Electronic Supplementary Material (ESI) for Organic & Biomolecular Chemistry.
This journal is © The Royal Society of Chemistry 2019

Fluorinated bisbenzimidazoles: a new class of drug-like anion transporters with chloride-mediated, cell apoptosis-inducing activity

Xi-Hui Yu[#], Xiao-Qiao Hong[#] and Wen-Hua Chen*

Guangdong Provincial Key Laboratory of New Drug Screening, School of Pharmaceutical Sciences, Southern Medical University, Guangzhou 510515, P. R. China

Supporting Information

Experimental procedures

Preparation of EYPC vesicles

Vesicles for pH discharge were prepared completely according to the reported protocols. [1] Entrapped within the vesicles was a 0.1 mM pyranine solution in 25 mM HEPES buffer (50 mM NaCl, pH 7.0), whereas the external solution was 25 mM HEPES buffer (50 mM NaCl, pH 7.0).

Vesicles for chloride efflux were prepared in a similar fashion, except that they were formed in 25 mM HEPES buffer (500 mM NaCl, pH 7.0), whereas the external solution was 25 mM HEPES buffer (500 mM $NaNO_3$, pH 7.0).

Vesicles for mobile carrier mechanism study were prepared in a similar fashion, except that EYPC-cholesterol (7/3) was used instead of EYPC.

Vesicles for calcein leakage experiments were prepared in a similar fashion, except that they were formed in a 100 mM calcein solution in 25 mM HEPES buffer (500 mM NaCl, pH 7.0); and that 25 mM HEPES buffer (500 mM NaCl, pH 7.0) was used to elute the Sephadex G-25 column to remove the non-entrapped calcein.

Measurement of anionophoric activity

Literature protocols described by us [2-4] and others [5-7] were used to prepare the vesicle preparations and conduct the pH discharge, the chloride efflux, cation and anion selective transport and calcein leakage experiments of each of compounds.

^{1}H NMR titrations [8]

^{1}H NMR titrations were performed by keeping the concentrations of each compound constant, while gradually increasing the concentration of TBACl. Typically, to a solution of Bimbe (1 mM) in acetonitrile-d_3 were added aliquots of Bimbe (1 mM) and TBACl (4-50 mM) in the same solvent. The association constants (K_a's) were derived from nonlinear least-square fit of the experimental data according to a 1 : 1 binding model, $\delta = \delta_0+((\delta_\infty-\delta_0)/2[C]_0)\{([N]_0+[C]_0+1/K_a)-(([N]_0+[C]_0+1/K_a)^2-4[N]_0[C]_0)^{1/2}\}$, wherein $[N]_0$ and $[C]_0$ are the initial analytical concentrations of TBACl and each compound, respectively; $\Delta\delta$ and δ_0 represent the chemical

shifts of the sample and compound alone, respectively, and δ_∞ is the chemical shift when compound is totally bound.

MTT-based cytotoxicity assay [2,7]

The cytotoxicity was measured in standard DMEM/high glucose media. Specifically, cells were dispersed in a 96-well flat bottom tissue culture treated plates (Corning) at density of 3000 cells/well (per 100 μL) and incubated at 37 ^{o}C in a 5% CO_2 incubator for 16 h. Then, they were treated for 48 h with each compound of fixed (50 μM) or varying (0.78-100 μM) concentrations. A solution of MTT (Amresco) in PBS buffer (5 mg MTT/mL) was added to each well and incubation continued for an additional 4 h. Then, the MTT solution was removed and DMSO (100 μL) was added in each well to dissolve the formed formazan crystals. The absorbance at 570 nm was recorded in a microplate reader (Tecan Infinite M1000 PRO). For each condition, at least three independent experiments were performed and the mean value was taken. DMSO (1%) was used as a control. Cell viability was expressed as a percentage of control cells, and the data are reported as the mean value ± S.D. The concentration of each compound resulting in 50% inhibition in cell growth (IC_{50} value) was calculated with SPSS 13.0 software.

The cytotoxicity in the presence or the absence of chloride anions was measured in a similar fashion, except that HBSS media were used with chloride anions (136.9 mM NaCl, 5.5 mM KCl, 0.34 mM Na_2HPO_4, 0.44 mM KH_2PO_4, 0.81 mM $MgSO_4$, 1.25 mM $CaCl_2$, 5.5 mM D-glucose, 4.2 mM $NaHCO_3$ and 10 mM HEPES, pH 7.4) or without chloride anions (136.9 mM Na-gluconate, 5.5 mM K-gluconate, 0.34 mM Na_2HPO_4, 0.44 mM KH_2PO_4, 0.81 mM $MgSO_4$, 1.25 mM $CaCl_2$, 5.5 mM D-glucose, 4.2 mM $NaHCO_3$ and 10 mM HEPES, pH 7.4).

The cytotoxicity in the presence of necrotic, autophagic or apoptotic inhibitors was measured in a similar fashion. HeLa cells were dispersed in a 96-well flat bottom tissue culture treated plates (Corning) at density of 3000 cells/well (per 100 μL) and incubated at 37 ^{o}C in a 5% CO_2 incubator for 24 h. Then, they were preincubated with Nec-1, 3-MA or Z-VAD-FMK for 2 h followed by incubation with $^{5,6}F_4$-FBimbe **12** or $^{4,5,6,7}F_8$-FBimbe **13** for 24 h. Finally, the samples were examined according to the standard protocols of MTT-based cytotoxicity assay.

MQAE assay

The experiments were conducted following the protocols reported in literatures. [2,5,7] Specifically, HeLa cells were seeded in a 96-well flat bottom tissue culture treated plates (Corning) at density of 10^4 cells/well (per 100 μL) and incubated in a 5% CO_2 incubator at 37 °C for 24 h. MQAE was added to each well by maintaining the final concentration at 5 mM for 3.5 h. Extracellular dye was removed by washing with PBS buffer thrice. Then, FBimbe **7**, $^{5}F_{2}$-FBimbe **9**, $^{5,6}F_{4}$-FBimbe **12** or $^{4,5,6,7}F_{8}$-FBimbe **13** of varying concentrations was added in DMEM (1% DMSO was used as a control) and the cells were incubated for additional 2 h. The MQAE fluorescence was measured using Infinite M1000 Pro (λ_{ex} = 350 nm, λ_{em} = 460 nm).

Acridine orange staining

The experiments were conducted following the protocols reported in literatures. [9-12] Specifically, HeLa cells were seeded on a 6-well plate for 24 h and then treated with 10 μM of FBimbe **7**, $^{5}F_{2}$-FBimbe **9**, $^{5,6}F_{4}$-FBimbe **12** or $^{4,5,6,7}F_{8}$-FBimbe **13** for 3 h. DMSO was added in control cells. Afterwards, the cells were washed twice with PBS buffer and incubated in a solution of acridine orange (5 μg/mL) at 37 °C in the dark for 30 min. Finally, the cells were washed with PBS-10% FBS buffer thrice and examined by fluorescence on an Axio Observer microscope.

Hoechst staining

The experiments were conducted following the protocols reported in literatures. [9,10] Specifically, HeLa cells were seeded on a 6-well plate for 17 h, and then treated with 10 μM of FBimbe **7**, $^{5}F_{2}$-FBimbe **9**, $^{5,6}F_{4}$-FBimbe **12** or $^{4,5,6,7}F_{8}$-FBimbe **13** for 24 h. DMSO was added in control cells. Afterwards, the cells were washed with PBS buffer and incubated with a solution of Hoechst 33342 (2 μg/mL) at 37 °C in the dark for 30 min. Finally, the cells were washed with PBS buffer and examined by fluorescence on an Axio Observer microscope.

JC-1 staining

The experiments were performed following the protocols reported in literatures. [2,7,13] Here the

mitochondrial membrane potential detection kit (Genview, USA) was employed to examine the mitochondrial membrane potential. Thus, HeLa cells were seeded on a 6-well plate for 17 h, and then treated with $^{5,6}F_4$-FBimbe **12** or $^{4,5,6,7}F_8$-FBimbe **13** (1.25 μM, 2.5 μM, 5 μM and 10 μM, respectively) for 24 h. DMSO was added in control cells. The HeLa cells were stained with JC-1 according to the manufacturer's instructions. Finally, the cells were examined by fluorescence on an Axio Observer microscope. The red/green pixel ratio was analyzed by Image*J*.

References

1. W.-H. Chen, S. L. Regen, *J. Am. Chem. Soc.*, **2005**, *127*, 6538-6539.
2. X.-H. Yu, C.-C. Peng, X.-X. Sun, W.-H. Chen, *Eur. J. Med. Chem.*, **2018**, *152*, 115-125.
3. Z. Li, X.-H. Yu, Y. Chen, D.-Q. Yuan, W.-H. Chen, *J. Org. Chem.*, **2017**, *82*, 13368-13375.
4. C.-C. Peng, M.-J. Zhang, X.-X. Sun, X.-J. Cai, Y. Chen, W.-H. Chen, *Org. Biomol. Chem.*, **2016**, *14*, 8232-8236.
5. N. Busschaert, S. H. Park, K. H. Baek, Y. P. Choi, J. Park, E. N. W. Howe, J. R. Hiscock, L. E. Karagiannidis, I. Marques, V. Felix, W. Namkung, J. L. Sessler, P. A. Gale, I. Shin, *Nat. Chem.*, **2017**, *9*, 667-675.
6. W. Van Rossom, D. J. Asby, A. Tavassoli, P. A. Gale, *Org. Biomol. Chem.*, **2016**, *14*, 2645-2650.
7. T. Saha, M. S. Hossain, D. Saha, M. Lahiri, P. Talukdar, *J. Am. Chem. Soc.*, **2016**, *138*, 7558-7567.
8. X. Bao, X. Wu, S. N. Berry, E. N. W. Howe, Y. T. Chang, P. A. Gale, *Chem. Commun.*, **2018**, *54*, 1363-1366.
9. E. Hernando, V. Soto-Cerrato, S. Cortes-Arroyo, R. Perez-Tomas, R. Quesada, *Org. Biomol. Chem.*, **2014**, *12*, 1771-1778.
10. N. Busschaert, M. Wenzel, M. E. Light, P. Iglesias-Hernandez, R. Perez-Tomas, P. A. Gale, *J. Am. Chem. Soc.*, **2011**, *133*, 14136-14148.
11. V. Soto-Cerrato, P. Manuel-Manresa, E. Hernando, S. Calabuig-Farinas, A. Martinez-Romero, V. Fernandez-Duenas, K. Sahlholm, T. Knopfel, M. Garcia-Valverde, A. M.

Rodilla, E. Jantus-Lewintre, R. Farras, F. Ciruela, R. Perez-Tomas, R. Quesada, *J. Am. Chem. Soc.*, **2015**, *137*, 15892-15898.

12. A. M. Rodilla, L. Korrodi-Gregorio, E. Hernando, P. Manuel-Manresa, R. Quesada, R. Perez-Tomas, V. Soto-Cerrato, *Biochem. Pharmacol.*, **2017**, *126*, 23-33.
13. T. Saha, A. Gautam, A. Mukherjee, M. Lahiri, P. Talukdar, *J. Am. Chem. Soc.*, **2016**, *138*, 16443-16451.

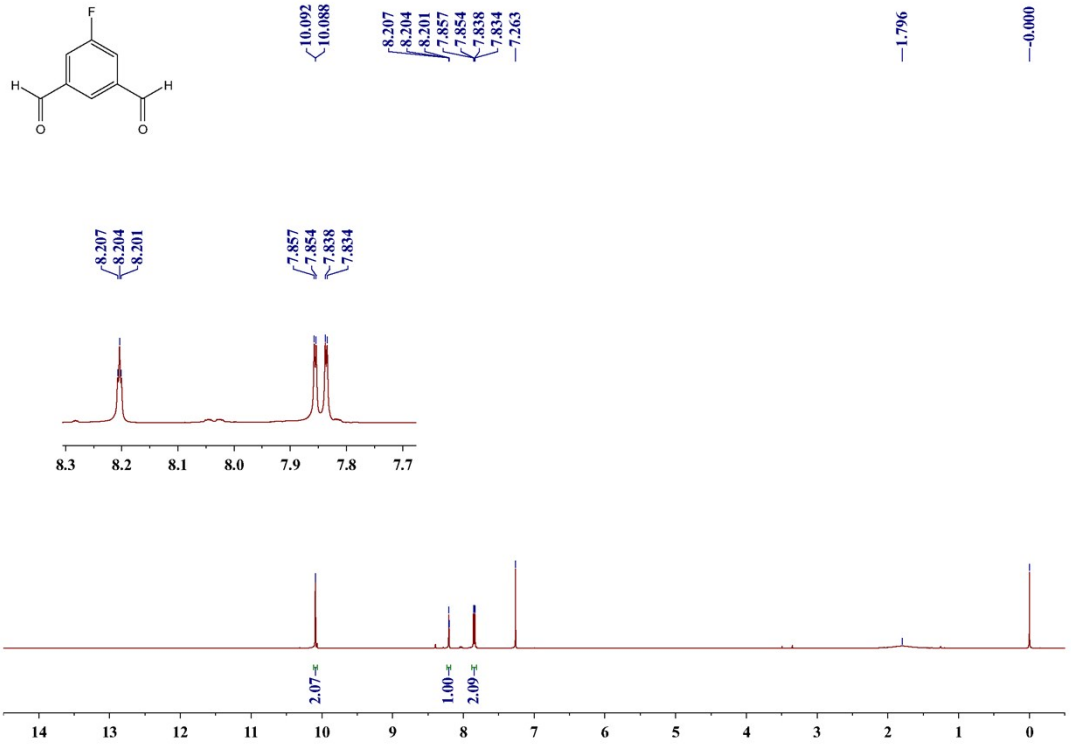

Fig. S1. ^{1}H NMR ($CDCl_3$, 400 MHz) of 5-fluoro-benzene-1,3-dicarbaldehyde.

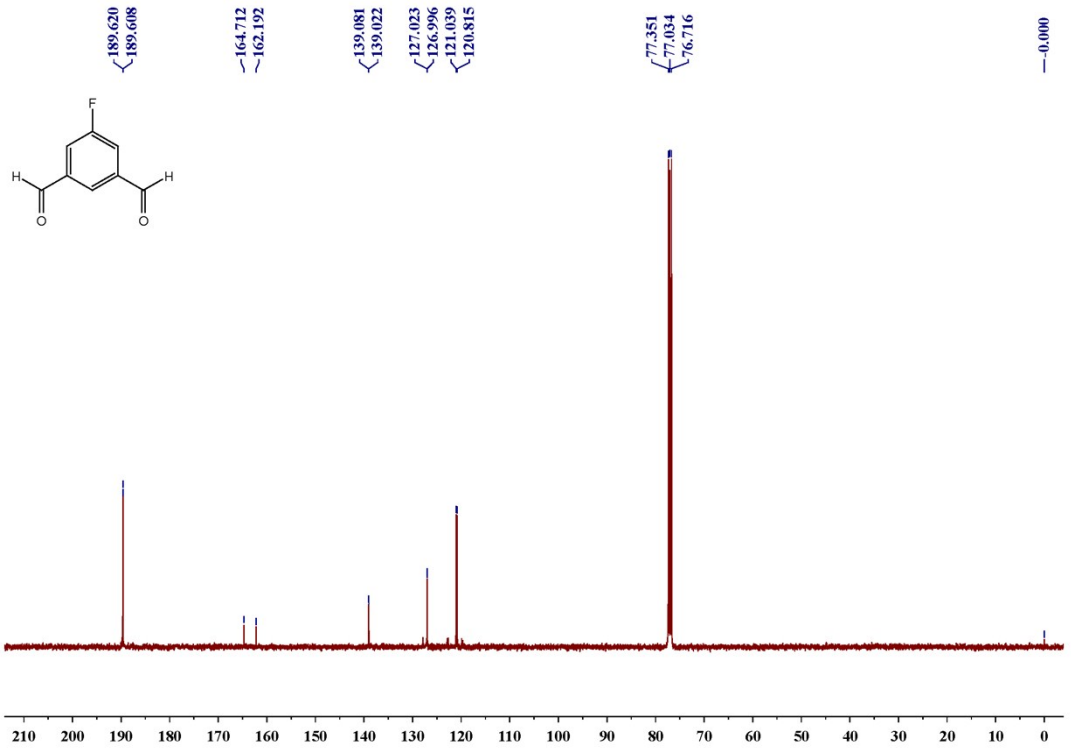

Fig. S2. ^{13}C NMR ($CDCl_3$, 100 MHz) of 5-fluoro-benzene-1,3-dicarbaldehyde.

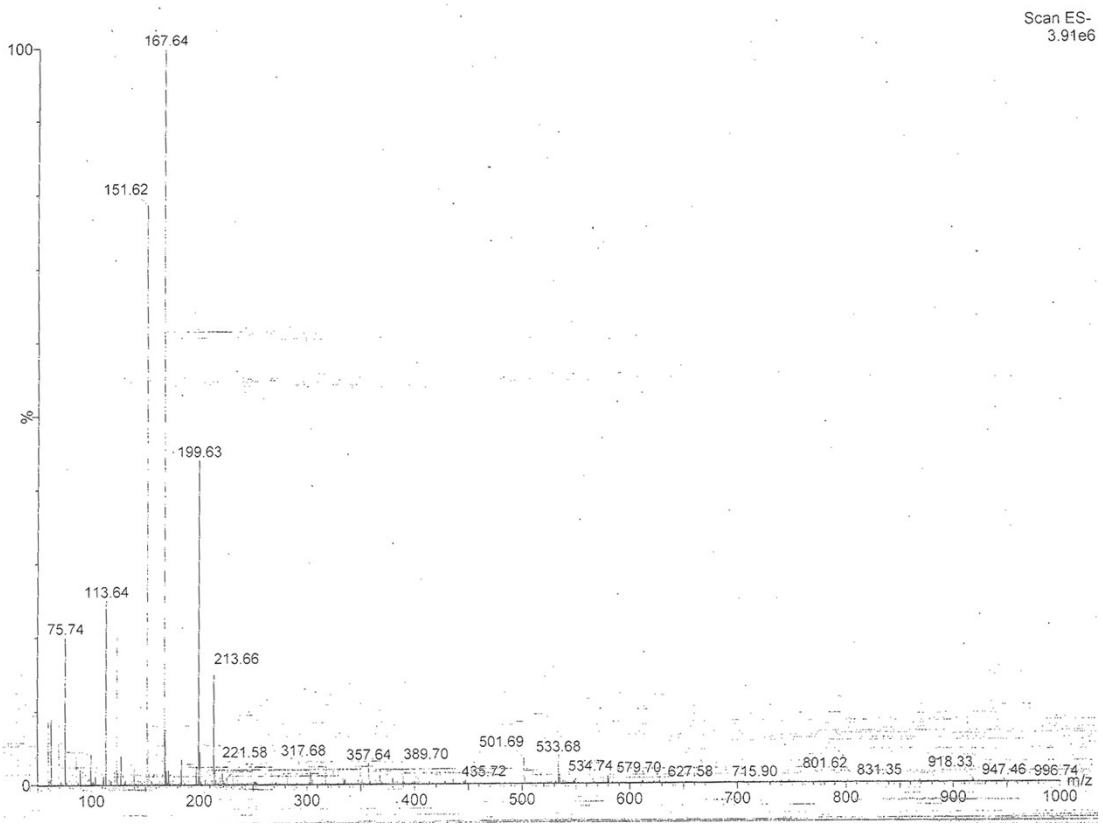

Fig. S3. ESI-MS of 5-fluoro-benzene-1,3-dicarbaldehyde.

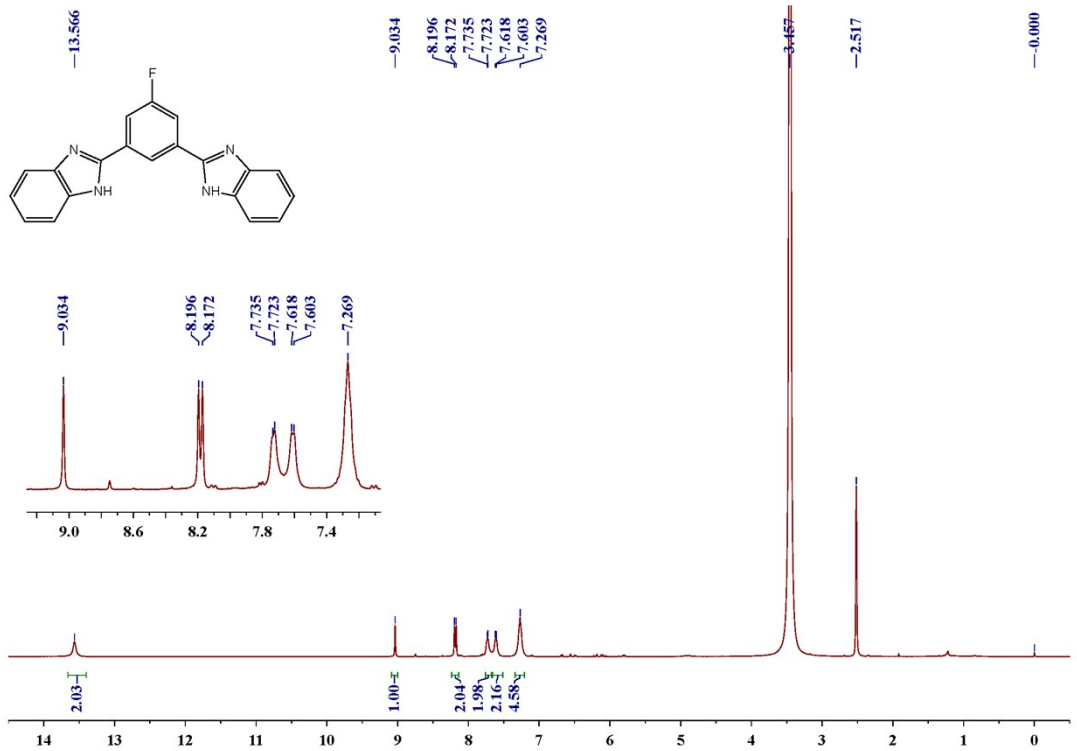

Fig. S4. ^{1}H NMR (DMSO-d_6, 400 MHz) of FBimbe **7**.

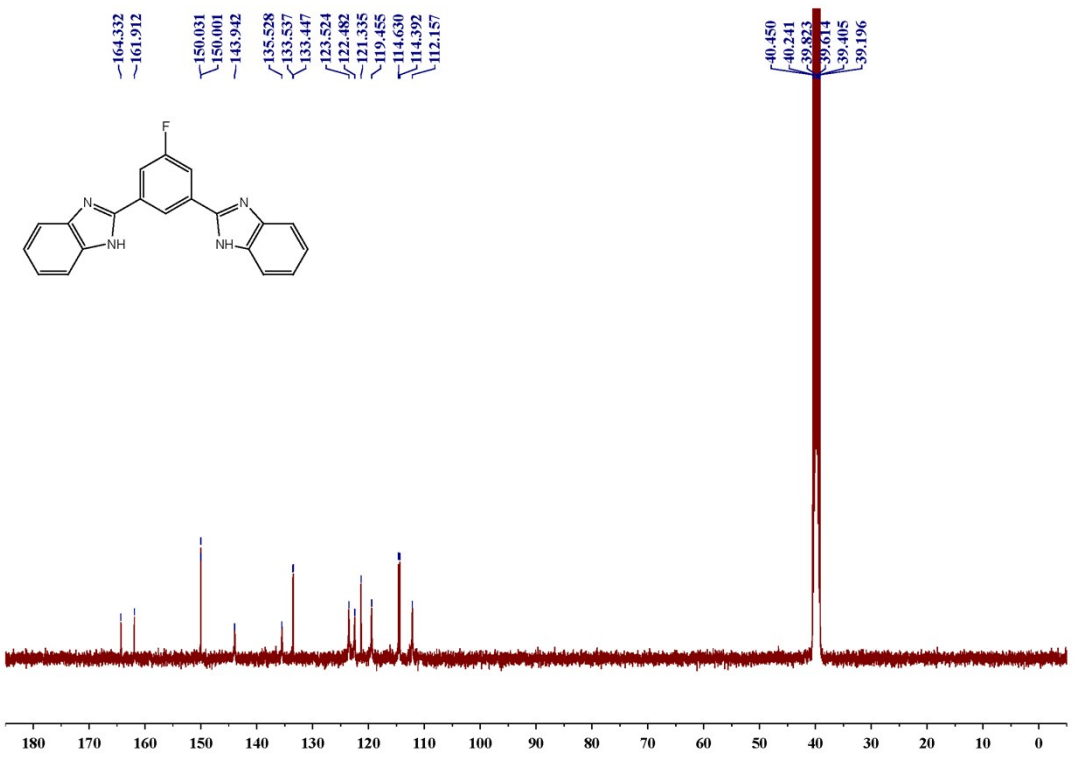

Fig. S5. ^{13}C NMR (DMSO-d_6, 100 MHz) of FBimbe **7**.

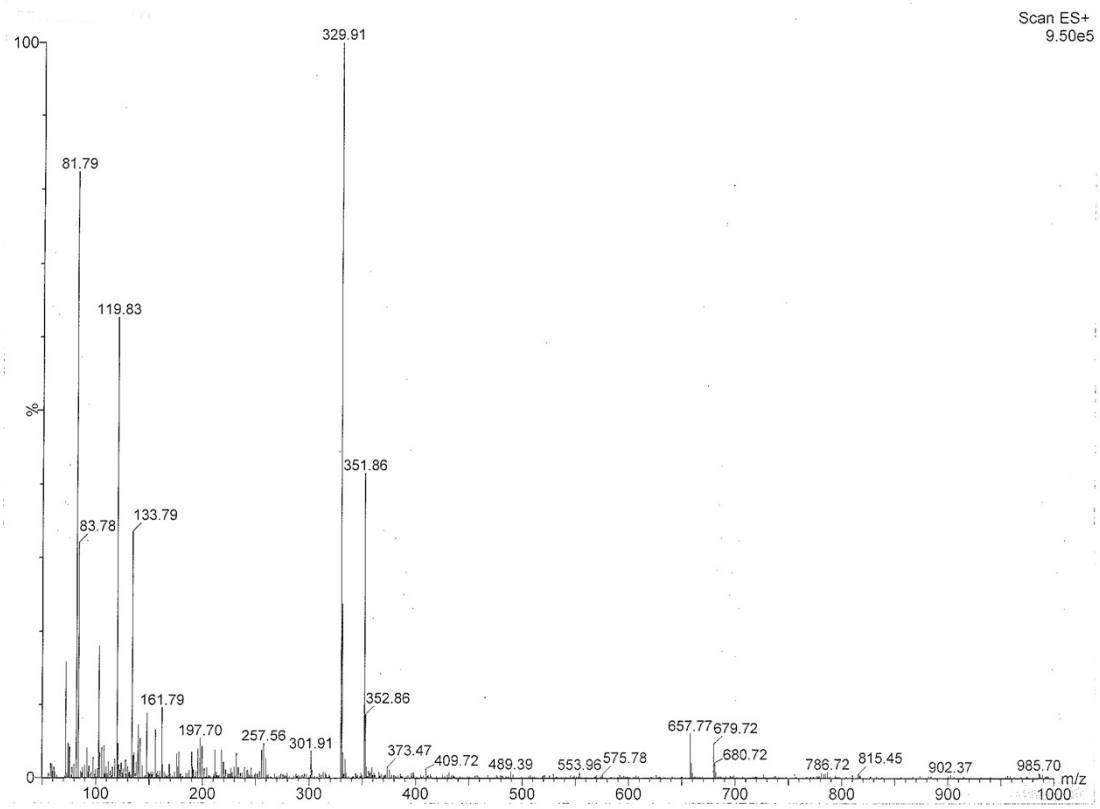

Fig. S6. ESI-MS of FBimbe **7**.

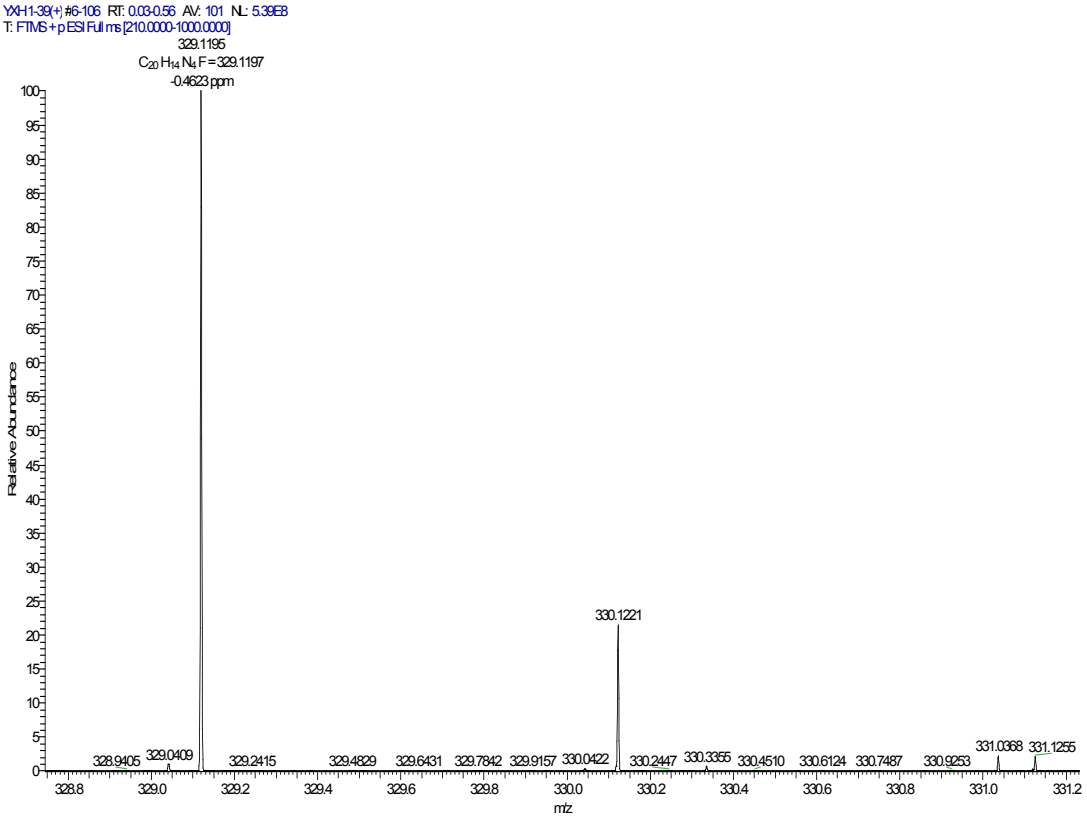

Fig. S7. HR ESI-MS of FBimbe **7**.

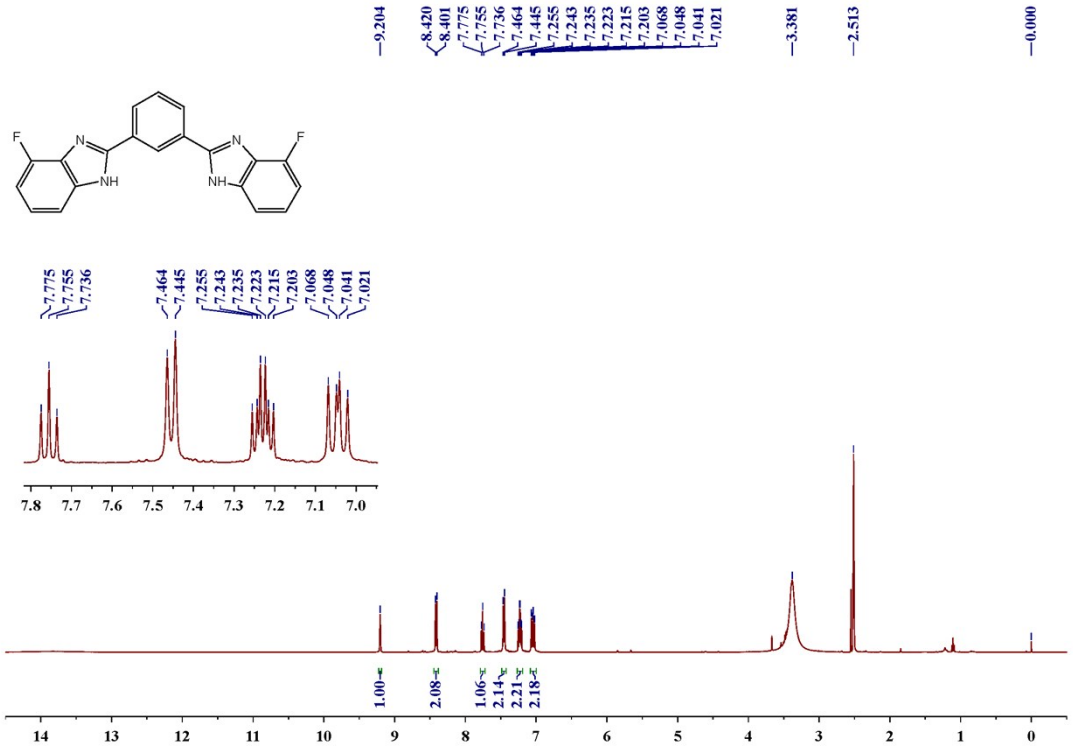

Fig. S8. ^{1}H NMR (DMSO-d_6, 400 MHz) of $^{4}F_2$-Bimbe **2**.

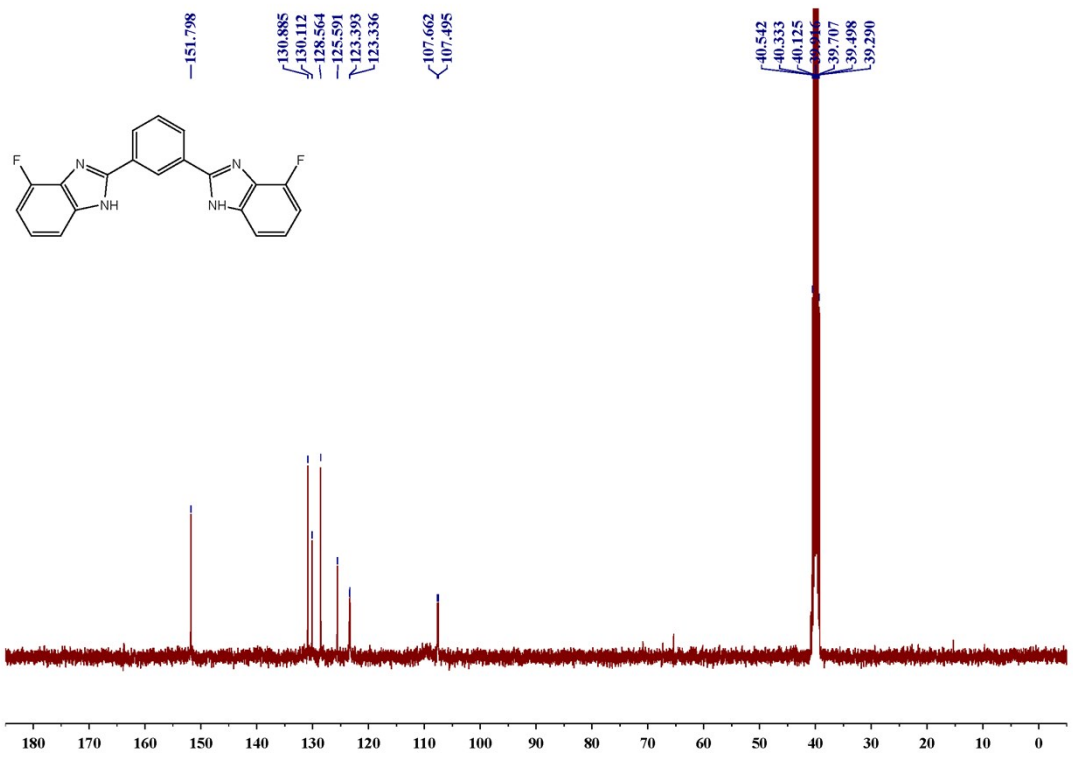

Fig. S9. ^{13}C NMR (DMSO-d_6, 100 MHz) of $^{4}F_2$-Bimbe **2**.

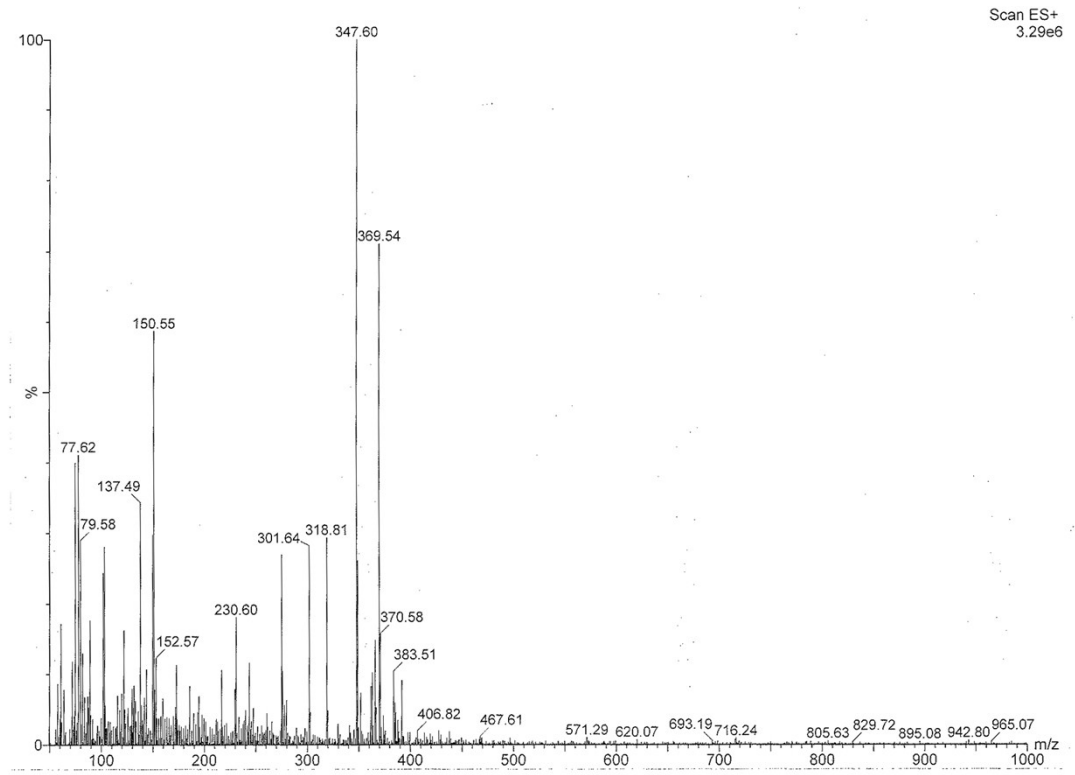

Fig. S10. ESI-MS of $^{4}F_2$-Bimbe **2**.

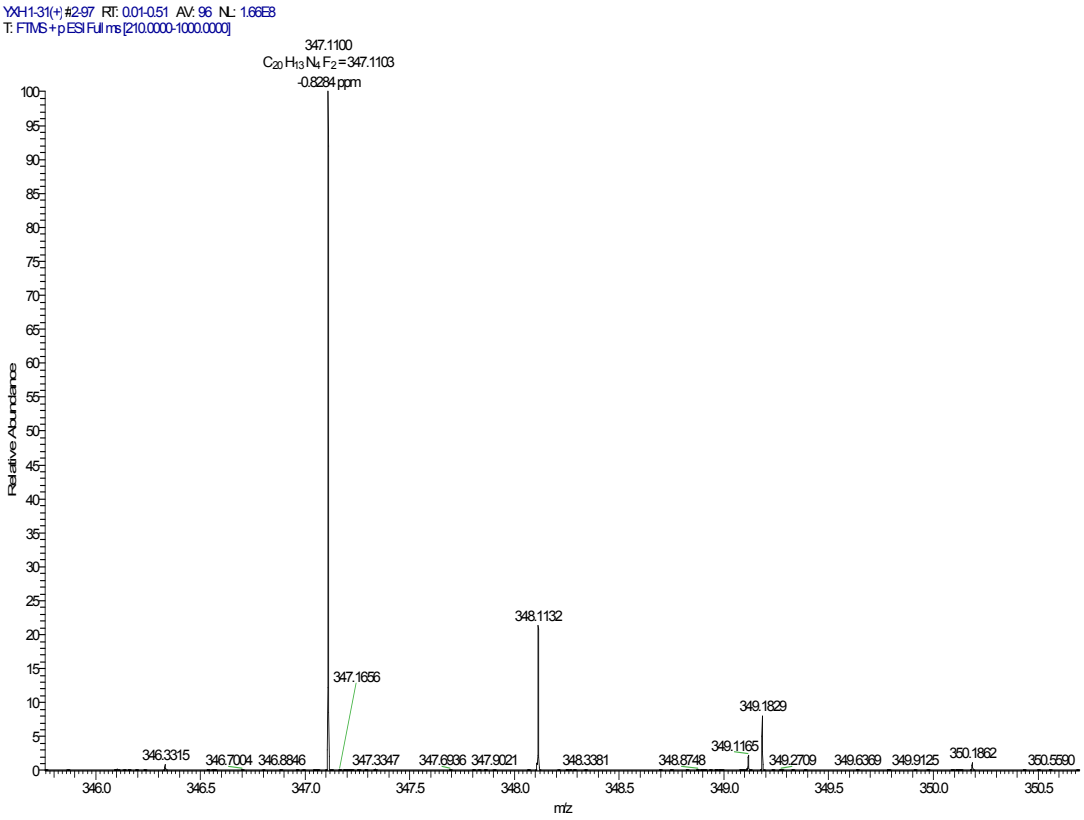

Fig. S11. HR ESI-MS of $^{4}F_{2}$-Bimbe **2**.

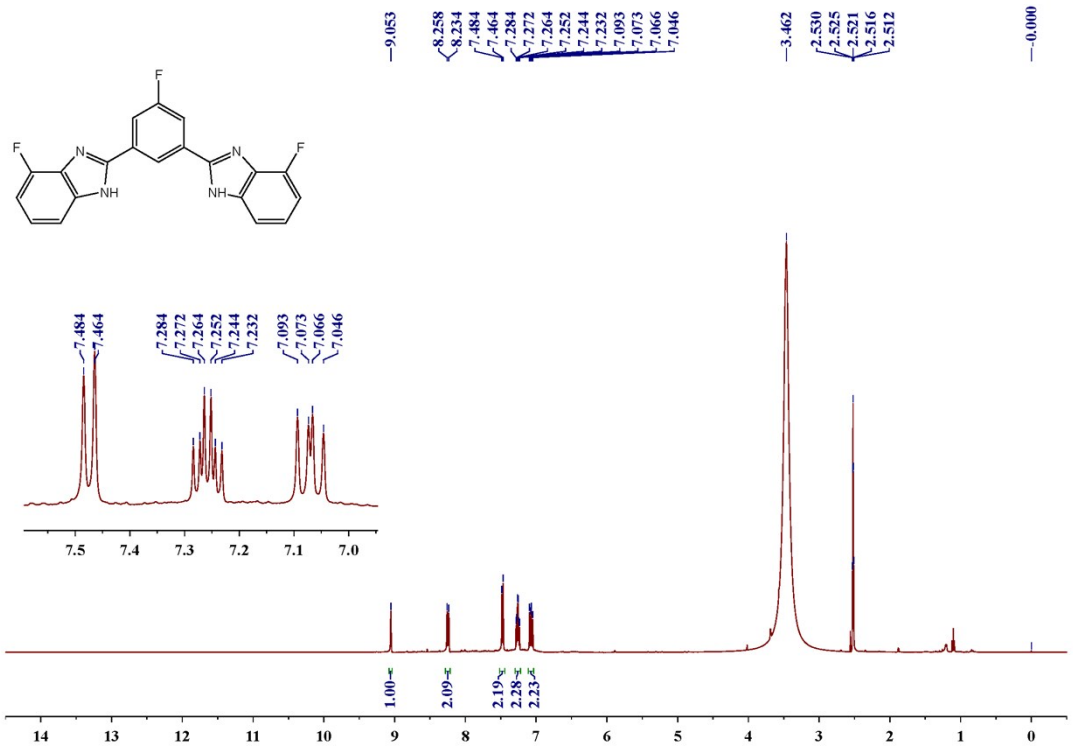

Fig. S12. ^{1}H NMR (DMSO-d_6, 400 MHz) of $^{4}F_{2}$-FBimbe **8**.

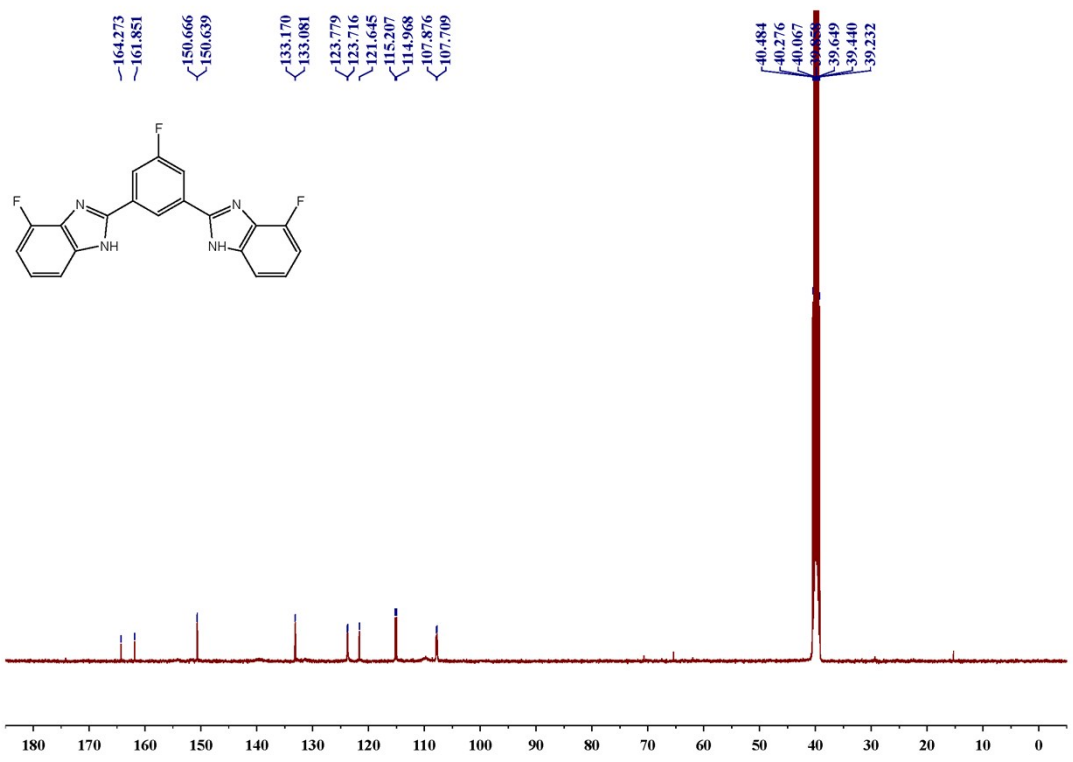

Fig. S13. ^{13}C NMR (DMSO-d_6, 100 MHz) of $^{4}F_2$-FBimbe **8**.

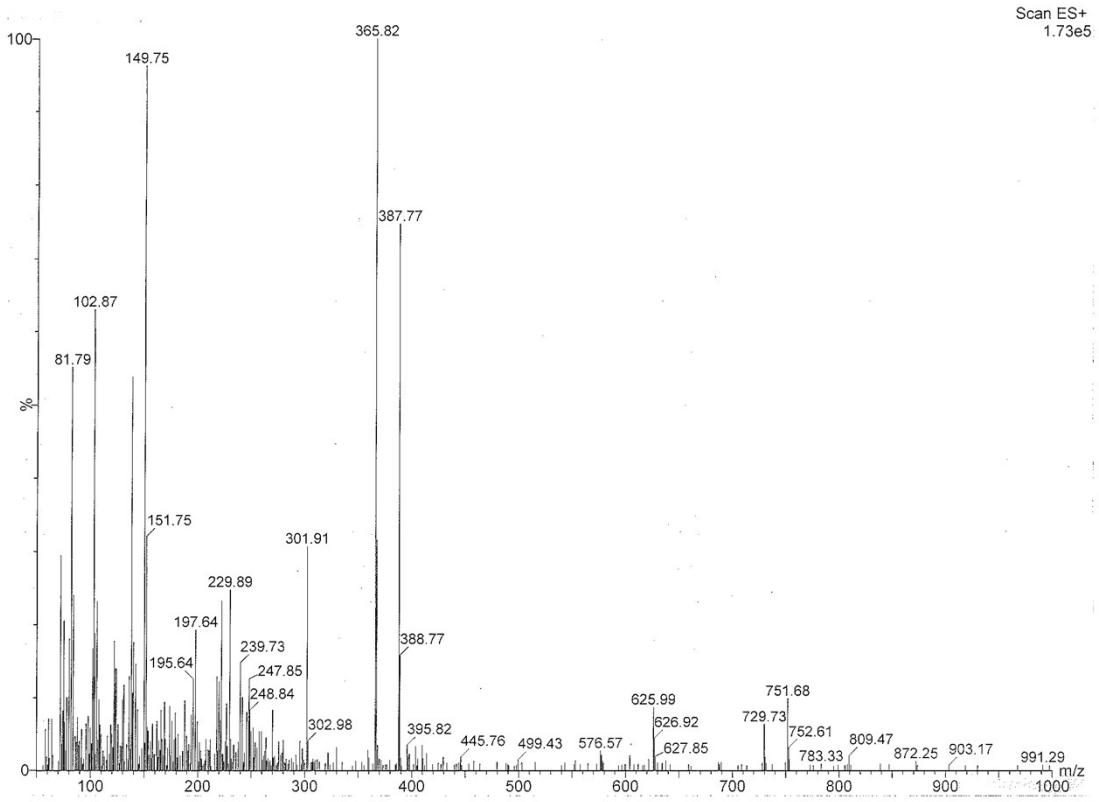

Fig. S14. ESI-MS of $^{4}F_2$-FBimbe **8**.

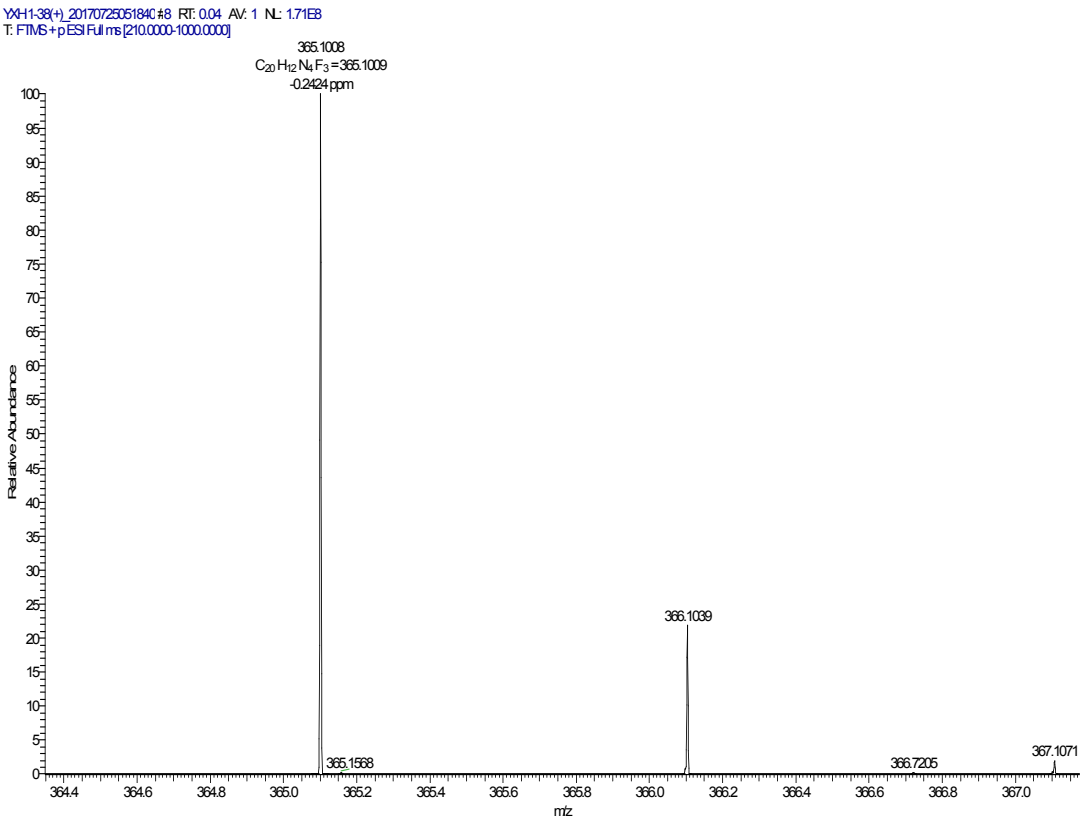

Fig. S15. HR ESI-MS of $^{4}F_{2}$-FBimbe **8**.

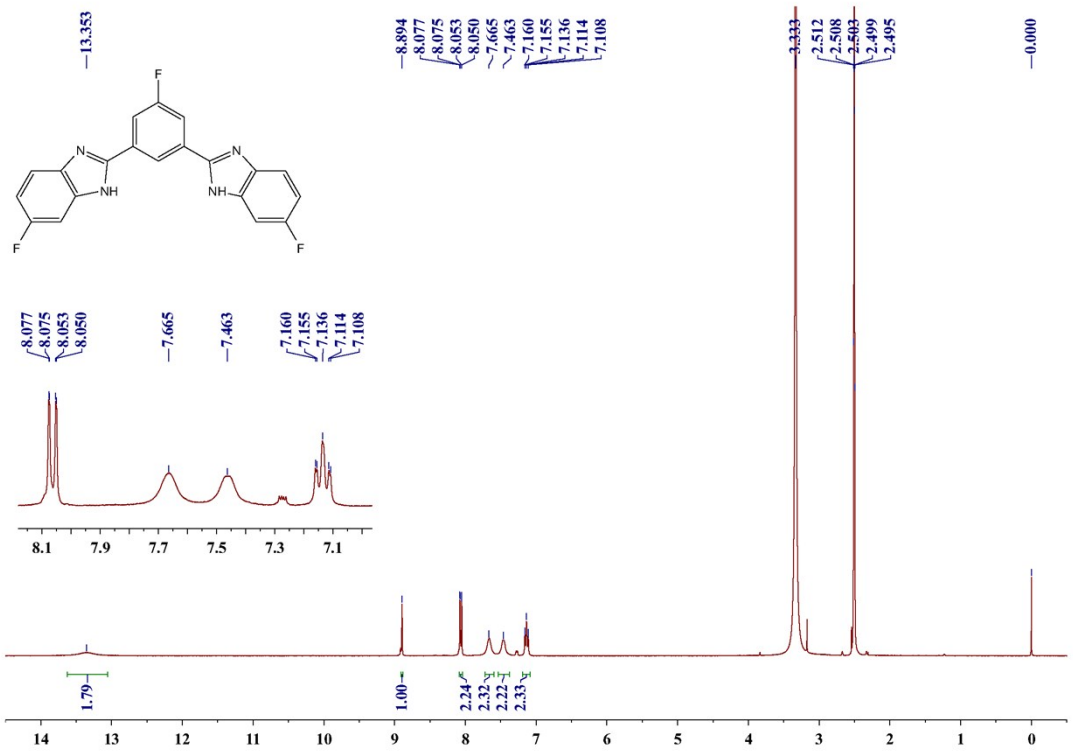

Fig. S16. ^{1}H NMR (DMSO-d_6, 400 MHz) of $^{5}F_{2}$-FBimbe **9**.

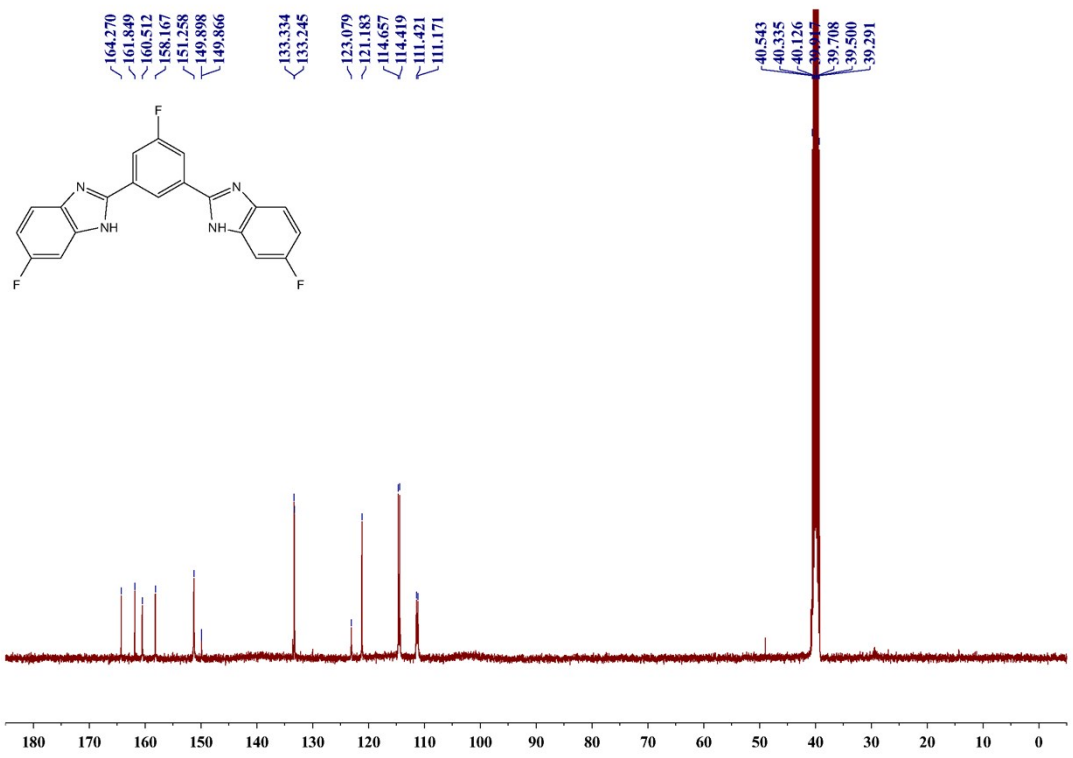

Fig. S17. ^{13}C NMR (DMSO-d_6, 100 MHz) of $^{5}F_2$-FBimbe **9**.

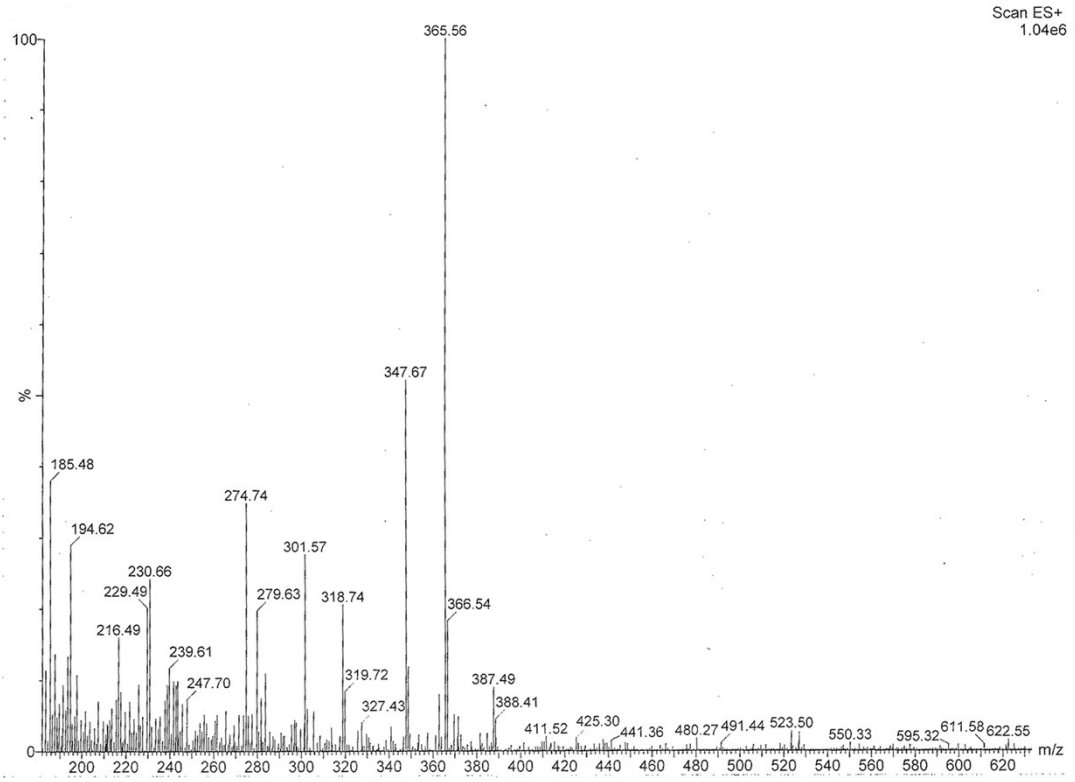

Fig. S18. ESI-MS of $^{5}F_2$-FBimbe **9**.

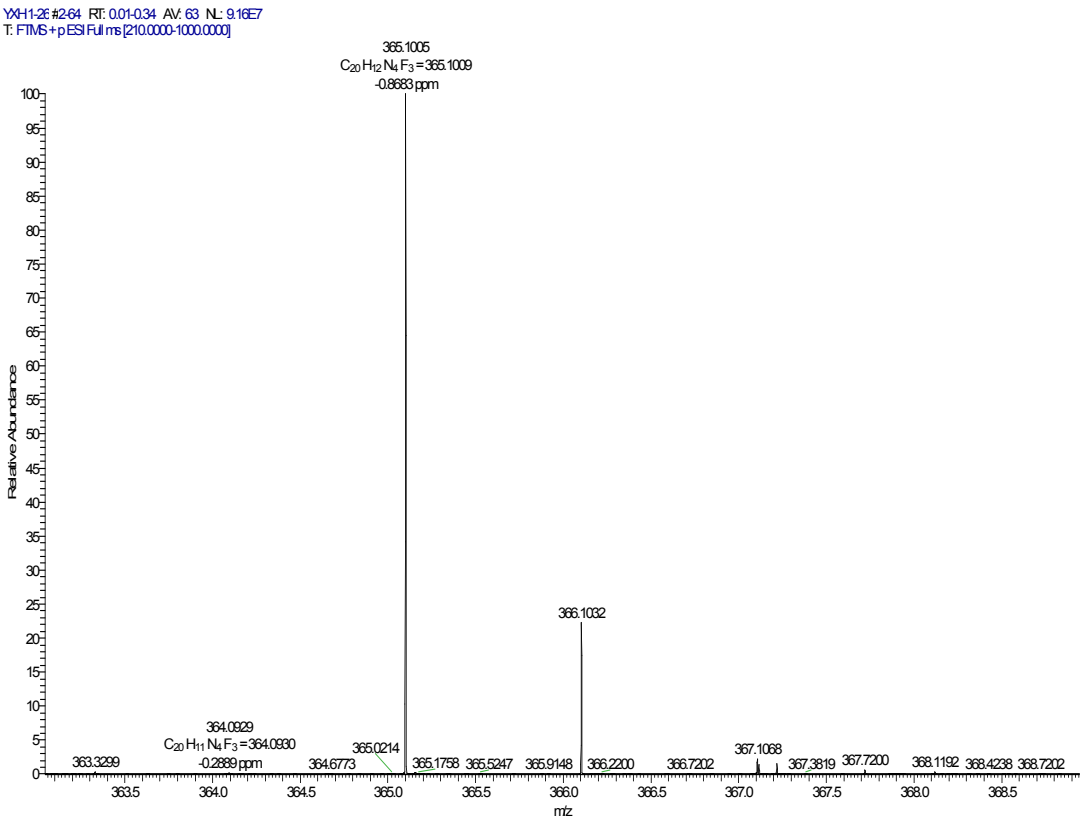

Fig. S19. HR ESI-MS of $^{5}F_{2}$-FBimbe **9**.

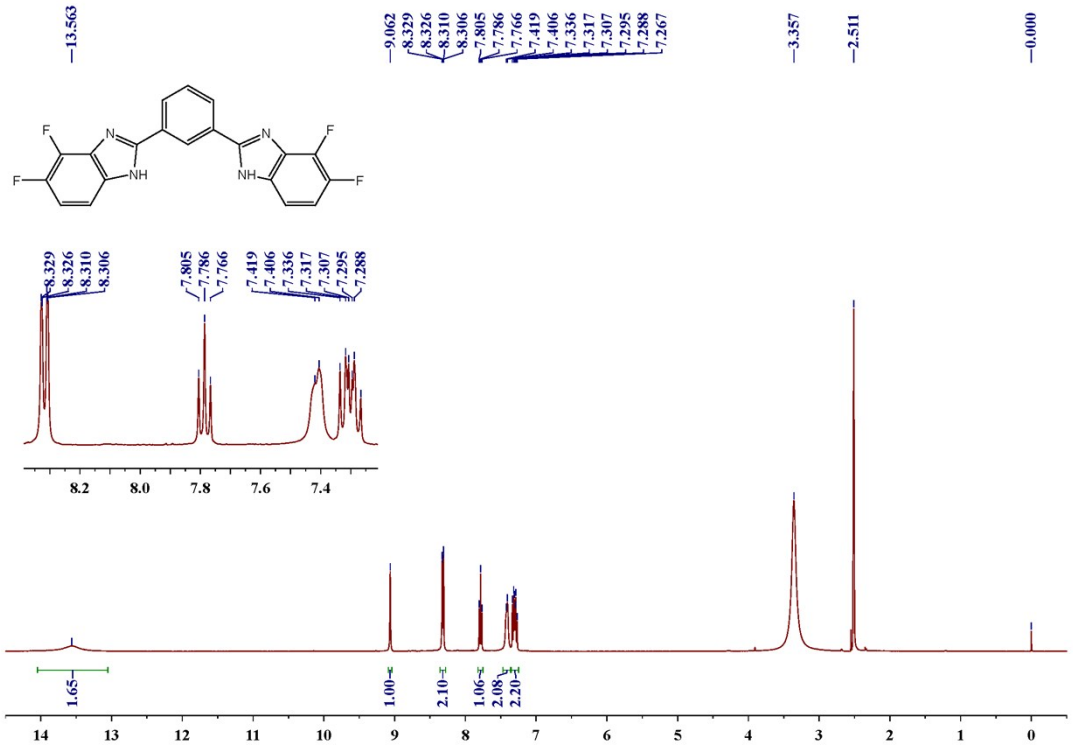

Fig. S20. ^{1}H NMR (DMSO-d_6, 400 MHz) of $^{4,5}F_{4}$-Bimbe **4**.

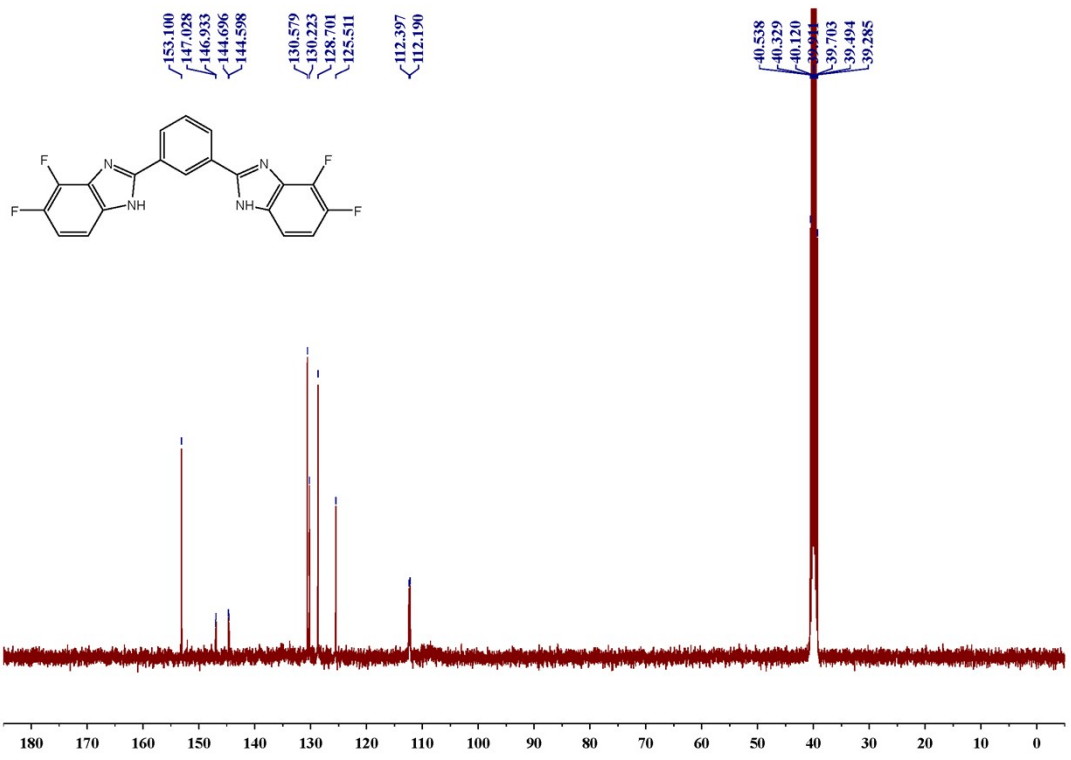

Fig. S21. ^{13}C NMR (DMSO-d_6, 100 MHz) of $^{4,5}F_4$-Bimbe **4**.

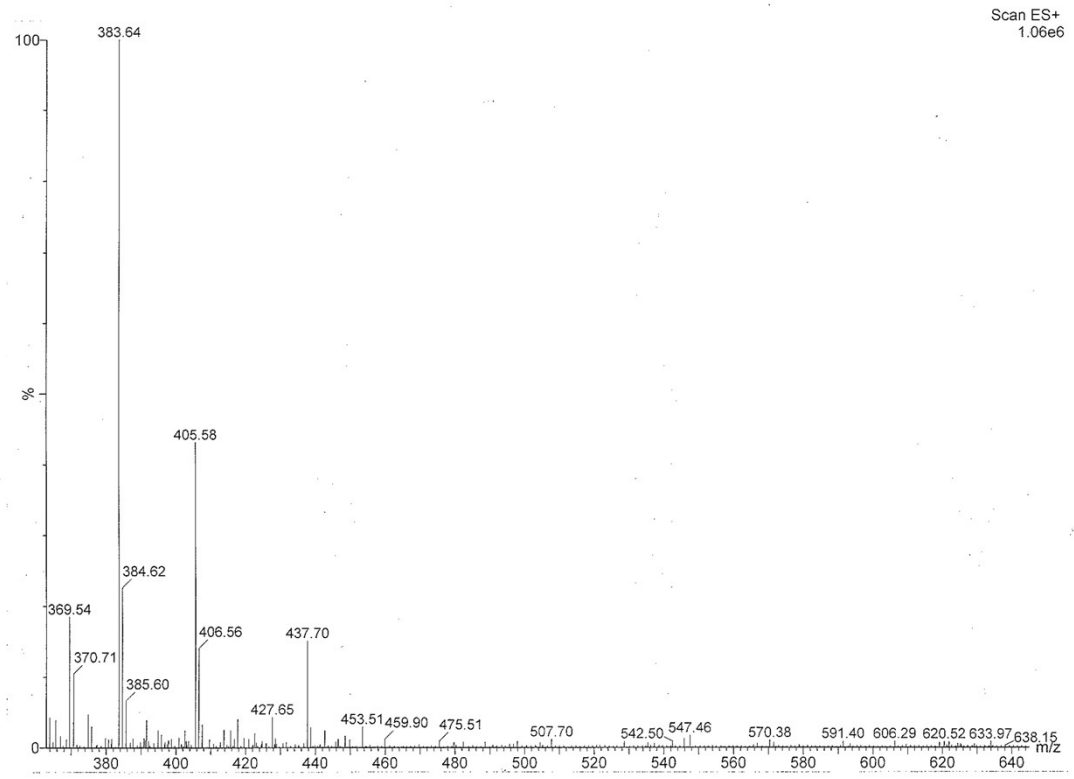

Fig. S22. ESI-MS of $^{4,5}F_4$-Bimbe **4**.

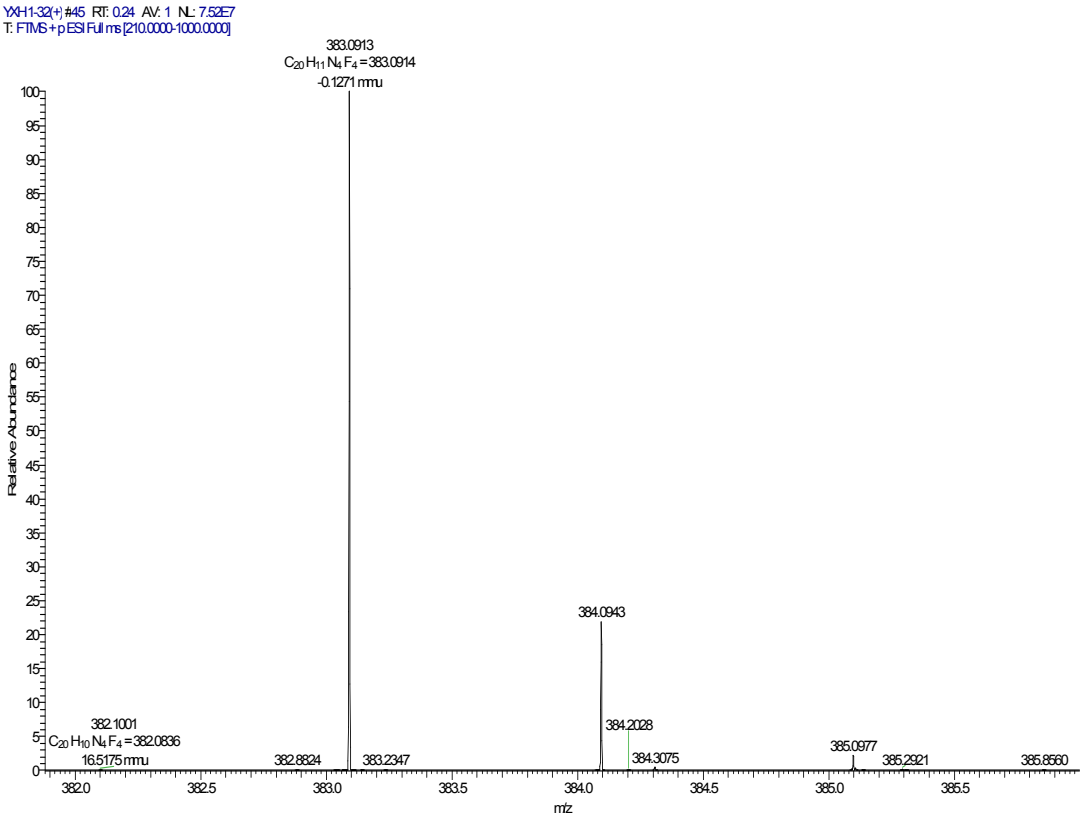

Fig. S23. HR ESI-MS of $^{4,5}F_4$-Bimbe **4**.

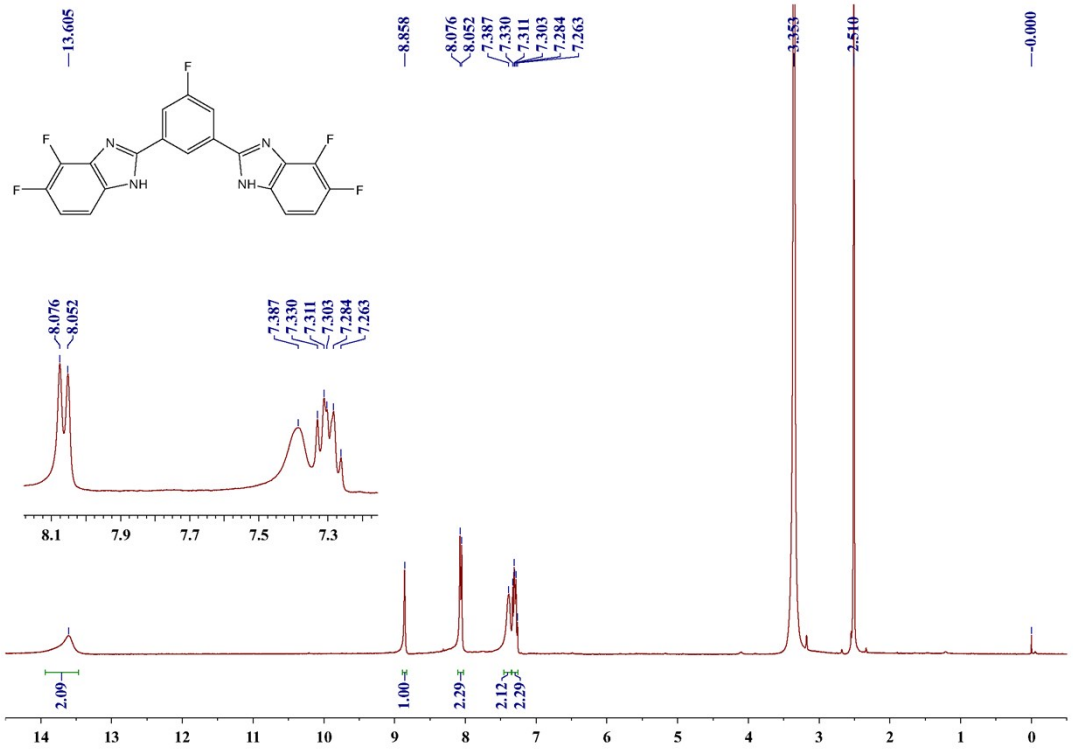

Fig. S24. ^{1}H NMR (DMSO-d_6, 400 MHz) of $^{4,5}F_4$-FBimbe **10**.

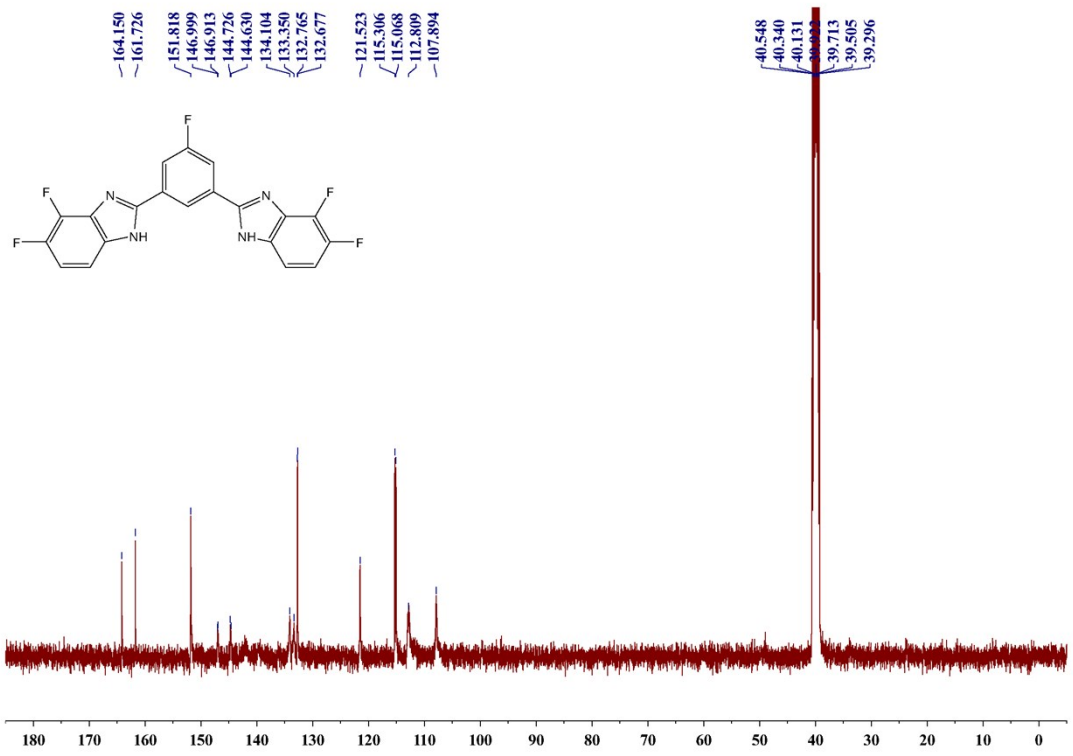

Fig. S25. ^{13}C NMR (DMSO-d_6, 100 MHz) of $^{4,5}F_4$-FBimbe **10**.

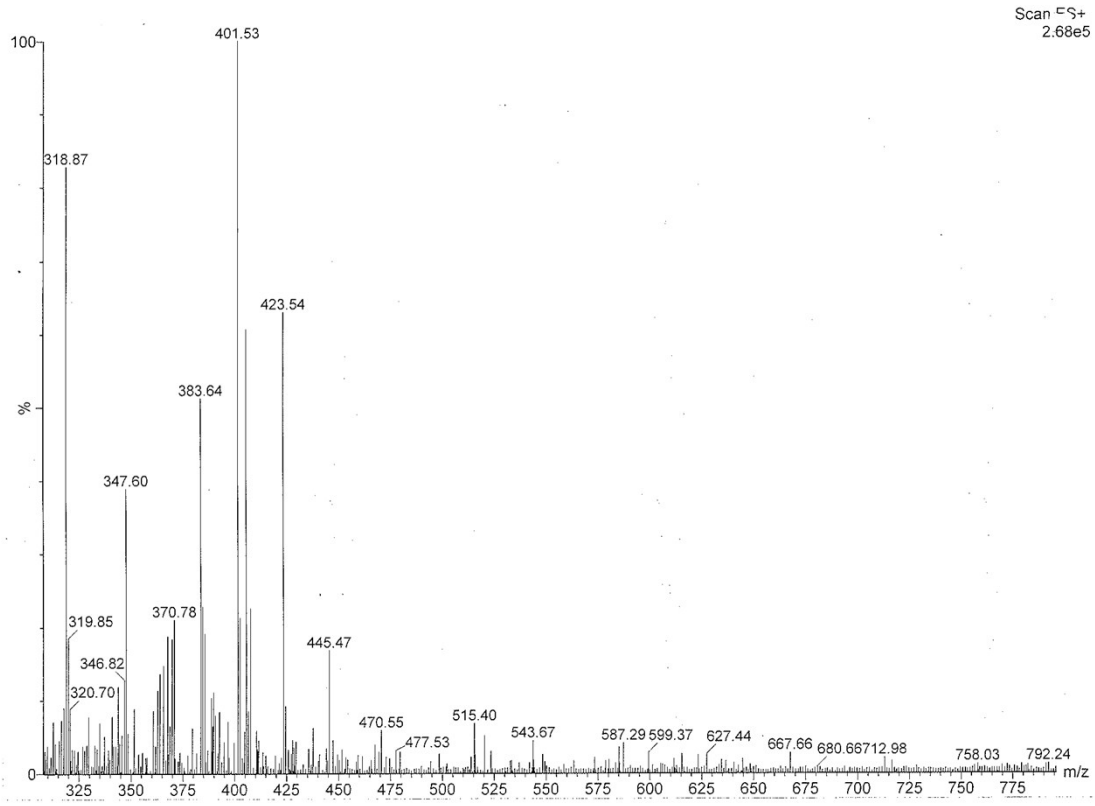

Fig. S26. ESI-MS of $^{4,5}F_4$-FBimbe **10**.

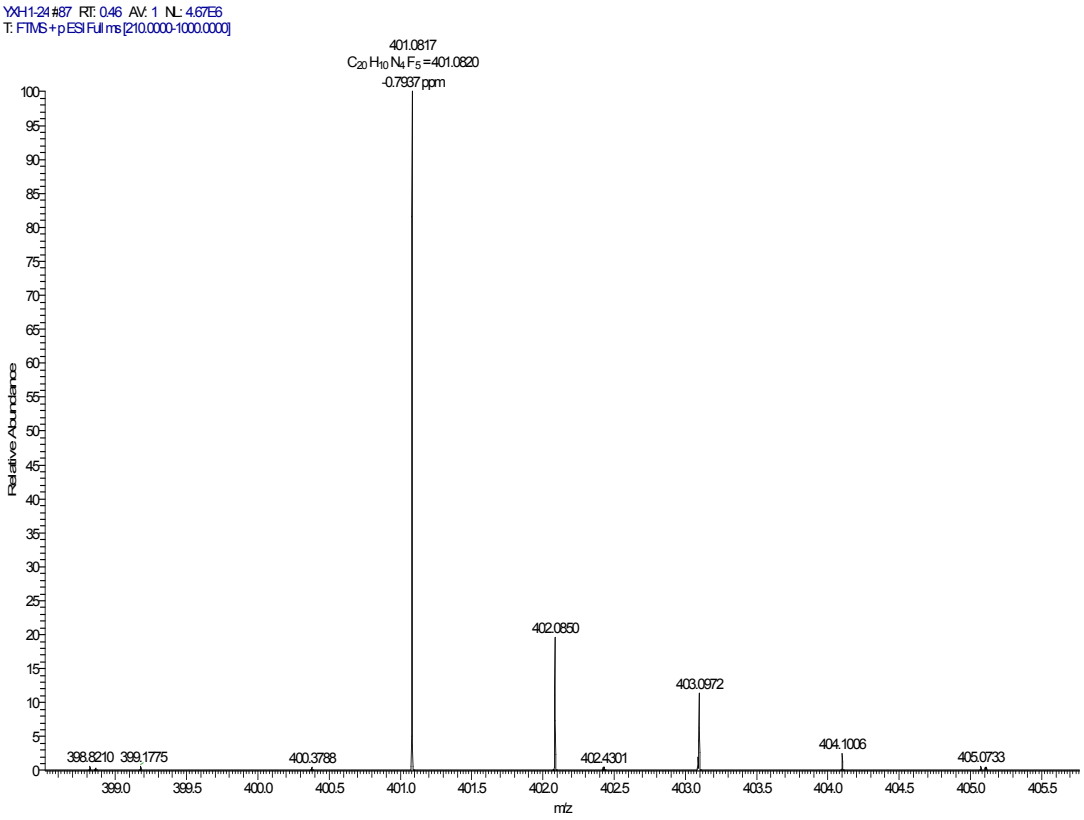

Fig. S27. HR ESI-MS of $^{4,5}F_4$-FBimbe **10**.

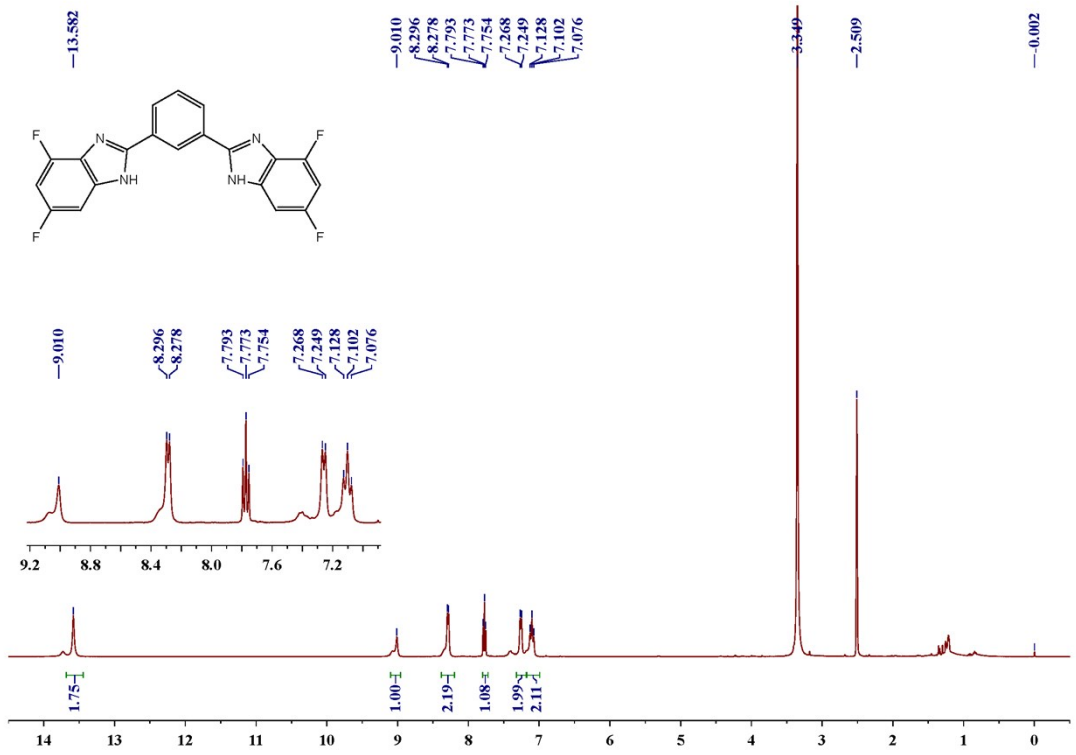

Fig. S28. ^{1}H NMR (DMSO-d_6, 400 MHz) of $^{4,6}F_4$-Bimbe **5**.

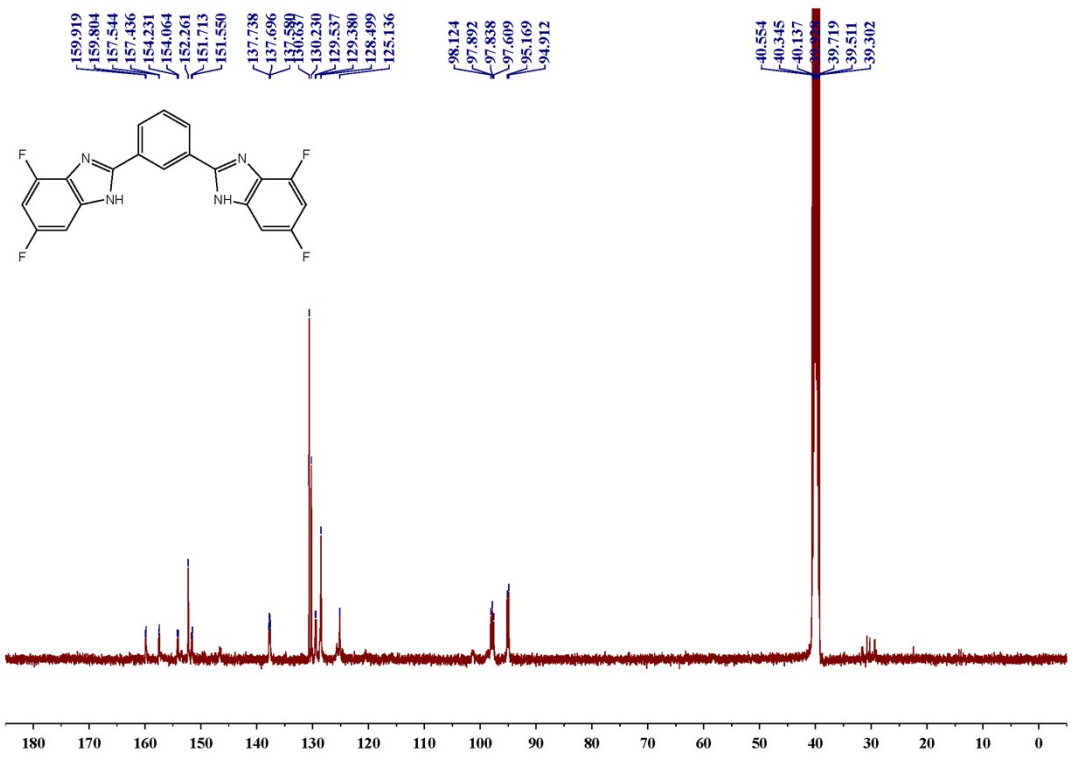

Fig. S29. ^{13}C NMR (DMSO-d_6, 100 MHz) of $^{4,6}F_4$-Bimbe **5**.

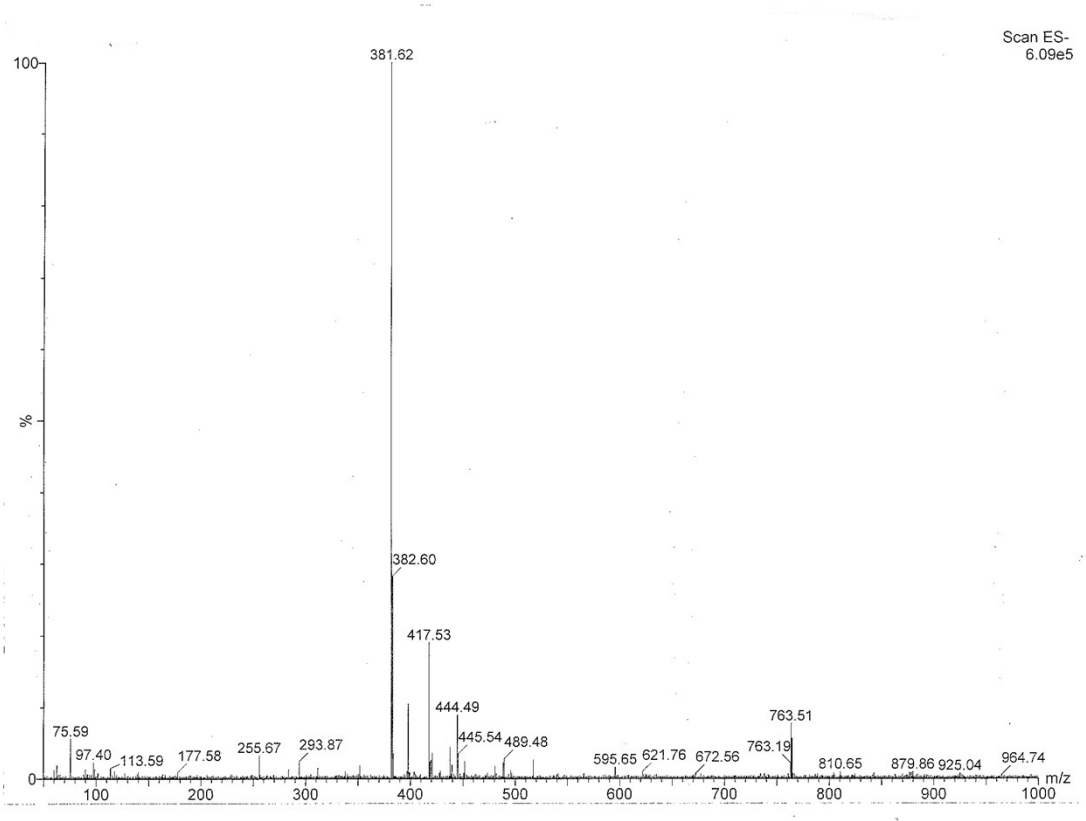

Fig. S30. ESI-MS of $^{4,6}F_4$-Bimbe **5**.

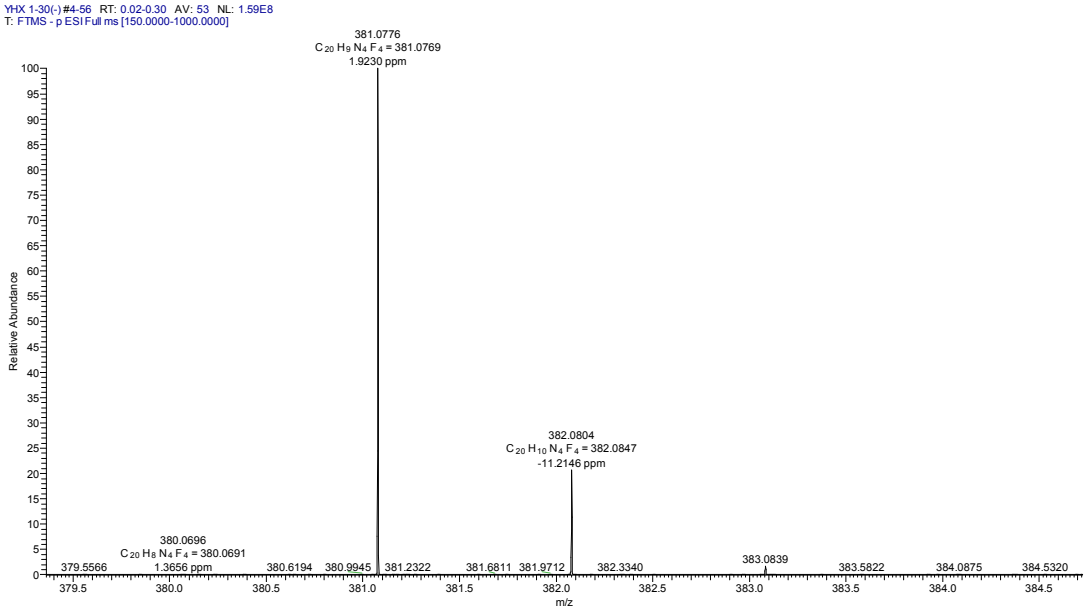

Fig. S31. HR ESI-MS of $^{4,6}F_4$-Bimbe **5**.

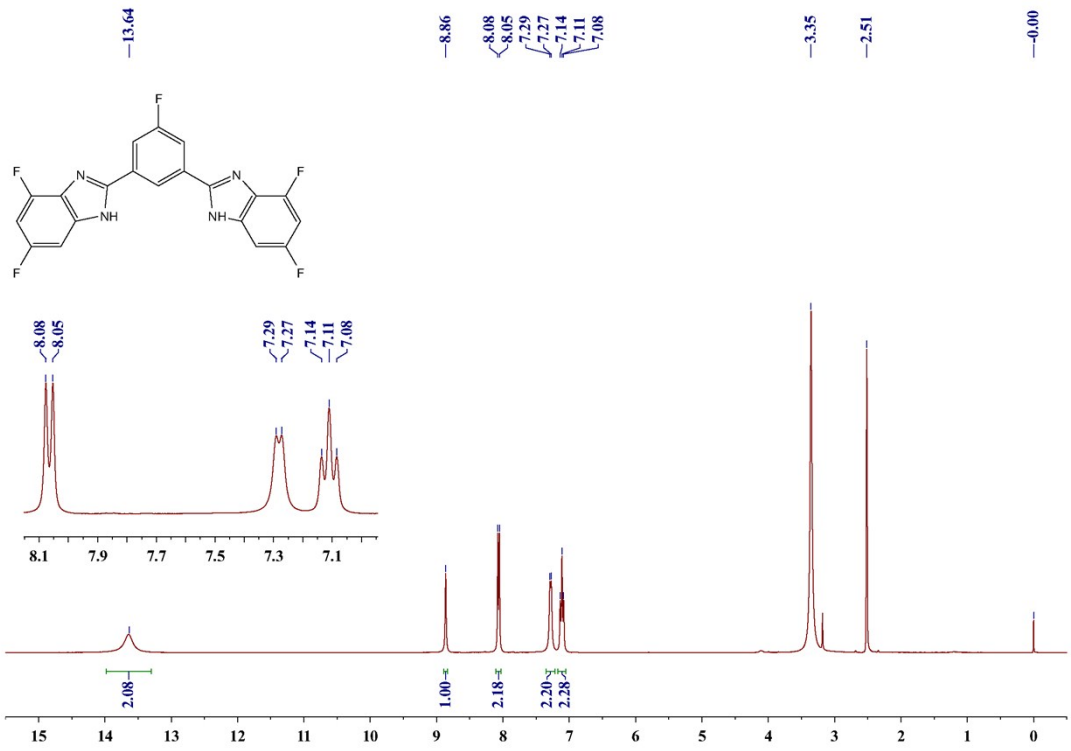

Fig. S32. ^{1}H NMR (DMSO-d_6, 400 MHz) of $^{4,6}F_4$-FBimbe **11**.

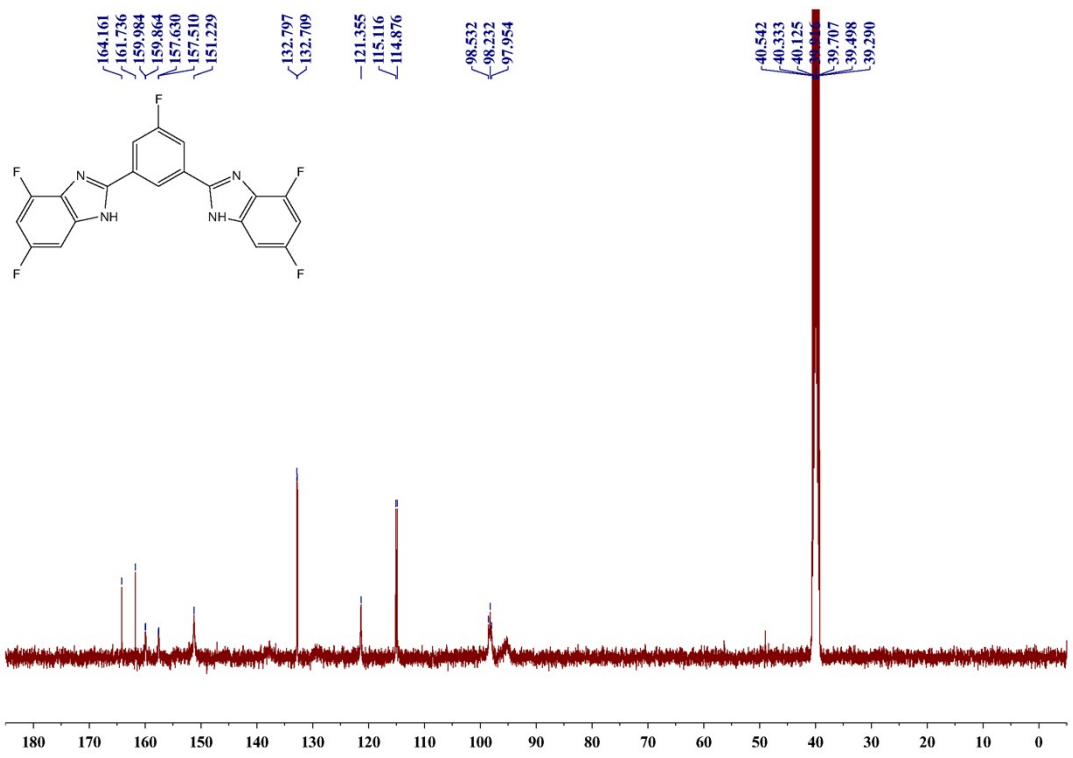

Fig. S33. ^{13}C NMR (DMSO-d_6, 100 MHz) of $^{4,6}F_4$-FBimbe **11**.

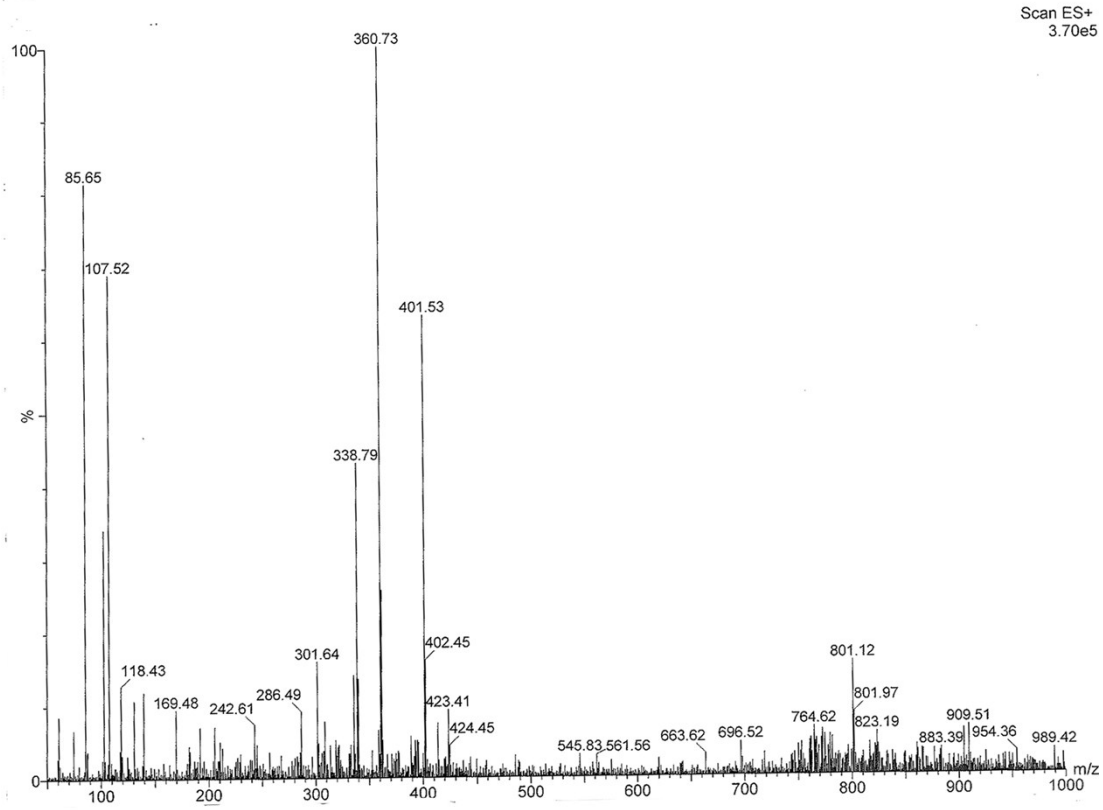

Fig. S34. ESI-MS of $^{4,6}F_4$-FBimbe **11**.

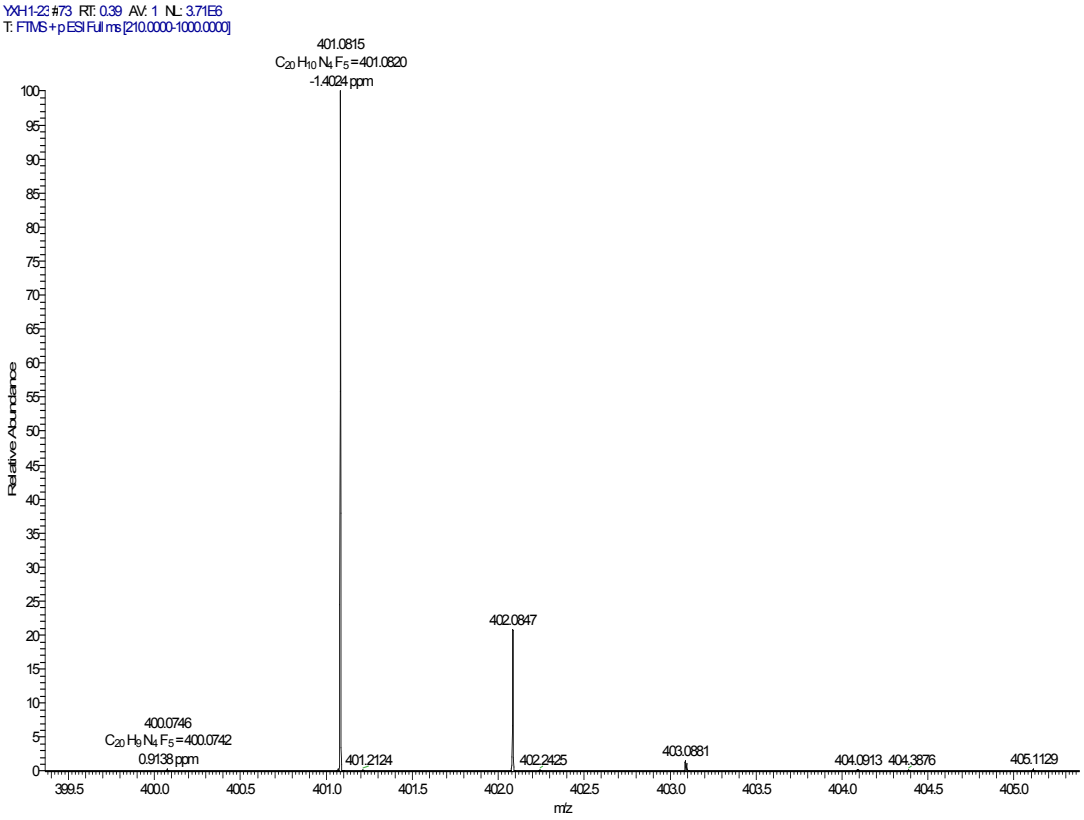

Fig. S35. HR ESI-MS of $^{4,6}F_4$-FBimbe **11**.

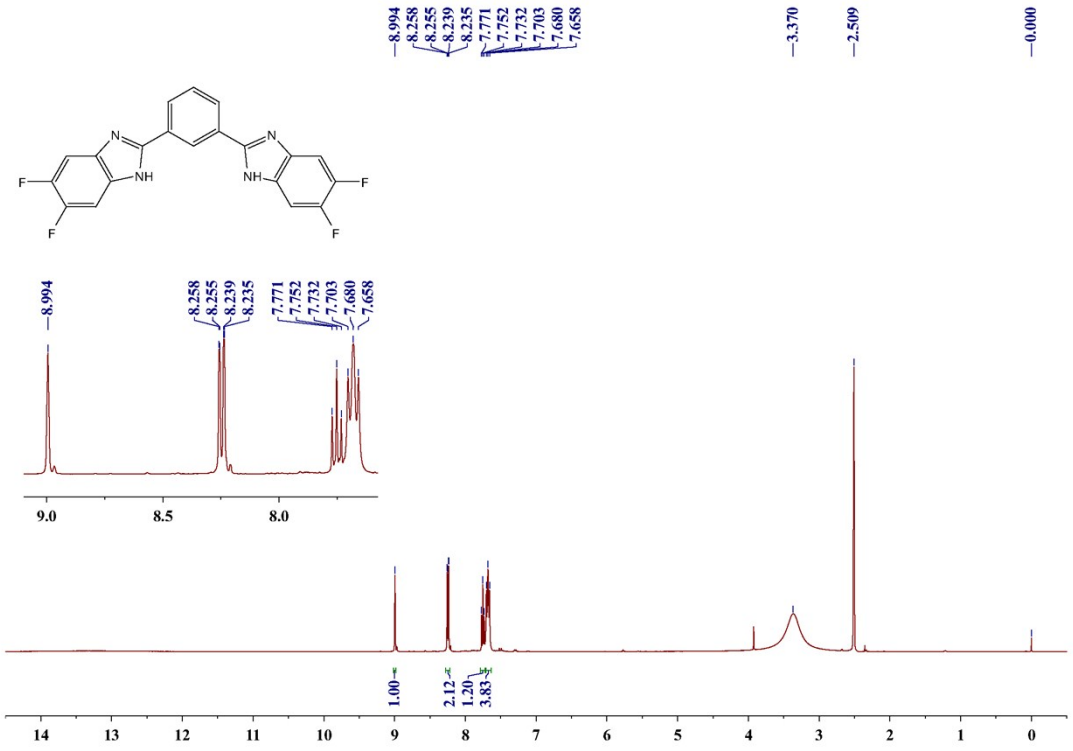

Fig. S36. ^{1}H NMR (DMSO-d_6, 400 MHz) of $^{5,6}F_4$-Bimbe **6**.

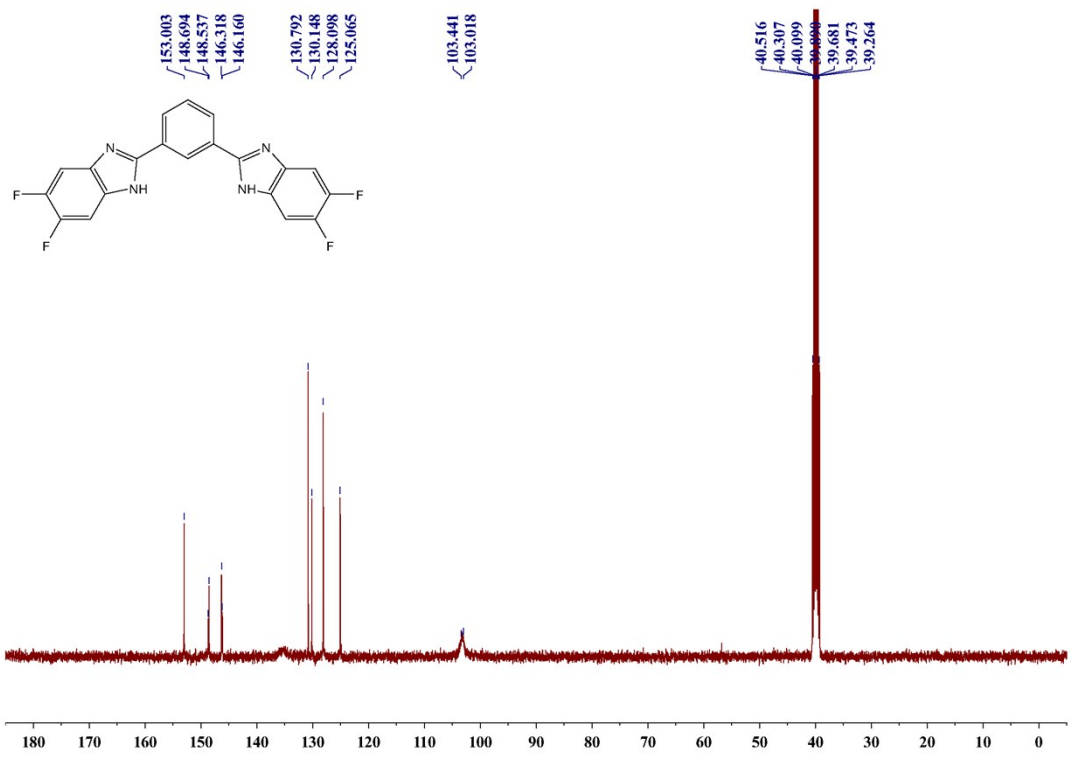

Fig. S37. ^{13}C NMR (DMSO-d_6, 100 MHz) of $^{5,6}F_4$-Bimbe **6**.

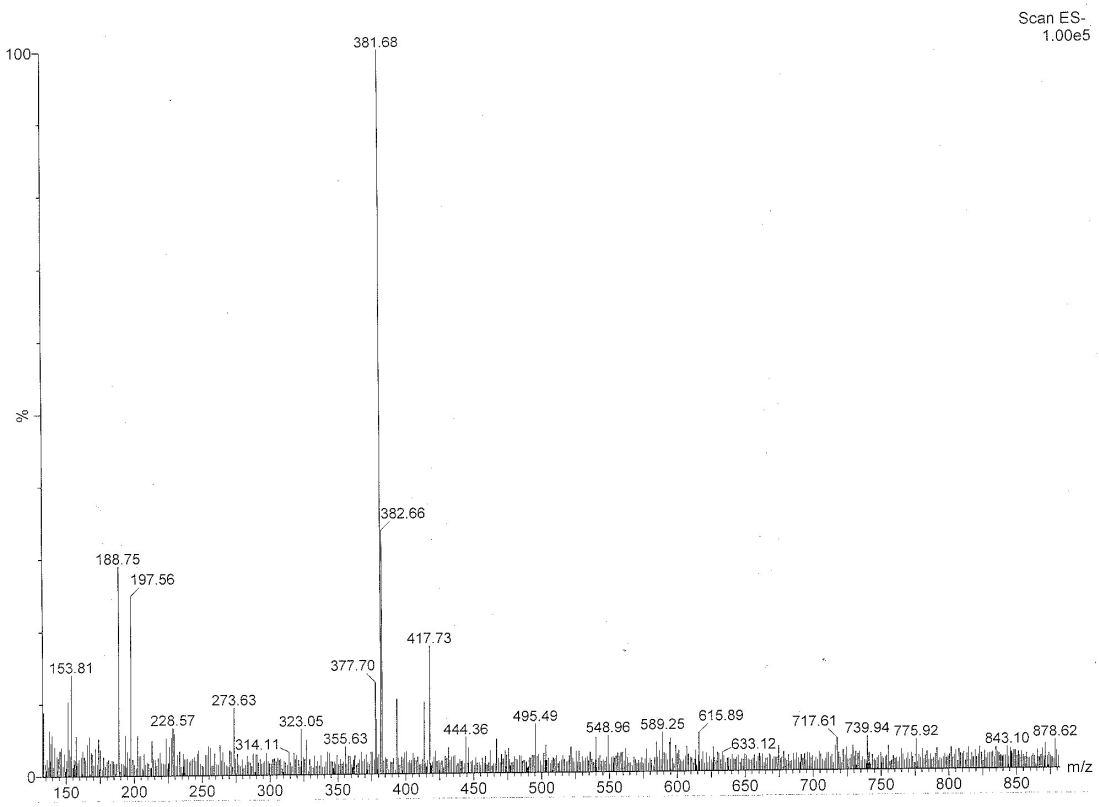

Fig. S38. ESI-MS of $^{5,6}F_4$-Bimbe **6**.

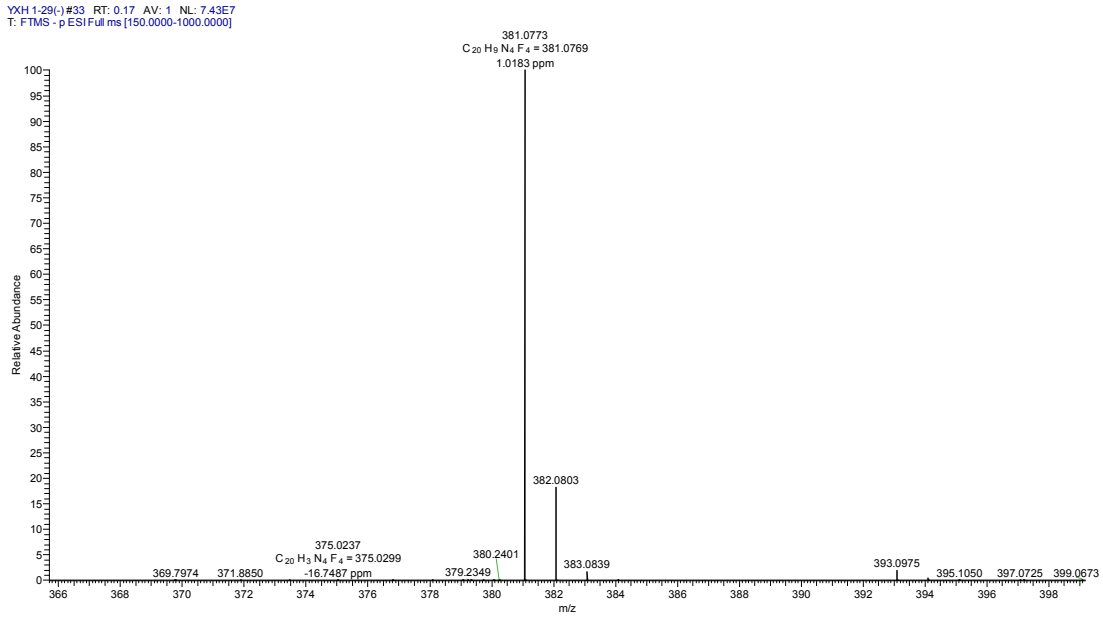

Fig. S39. HR ESI-MS of $^{5,6}F_4$-Bimbe **6**.

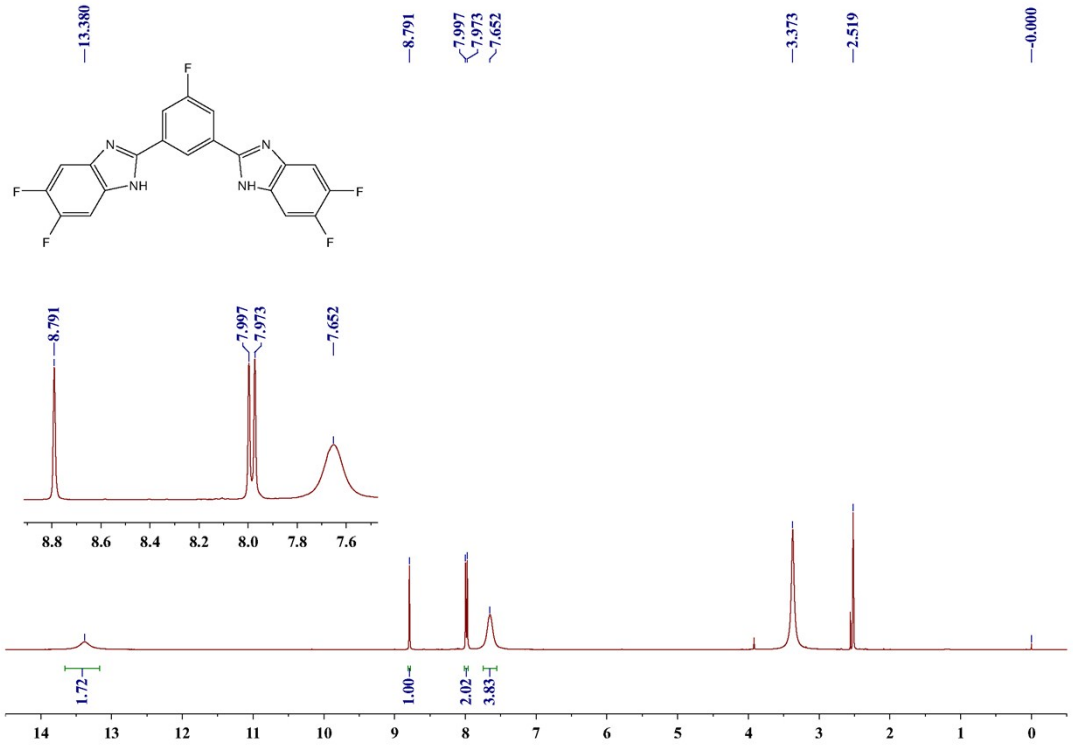

Fig. S40. ^{1}H NMR (DMSO-d_6, 400 MHz) of $^{5,6}F_4$-FBimbe **12**.

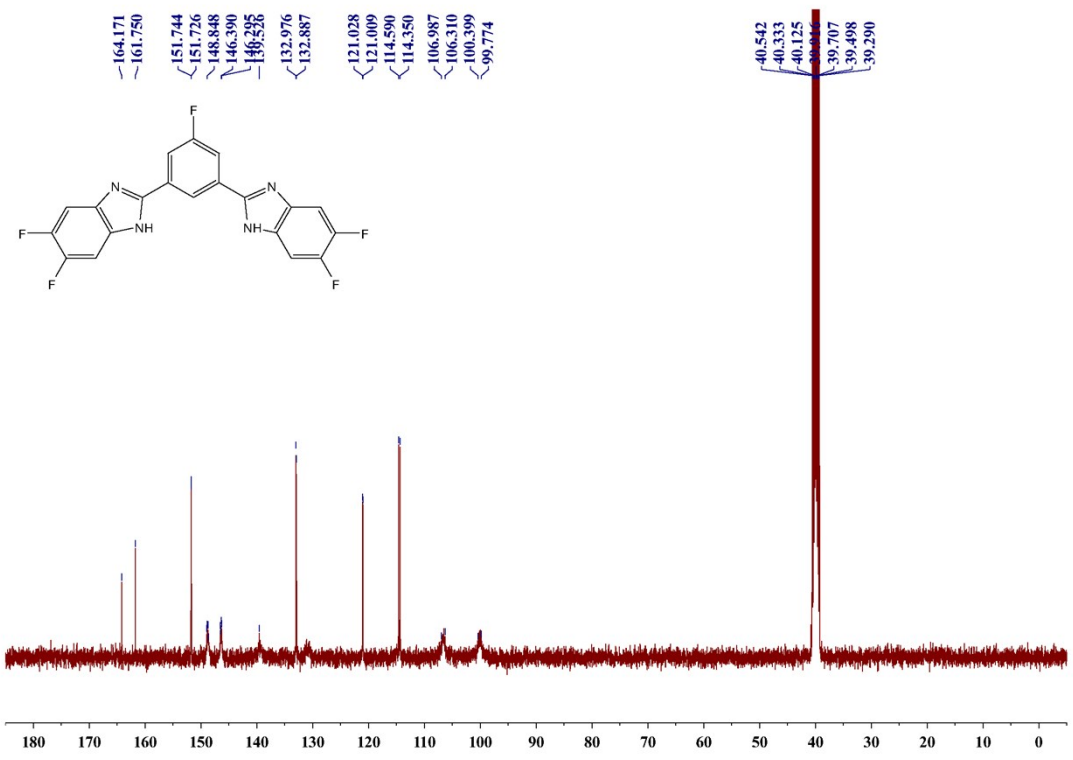

Fig. S41. ^{13}C NMR (DMSO-d_6, 100 MHz) of $^{5,6}F_4$-FBimbe **12**.

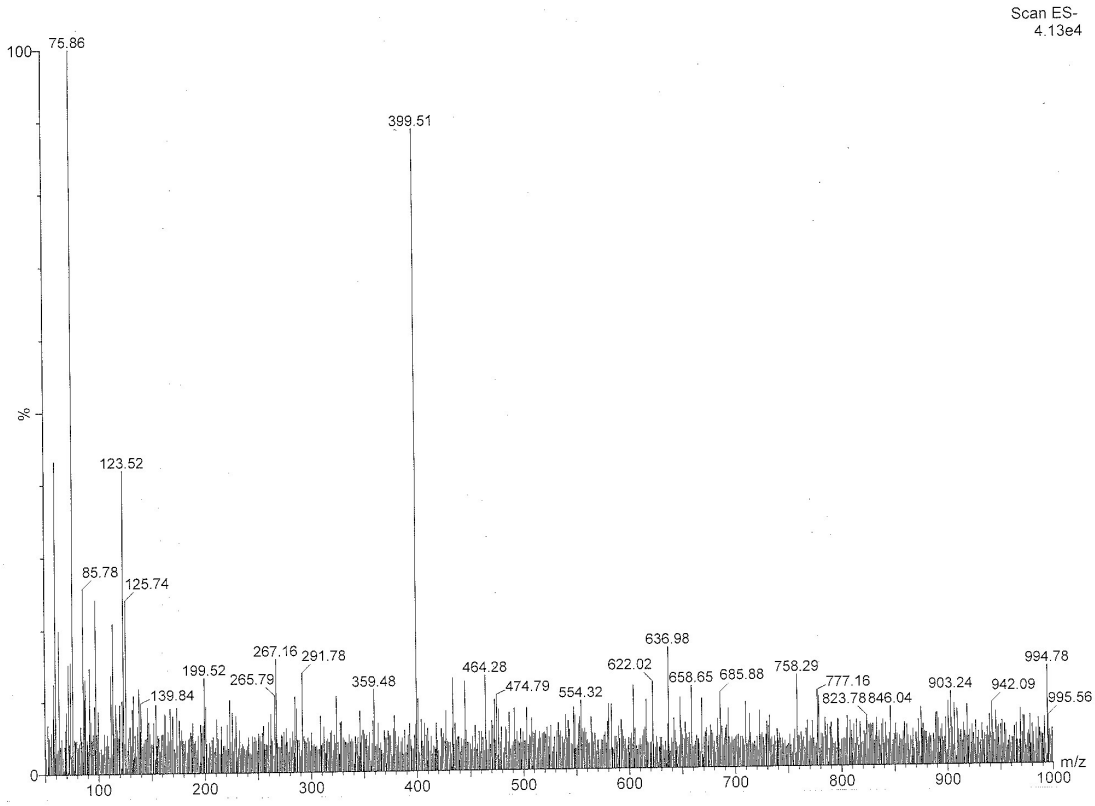

Fig. S42. ESI-MS of $^{5,6}F_4$-FBimbe **12**.

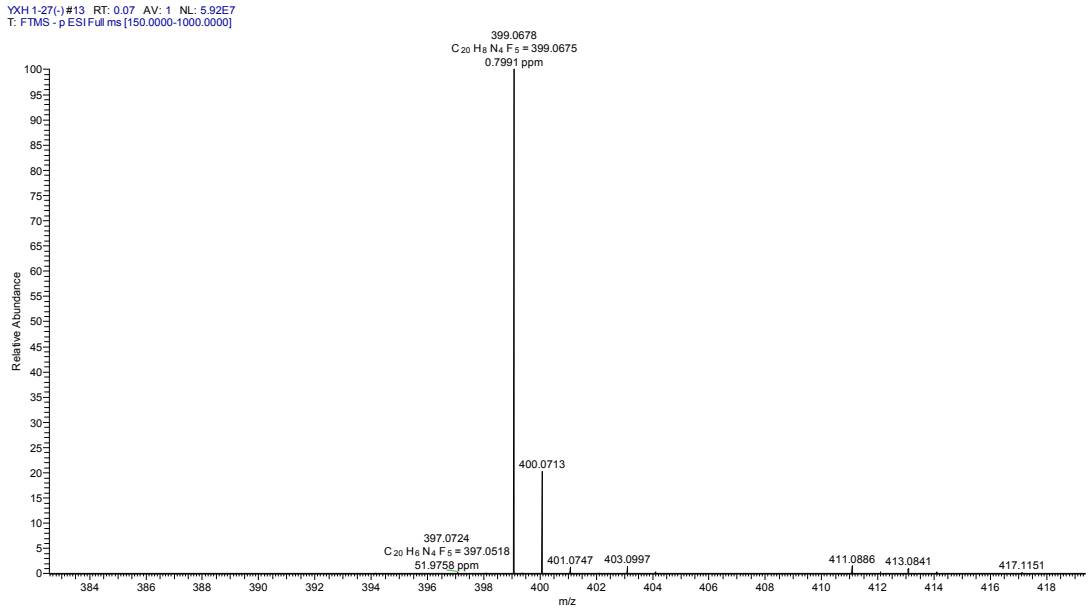

Fig. S43. HR ESI-MS of $^{5,6}F_4$-FBimbe **12**.

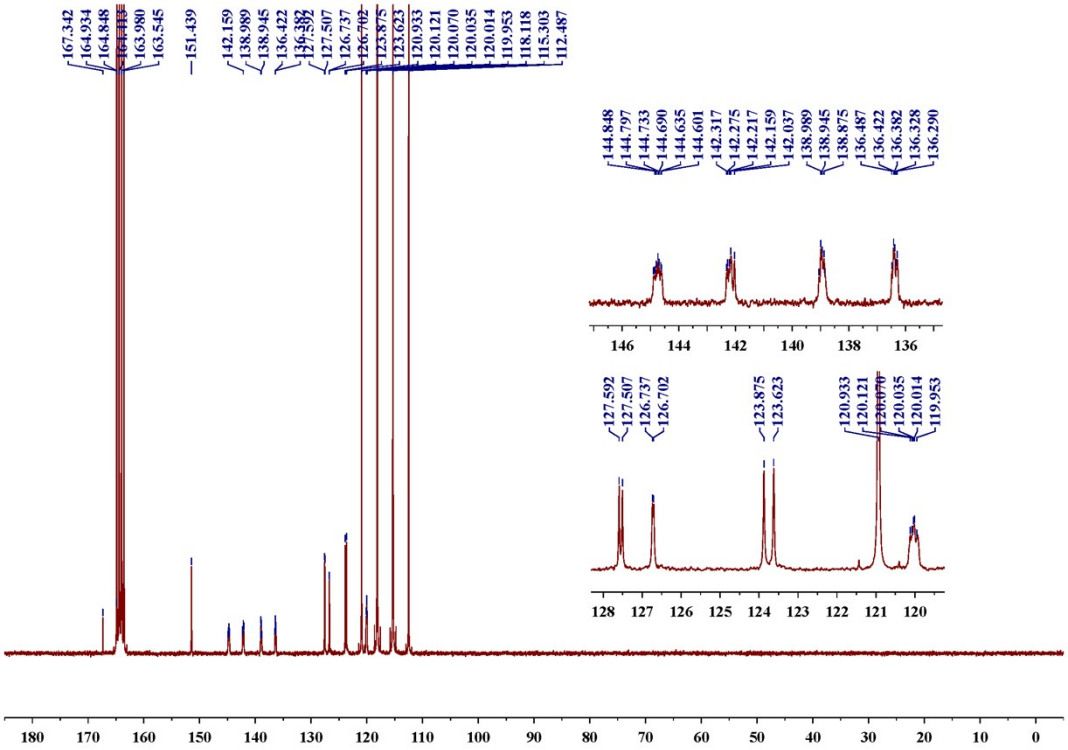

Fig. S44. ^{13}C NMR (TFA-*d*, 100 MHz) of $^{4,5,6,7}F_8$-FBimbe **13**.

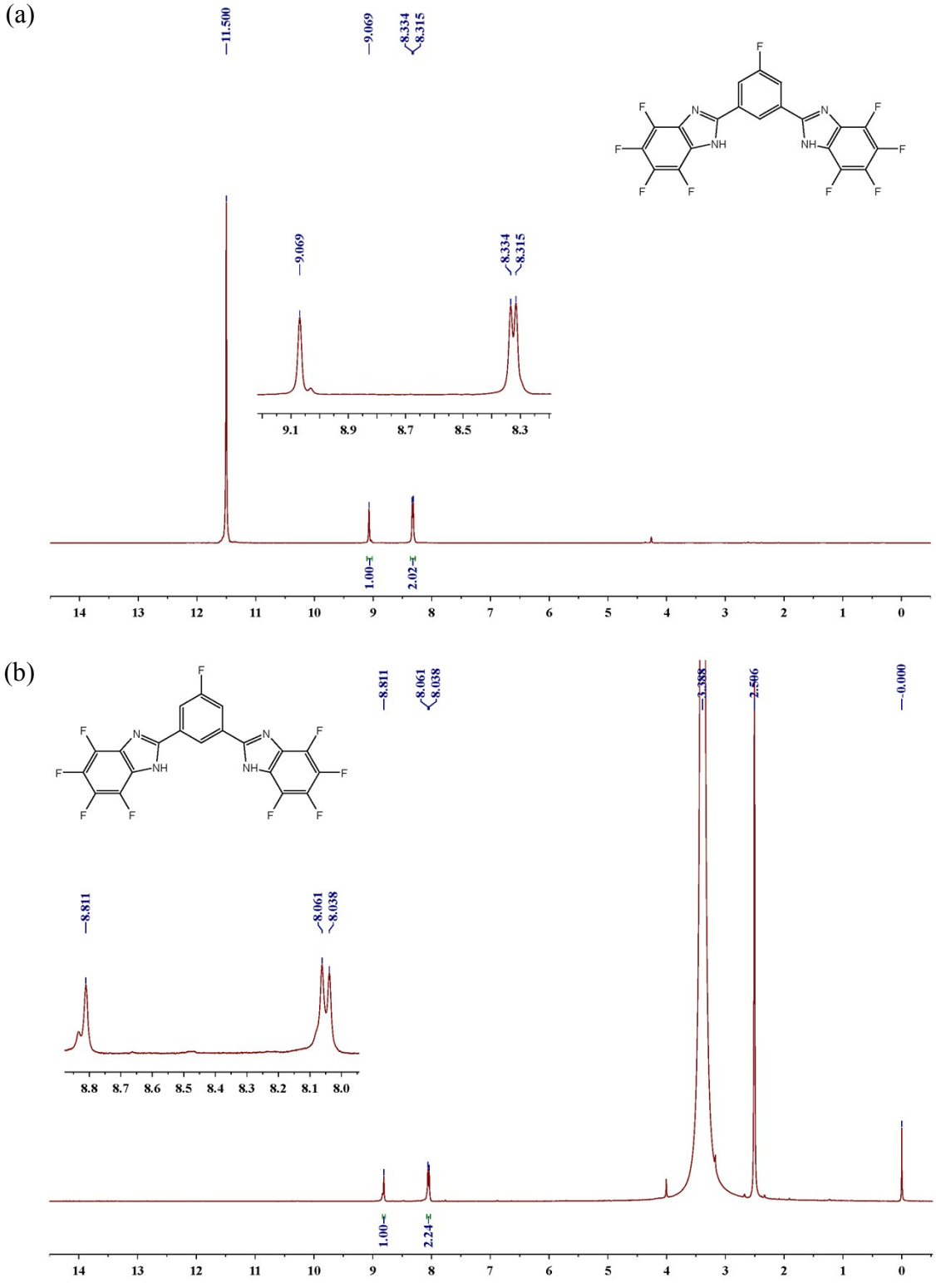

Fig. S45. ^{1}H NMR (400 MHz) of $^{4,5,6,7}F_8$-FBimbe **13** in (a) TFA-*d* and (b) DMSO-d_6.

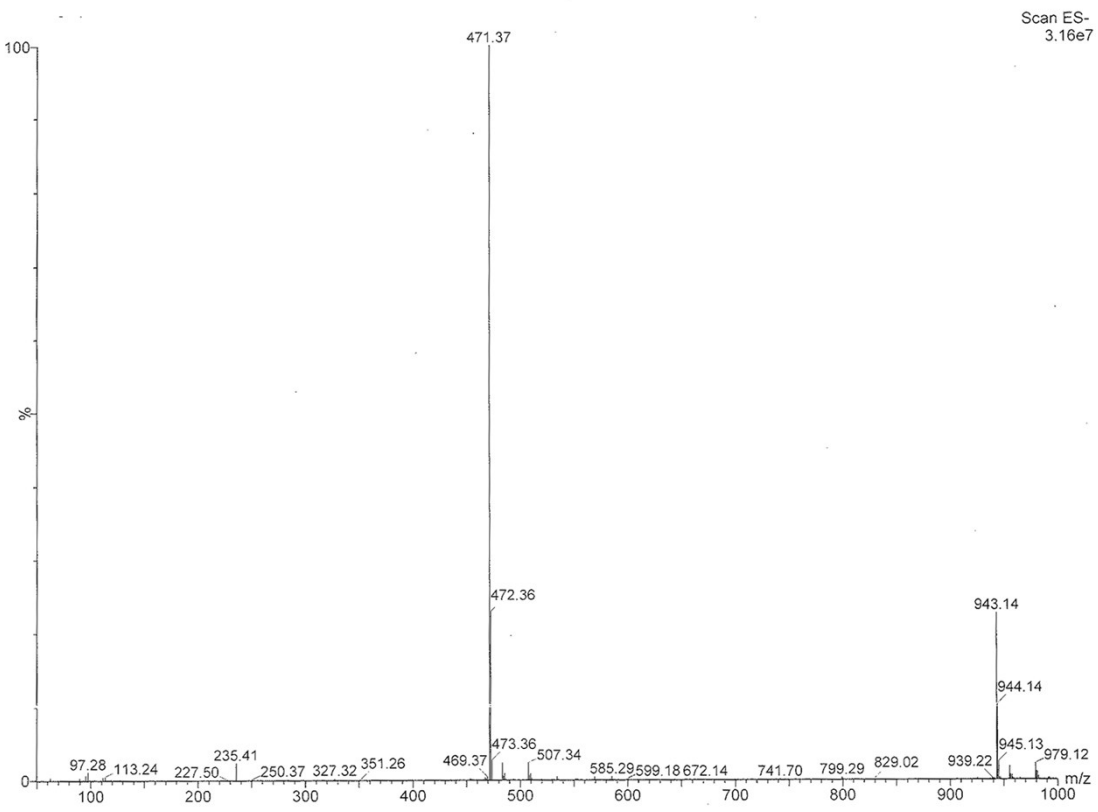

Fig. S46. ESI-MS of $^{4,5,6,7}F_8$-FBimbe **13**.

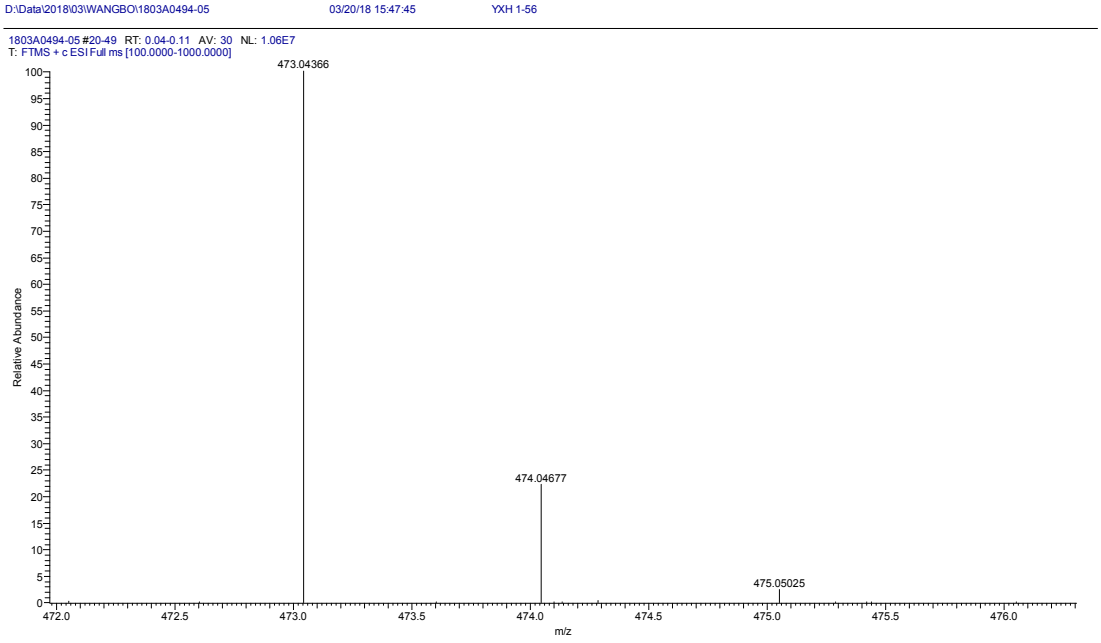

Fig. S47. HR ESI-MS of $^{4,5,6,7}F_8$-FBimbe **13**.

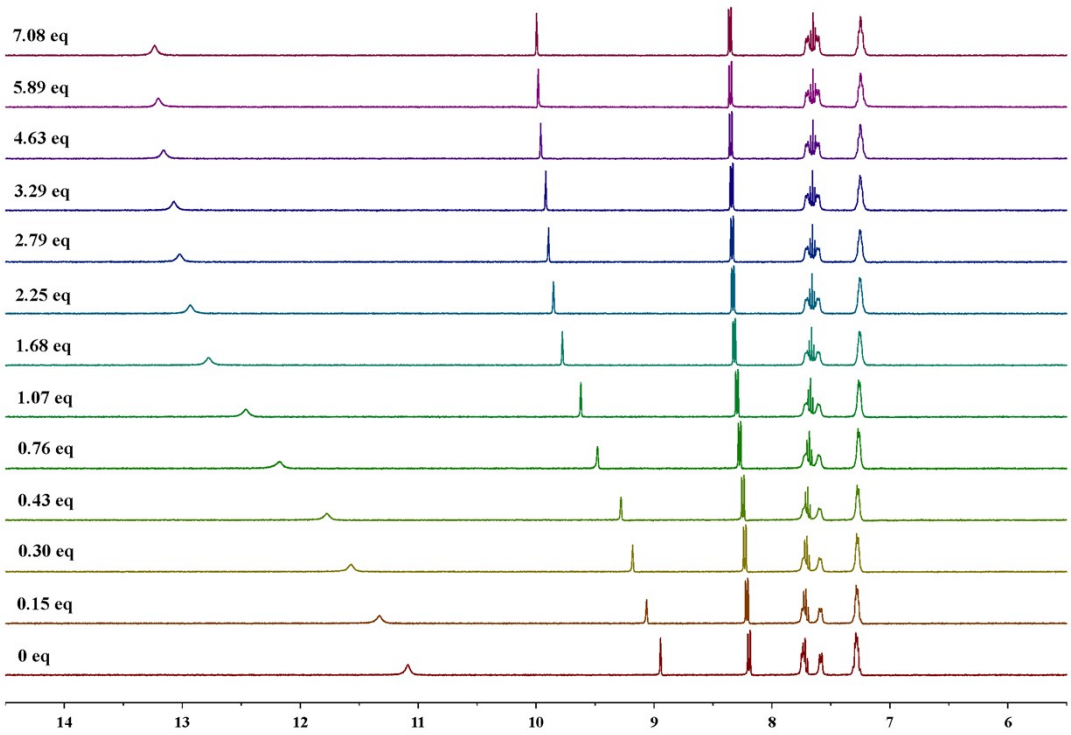

Fig. S48. ^{1}H NMR (acetonitrile-d_3, 400 MHz) of Bimbe **1** (1.0×10^{-3} M) titrated with TBACl of varying concentrations at 298 K.

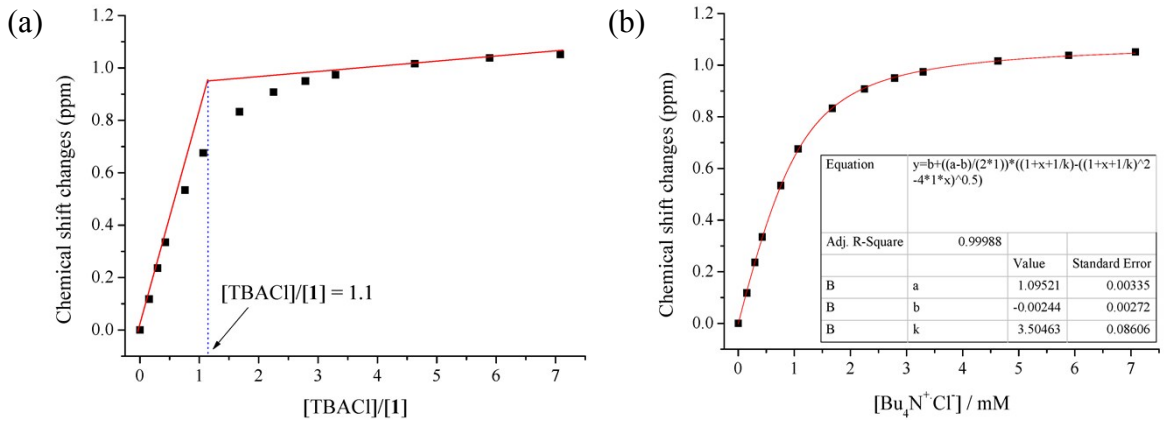

Fig. S49. (a) Plot of the chemical shift changes of -C_2H of the central aromatic ring versus the concentration ratios of TBACl to Bimbe **1** (1.0×10^{-3} M). (b) Fitting binding isotherms of Bimbe **1** (1.0×10^{-3} M) with TBACl in acetonitrile-d_3 at 298 K, showing the changes in chemical shifts for the -C_2H of the central aromatic ring, fitted to a 1 : 1 binding model.

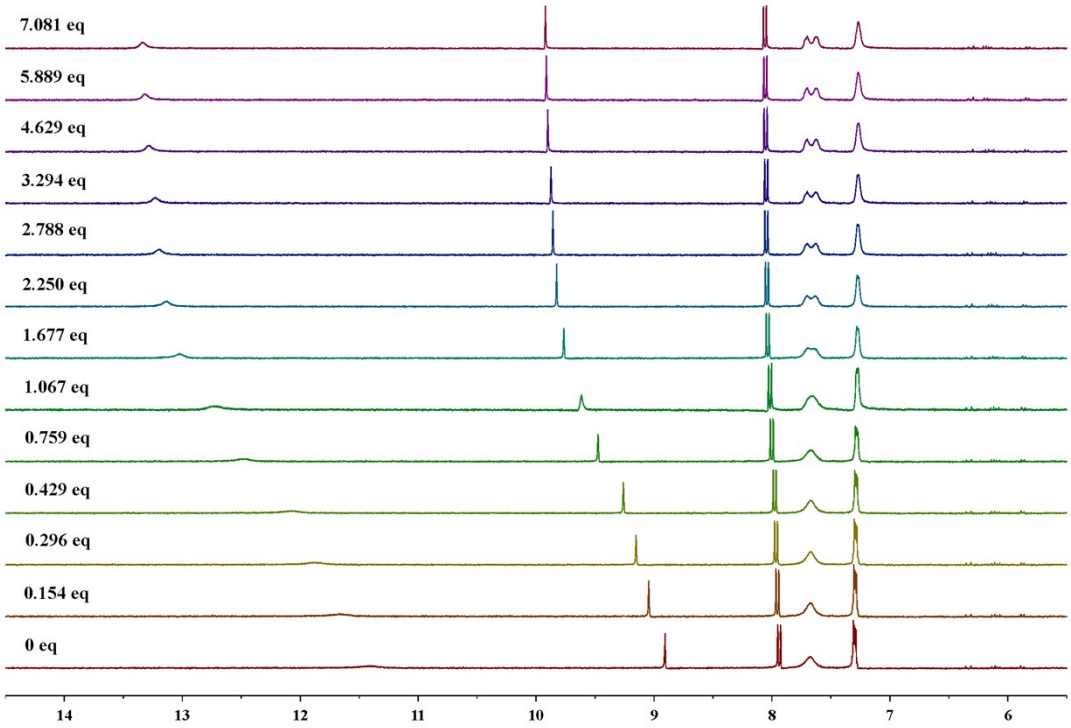

Fig. S50. ^{1}H NMR (400 MHz, acetonitrile-d_3) of FBimbe **7** (1.0×10^{-3} M) titrated with TBACl of varying concentrations at 298 K.

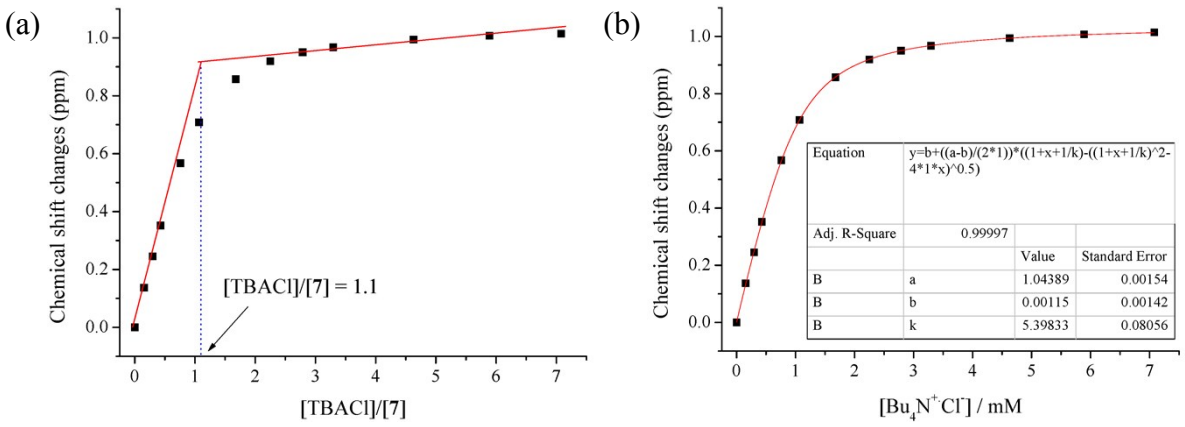

Fig. S51. (a) Plot of the chemical shift changes of -C_2H of the central aromatic ring versus the concentration ratios of TBACl to FBimbe **7** (1.0×10^{-3} M). (b) Fitting binding isotherms of FBimbe **7** (1.0×10^{-3} M) with TBACl in acetonitrile-d_3 at 298 K, showing the changes in chemical shifts for the -C_2H of the central aromatic ring, fitted to a 1 : 1 binding model.

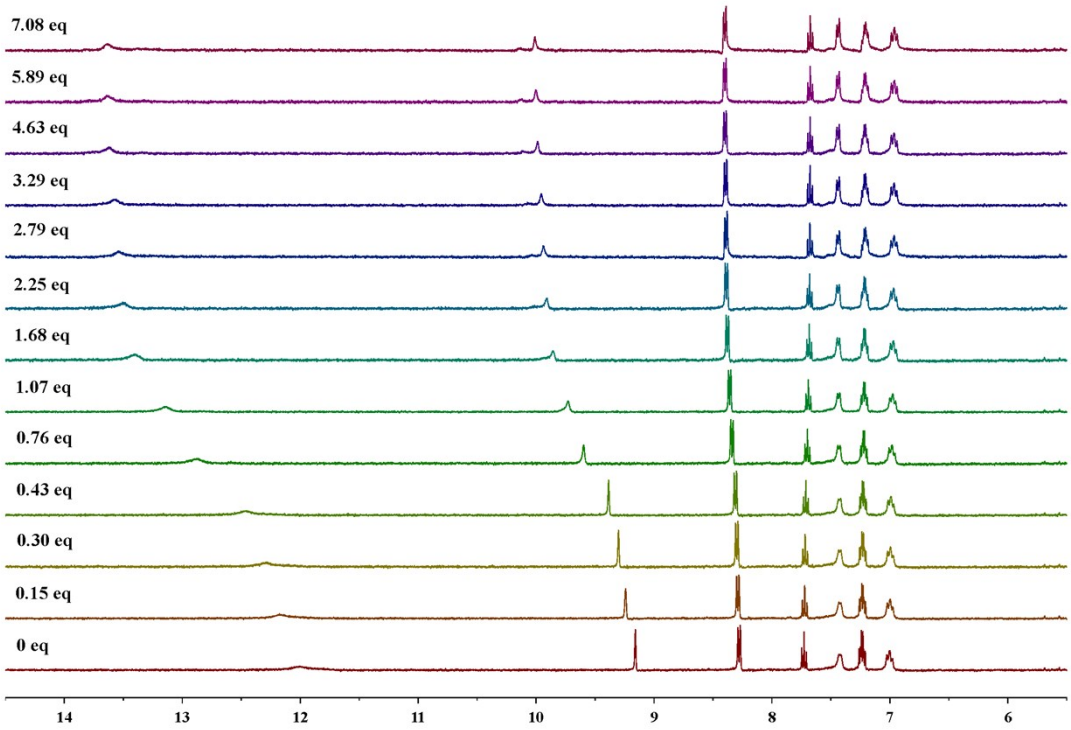

Fig. S52. ^{1}H NMR (400 MHz, acetonitrile-d_3) of $^{4}F_2$-Bimbe **2** (1.0×10^{-3} M) titrated with TBACl of varying concentrations at 298 K.

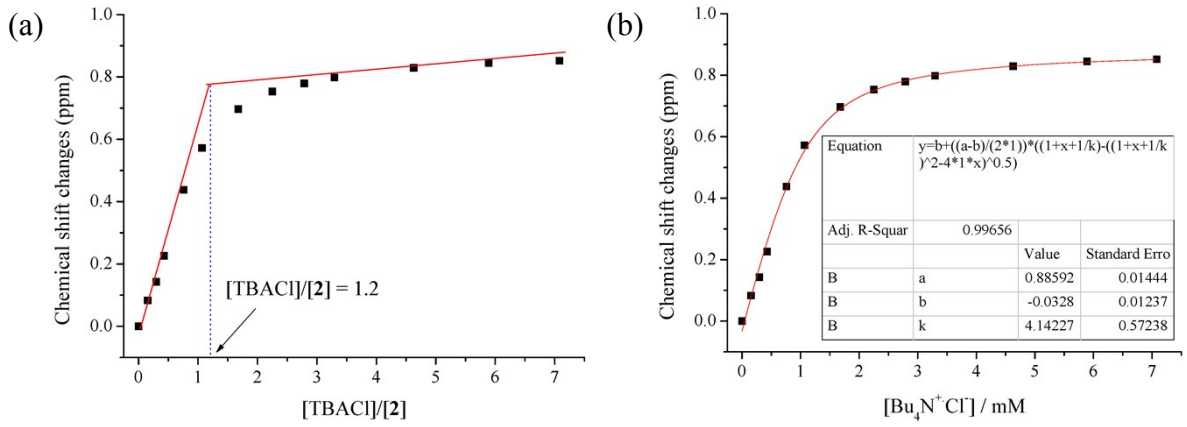

Fig. S53. (a) Plot of the chemical shift changes of -C_2H of the central aromatic ring versus the concentration ratios of TBACl to $^{4}F_2$-Bimbe **2** (1.0×10^{-3} M). (b) Fitting binding isotherms of $^{4}F_2$-Bimbe **2** (1.0×10^{-3} M) with TBACl in acetonitrile-d_3 at 298 K, showing the changes in chemical shifts for the -C_2H of the central aromatic ring, fitted to a 1 : 1 binding model.

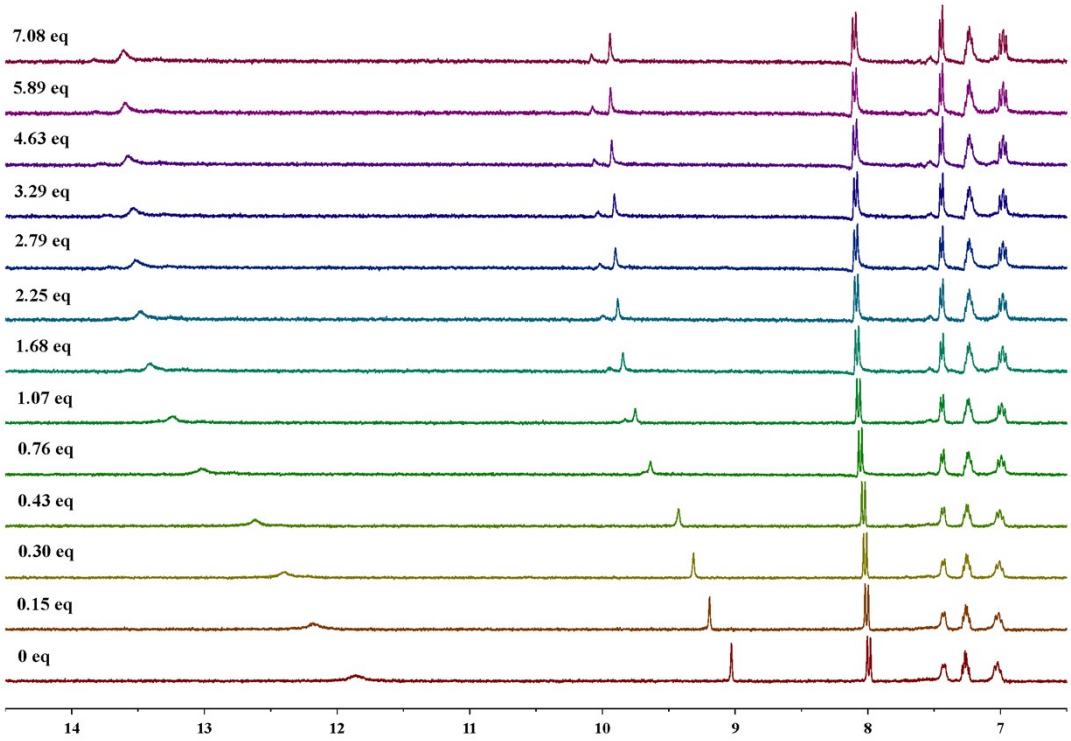

Fig. S54. ^{1}H NMR (400 MHz, acetonitrile-d_3) of $^{4}F_2$-FBimbe **8** (1.0×10^{-3} mM) with TBACl of varying concentrations at 298 K.

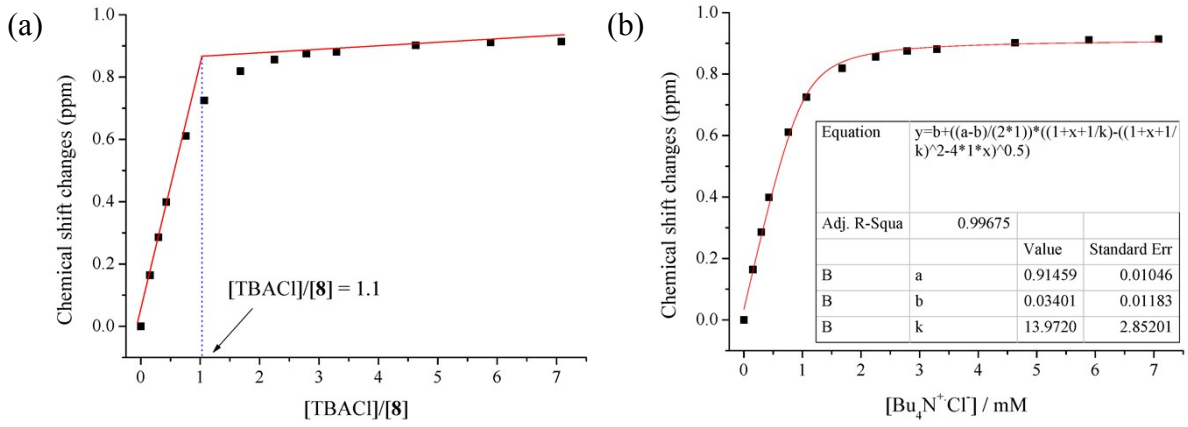

Fig. S55. (a) Plot of the chemical shift changes of -C_2H of the central aromatic ring versus the concentration ratios of TBACl to $^{4}F_2$-FBimbe **8** (1.0×10^{-3} M). (b) Fitting binding isotherms of $^{4}F_2$-FBimbe **8** (1.0×10^{-3} M) with TBACl in acetonitrile-d_3 at 298 K, showing the changes in chemical shifts for the -C_2H of the central aromatic ring, fitted to the 1:1 binding model.

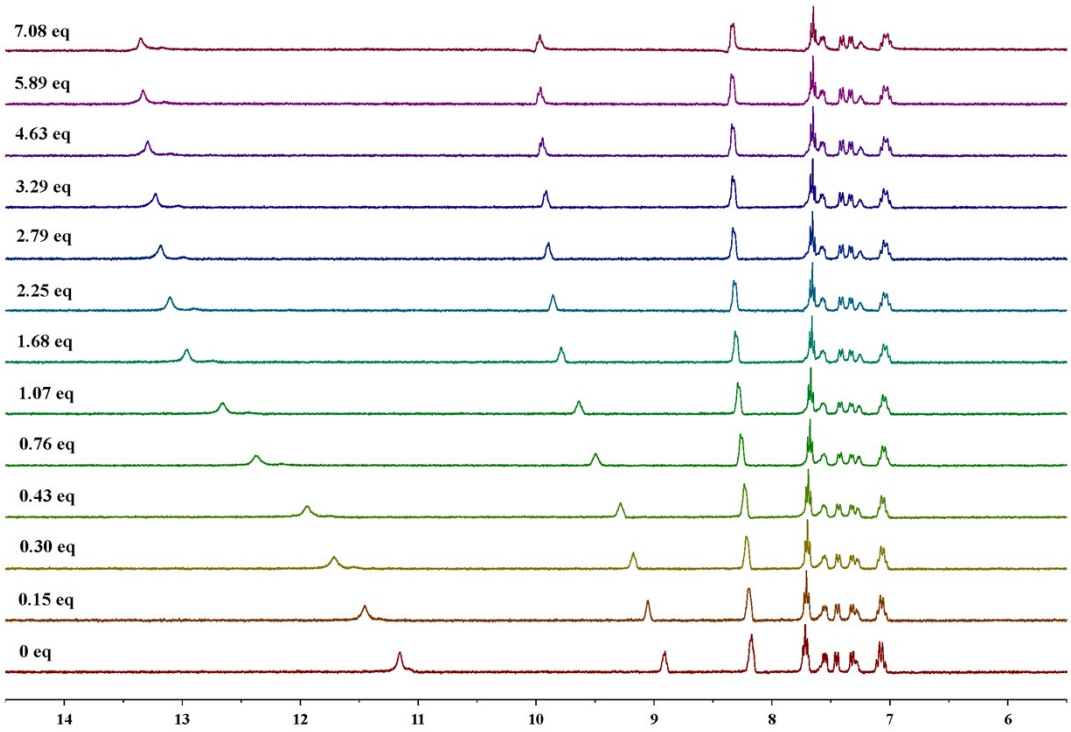

Fig. S56. ^{1}H NMR (400 MHz, acetonitrile-d_3) of $^{5}F_2$-Bimbe **3** (1.0×10^{-3} M) with TBACl of varying concentrations at 298 K.

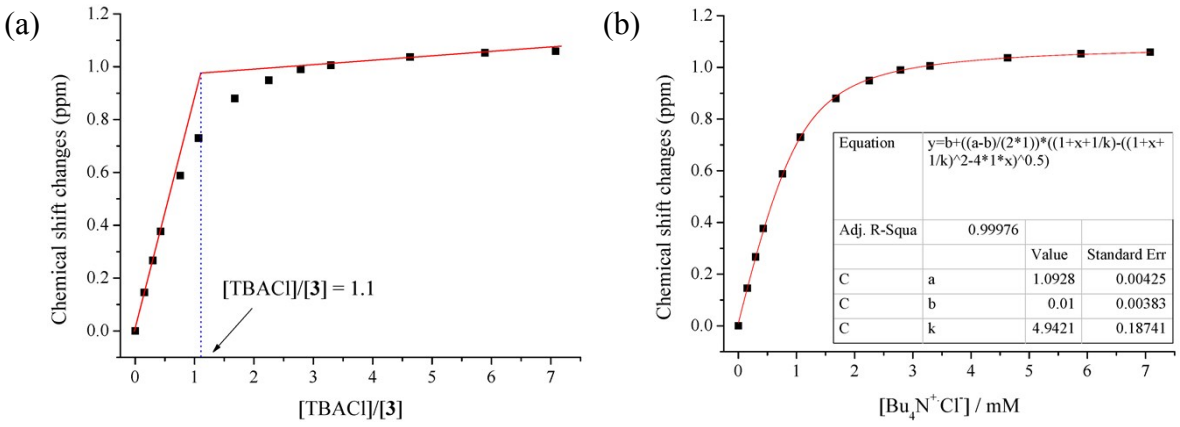

Fig. S57. (a) Plot of the chemical shift changes of -C_2H of the central aromatic ring versus the concentration ratios of TBACl to $^{5}F_2$-Bimbe **3** (1.0×10^{-3} M). (b) Fitting binding isotherms of $^{5}F_2$-Bimbe **3** (1.0×10^{-3} M) with TBACl in acetonitrile-d_3 at 298 K, showing the changes in chemical shifts for the -C_2H of the central aromatic ring, fitted to the 1:1 binding model.

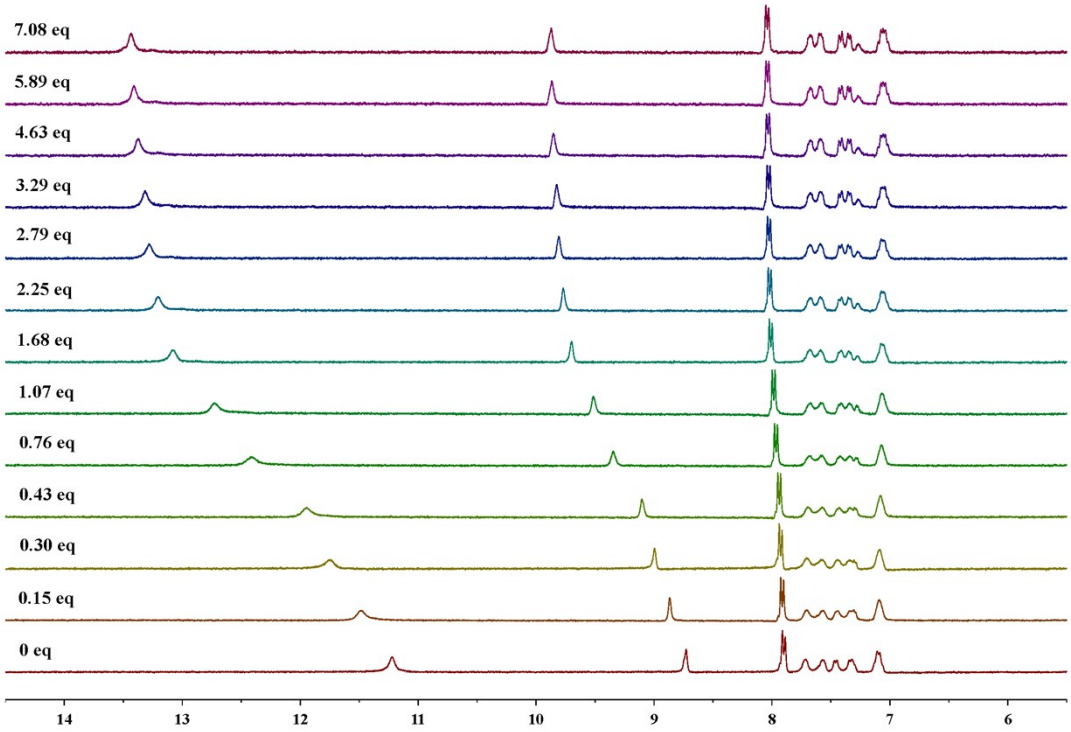

Fig. S58. ^{1}H NMR (400 MHz, acetonitrile-d_3) titration of $^{5}F_2$-FBimbe **9** (1.0×10^{-3} M) with TBACl of varying concentrations at 298 K.

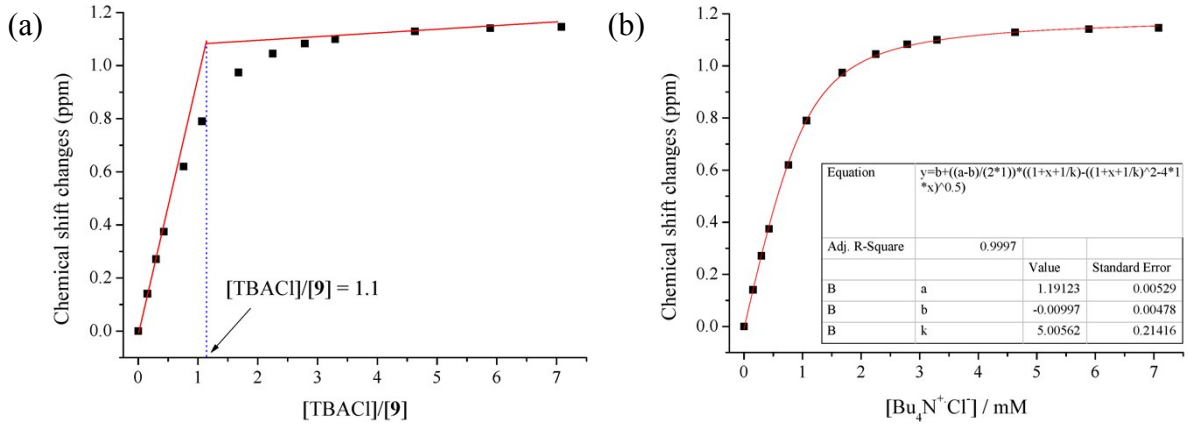

Fig. S59. (a) Plot of the chemical shift changes of -C_2H of the central aromatic ring versus the concentration ratios of TBACl to $^{5}F_2$-FBimbe **9** (1.0×10^{-3} M). (b) Fitting binding isotherms of $^{5}F_2$-FBimbe **9** (1.0×10^{-3} M) with TBACl in acetonitrile-d_3 at 298 K, showing the changes in chemical shifts for the -C_2H of the central aromatic ring, fitted to the 1:1 binding model.

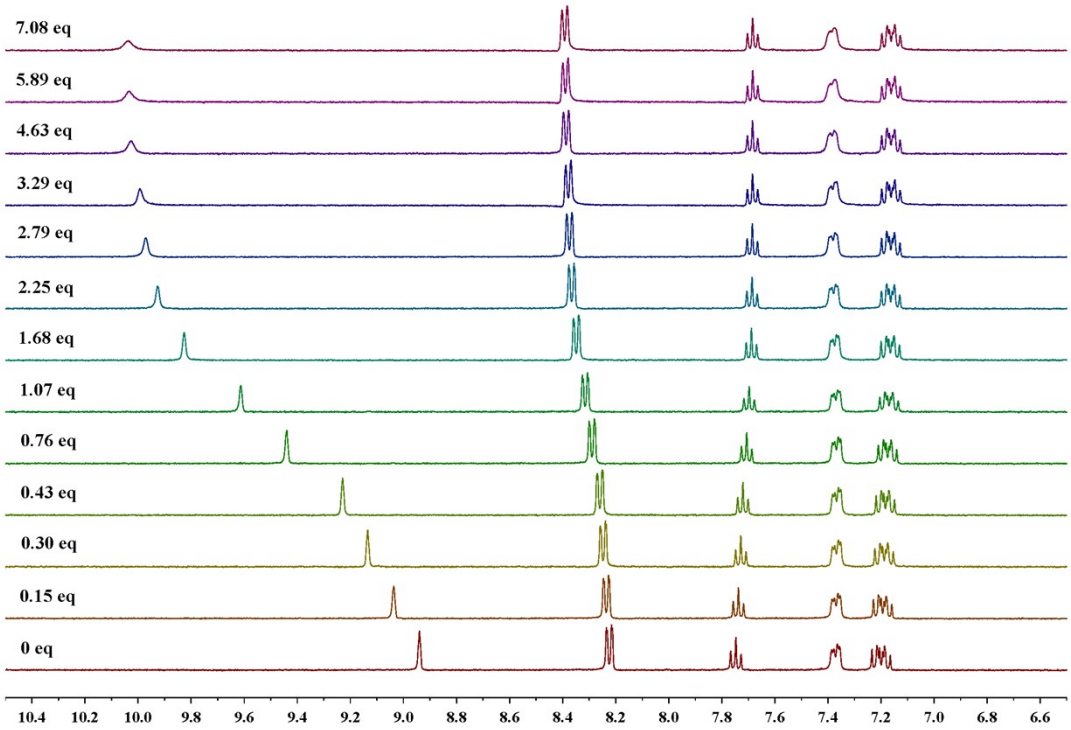

Fig. S60. ^{1}H NMR (400 MHz, acetonitrile-d_3) titration of $^{4,5}F_4$-Bimbe **4** (1.0×10^{-3} M) with TBACl of varying concentrations at 298 K.

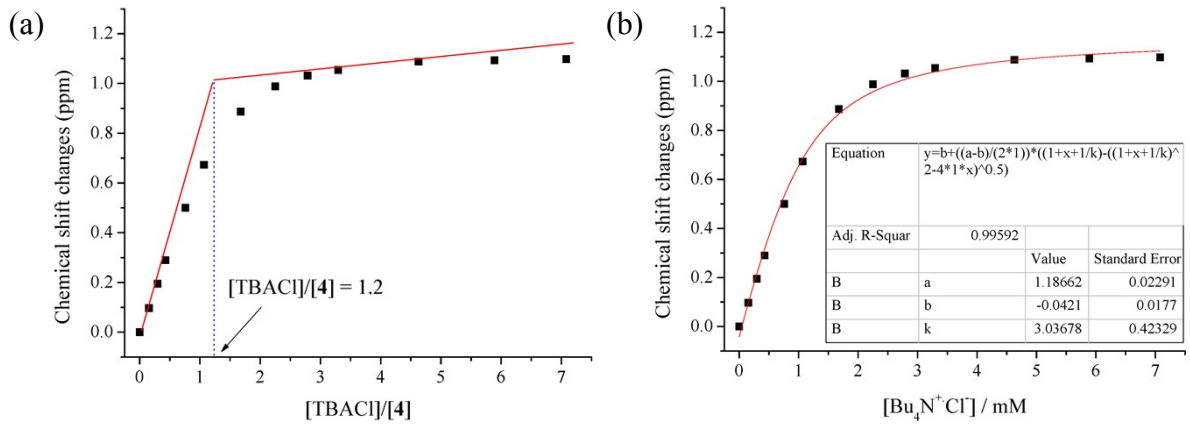

Fig. S61. (a) Plot of the chemical shift changes of -C_2H of the central aromatic ring versus the concentration ratios of TBACl to $^{4,5}F_4$-Bimbe **4** (1.0×10^{-3} M). (b) Fitting binding isotherms of $^{4,5}F_4$-Bimbe **4** (1.0×10^{-3} M) with TBACl in acetonitrile-d_3 at 298 K, showing the changes in chemical shifts for the -C_2H of the central aromatic ring, fitted to the 1:1 binding model.

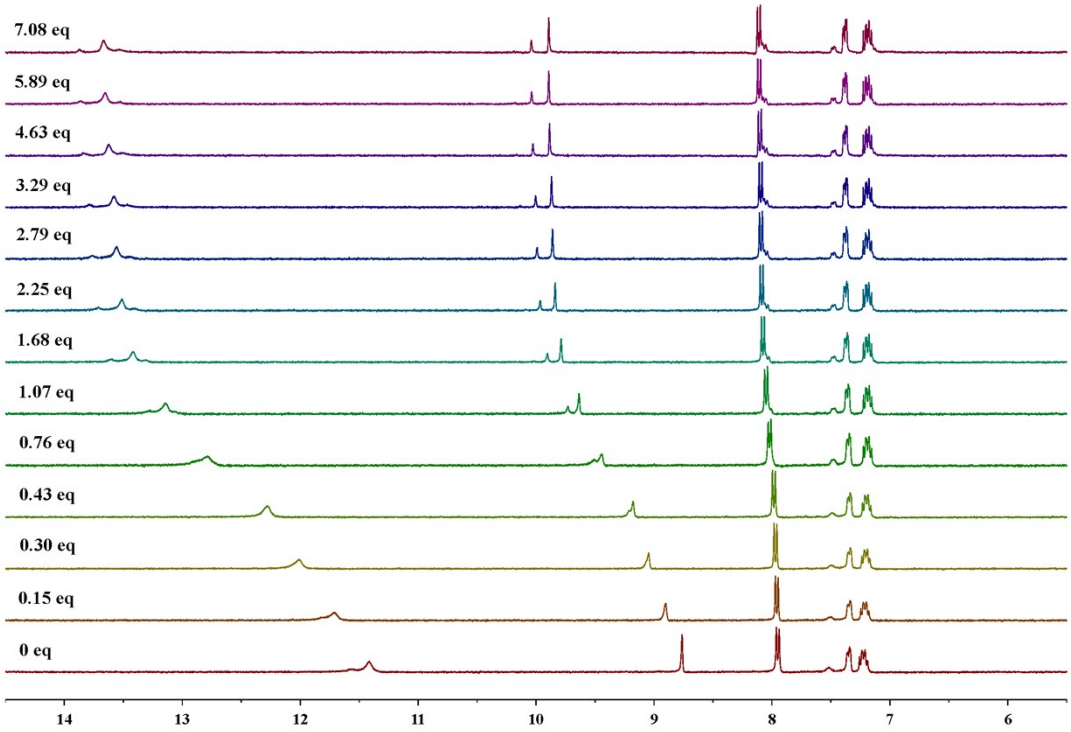

Fig. S62. ^{1}H NMR (400 MHz, acetonitrile-d_3) titration of $^{4,5}F_4$-FBimbe **10** (1.0×10^{-3} M) with TBACl of varying concentrations at 298 K.

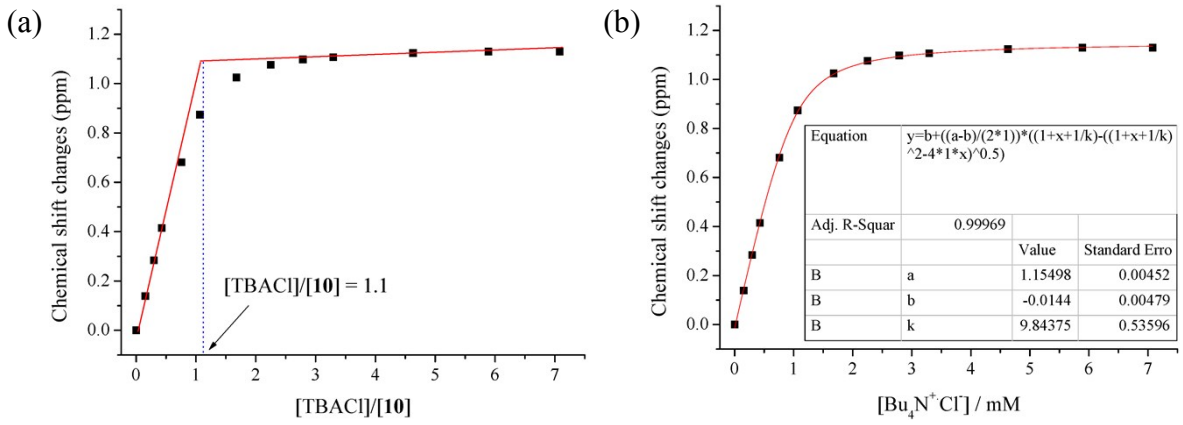

Fig. S63. (a) Plot of the chemical shift changes of -C_2H of the central aromatic ring versus the concentration ratios of TBACl to $^{4,5}F_4$-FBimbe **10** (1.0×10^{-3} M). (b) Fitting binding isotherms of $^{4,5}F_4$-FBimbe **10** (1.0×10^{-3} M) with TBACl in acetonitrile-d_3 at 298 K, showing the changes in chemical shifts for the -C_2H of the central aromatic ring, fitted to the 1:1 binding model.

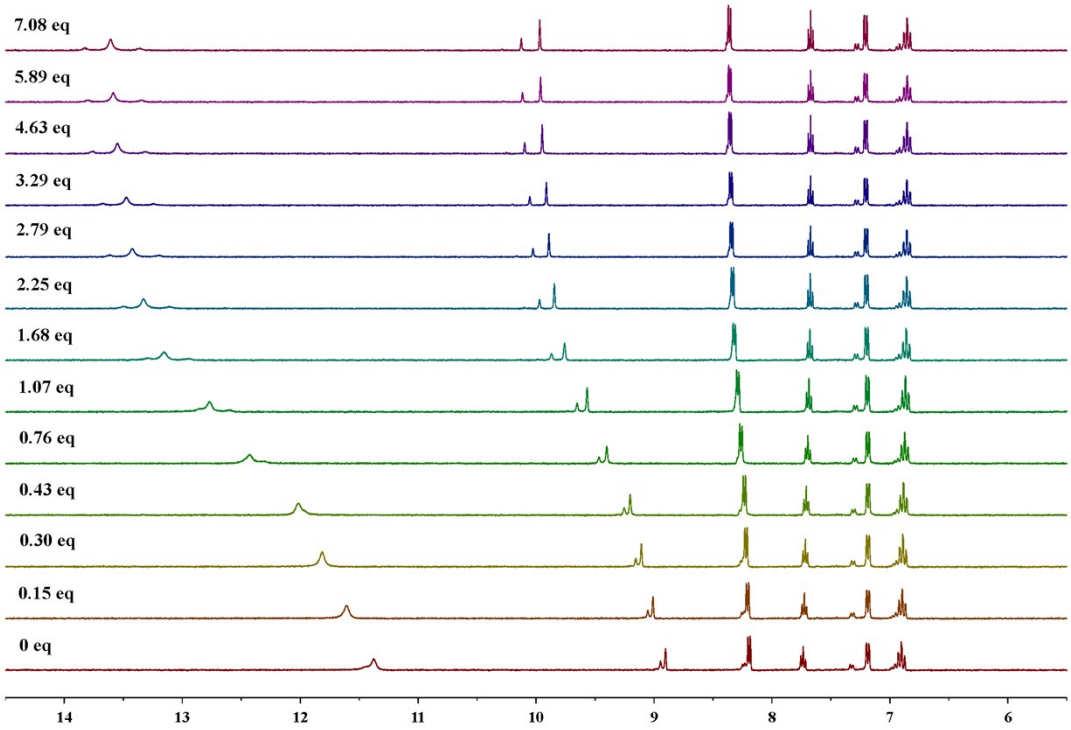

Fig. S64. ^{1}H NMR (400 MHz, acetonitrile-d_3) titration of $^{4,6}F_4$-Bimbe **5** (1.0×10^{-3} M) with TBACl of varying concentrations at 298 K.

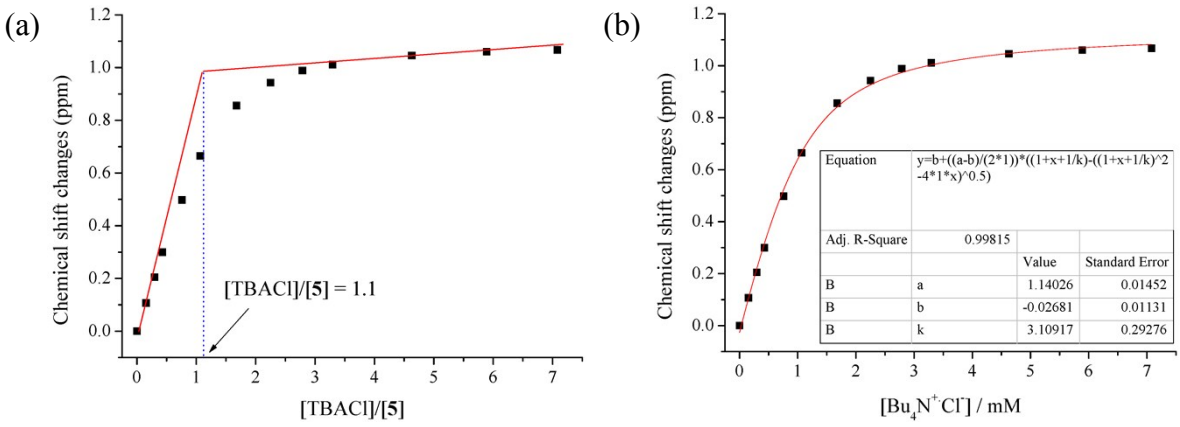

Fig. S65. (a) Plot of the chemical shift changes of -C_2H of the central aromatic ring versus the concentration ratios of TBACl to $^{4,6}F_4$-Bimbe **5** (1.0×10^{-3} M). (b) Fitting binding isotherms of $^{4,6}F_4$-Bimbe **5** (1.0×10^{-3} M) with TBACl in acetonitrile-d_3 at 298 K, showing the changes in chemical shifts for the -C_2H of the central aromatic ring, fitted to the 1:1 binding model.

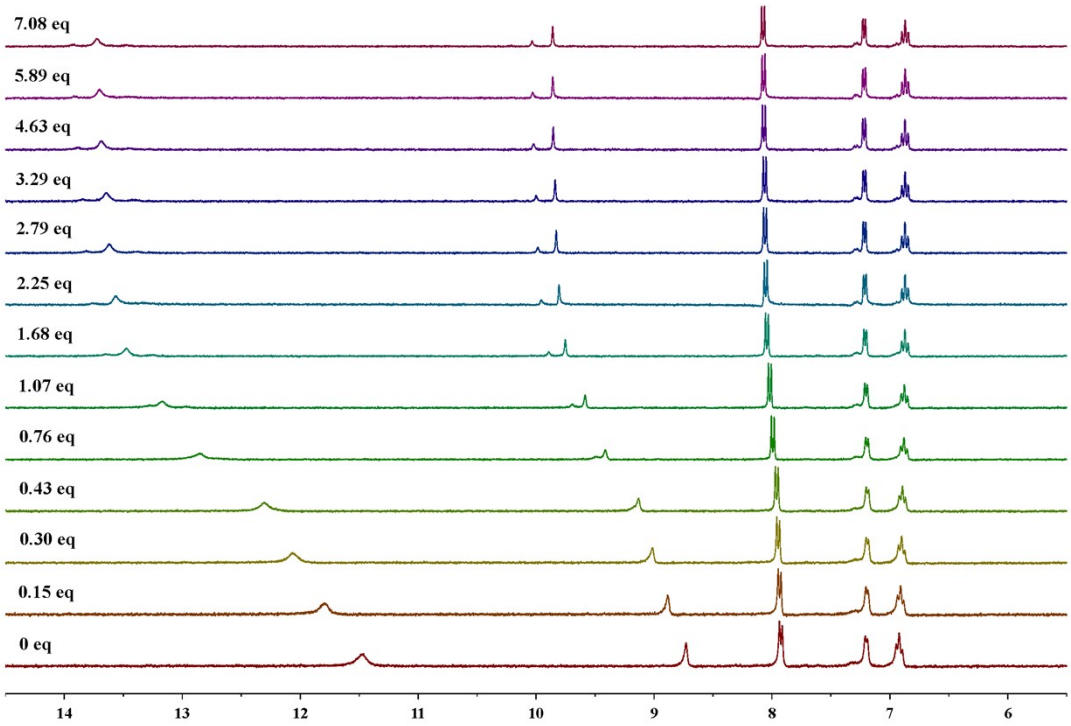

Fig. S66. ^{1}H NMR (400 MHz, acetonitrile-d_3) titration of $^{4,6}F_4$-FBimbe **11** (1.0×10^{-3} M) with TBACl of varying concentrations at 298 K.

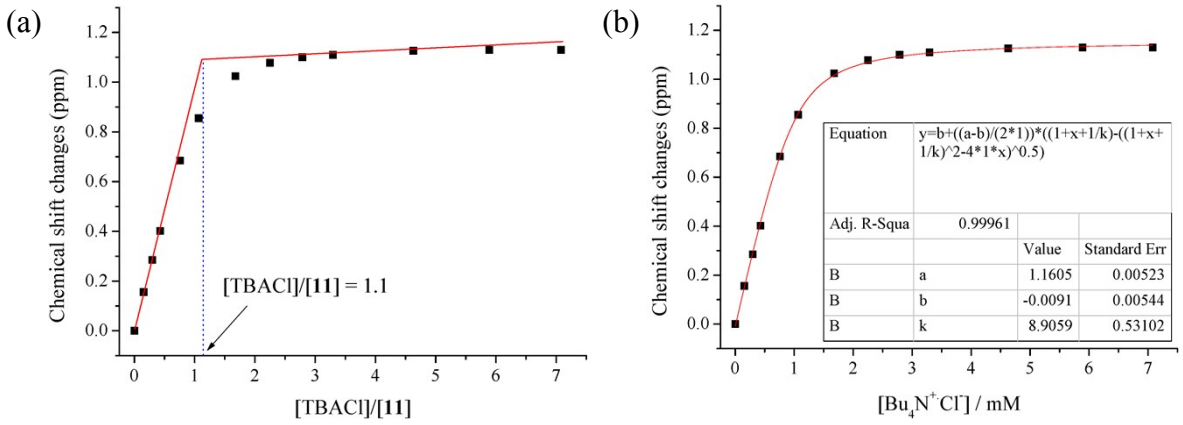

Fig. S67. (a) Plot of the chemical shift changes of -C_2H of the central aromatic ring versus the concentration ratios of TBACl to $^{4,6}F_4$-FBimbe **11** (1.0×10^{-3} M). (b) Fitting binding isotherms of $^{4,6}F_4$-FBimbe **11** (1.0×10^{-3} M) with TBACl in acetonitrile-d_3 at 298 K, showing the changes in chemical shifts for the -C_2H of the central aromatic ring, fitted to the 1:1 binding model.

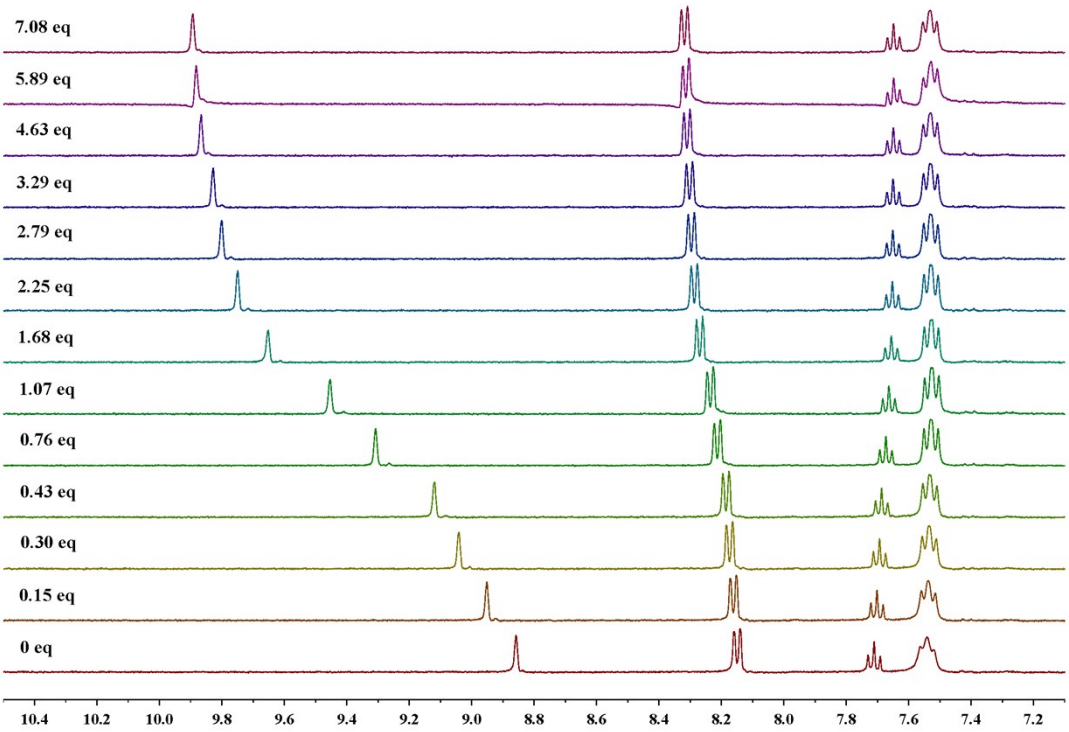

Fig. S68. ^{1}H NMR (400 MHz, acetonitrile-d_3) titration of $^{5,6}F_4$-Bimbe **6** (1.0×10^{-3} M) with TBACl of varying concentrations at 298 K.

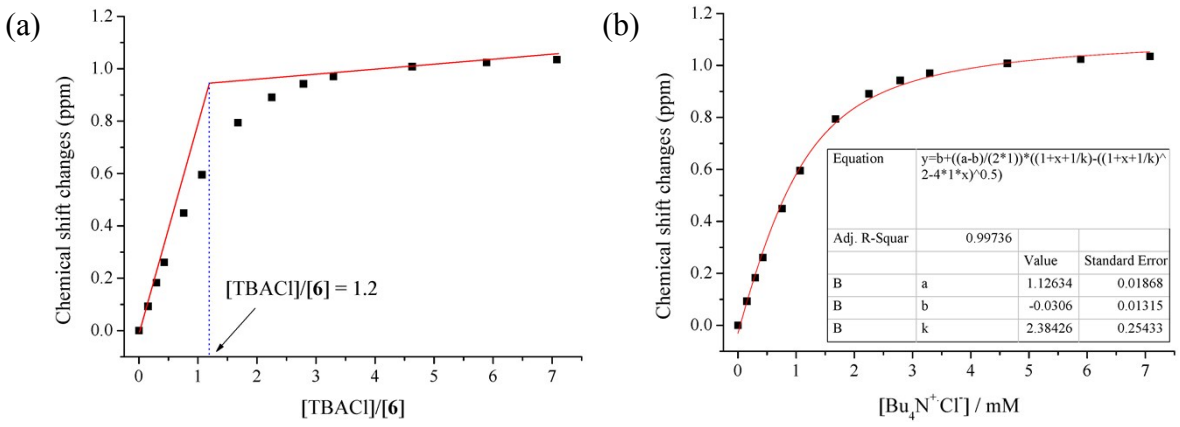

Fig. S69. (a) Plot of the chemical shift changes of -C_2H of the central aromatic ring versus the concentration ratios of TBACl to $^{5,6}F_4$-Bimbe **6** (1.0×10^{-3} M). (b) Fitting binding isotherms of $^{5,6}F_4$-Bimbe **6** (1.0×10^{-3} M) with TBACl in acetonitrile-d_3 at 298 K, showing the changes in chemical shifts for the -C_2H of the central aromatic ring, fitted to the 1:1 binding model.

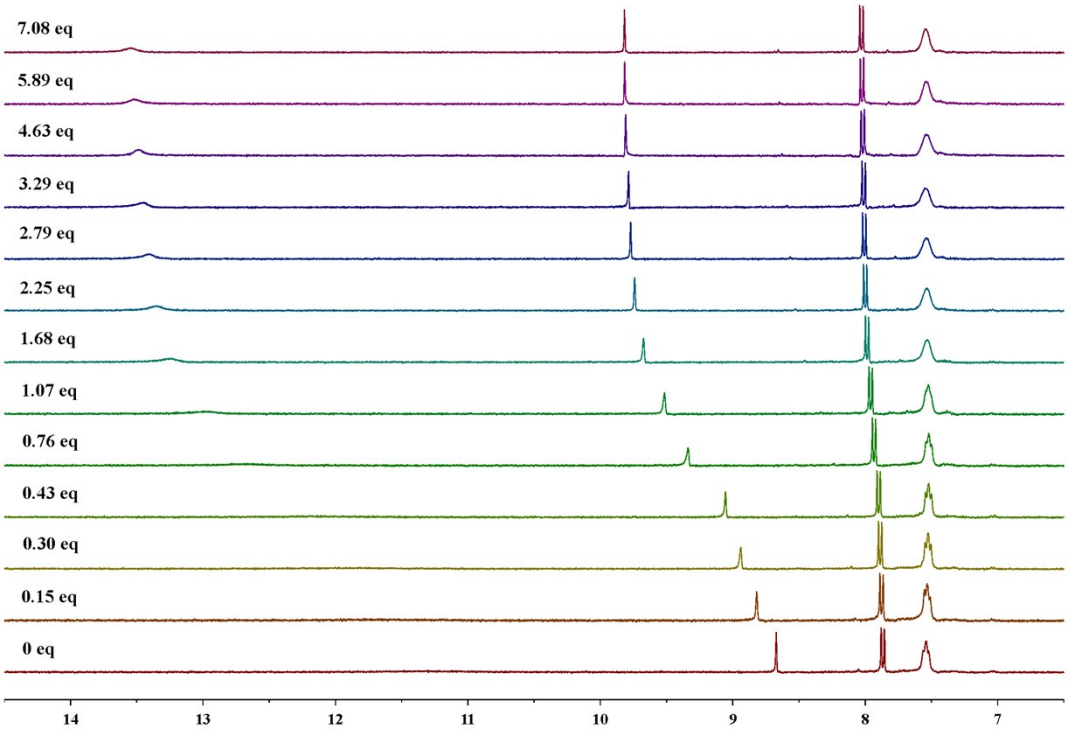

Fig. S70. ^{1}H NMR (400 MHz, acetonitrile-d_3) titration of $^{5,6}F_4$-FBimbe **12** (1.0×10^{-3} M) with TBACl of varying concentrations at 298 K.

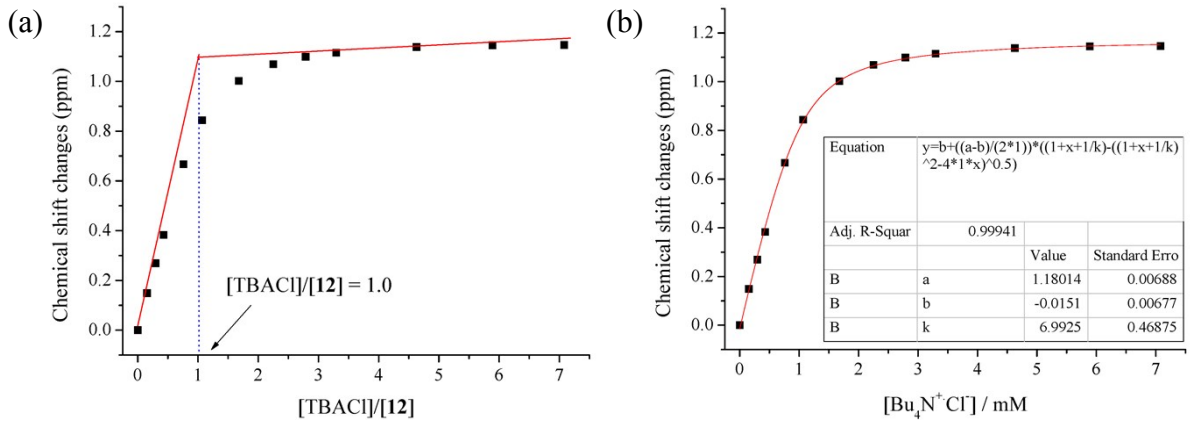

Fig. S71. (a) Plot of the chemical shift changes of -C_2H of the central aromatic ring versus the concentration ratios of TBACl to $^{5,6}F_4$-FBimbe **12** (1.0×10^{-3} M). (b) Fitting binding isotherms of $^{5,6}F_4$-FBimbe **12** (1.0×10^{-3} M) with TBACl in acetonitrile-d_3 at 298 K, showing the changes in chemical shifts for the -C_2H of the central aromatic ring, fitted to the 1:1 binding model.

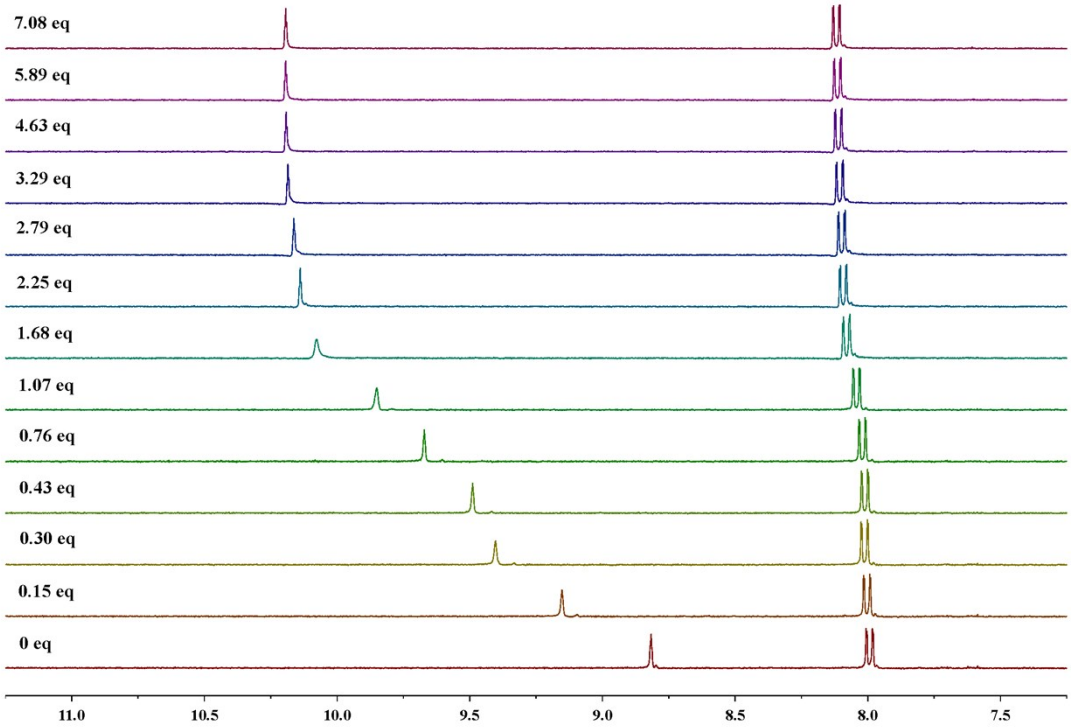

Fig. S72. ^{1}H NMR (400 MHz, acetonitrile-d_3) titration of $^{4,5,6,7}F_8$-FBimbe **13** (1.0×10^{-3} M) with TBACl of varying concentrations at 298 K.

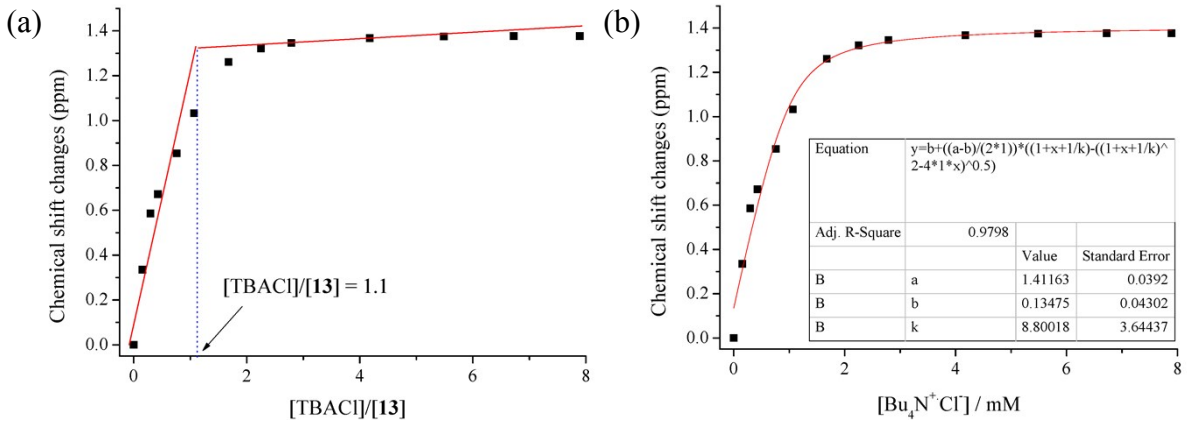

Fig. S73. (a) Plot of the chemical shift changes of -C_2H of the central aromatic ring versus the concentration ratios of TBACl to $^{4,5,6,7}F_8$-FBimbe **13** (1.0×10^{-3} M). (b) Fitting binding isotherms of $^{4,5,6,7}F_8$-FBimbe **13** (1.0×10^{-3} M) with TBACl in acetonitrile-d_3 at 298 K, showing the changes in chemical shifts for the -C_2H of the central aromatic ring, fitted to the 1:1 binding model.

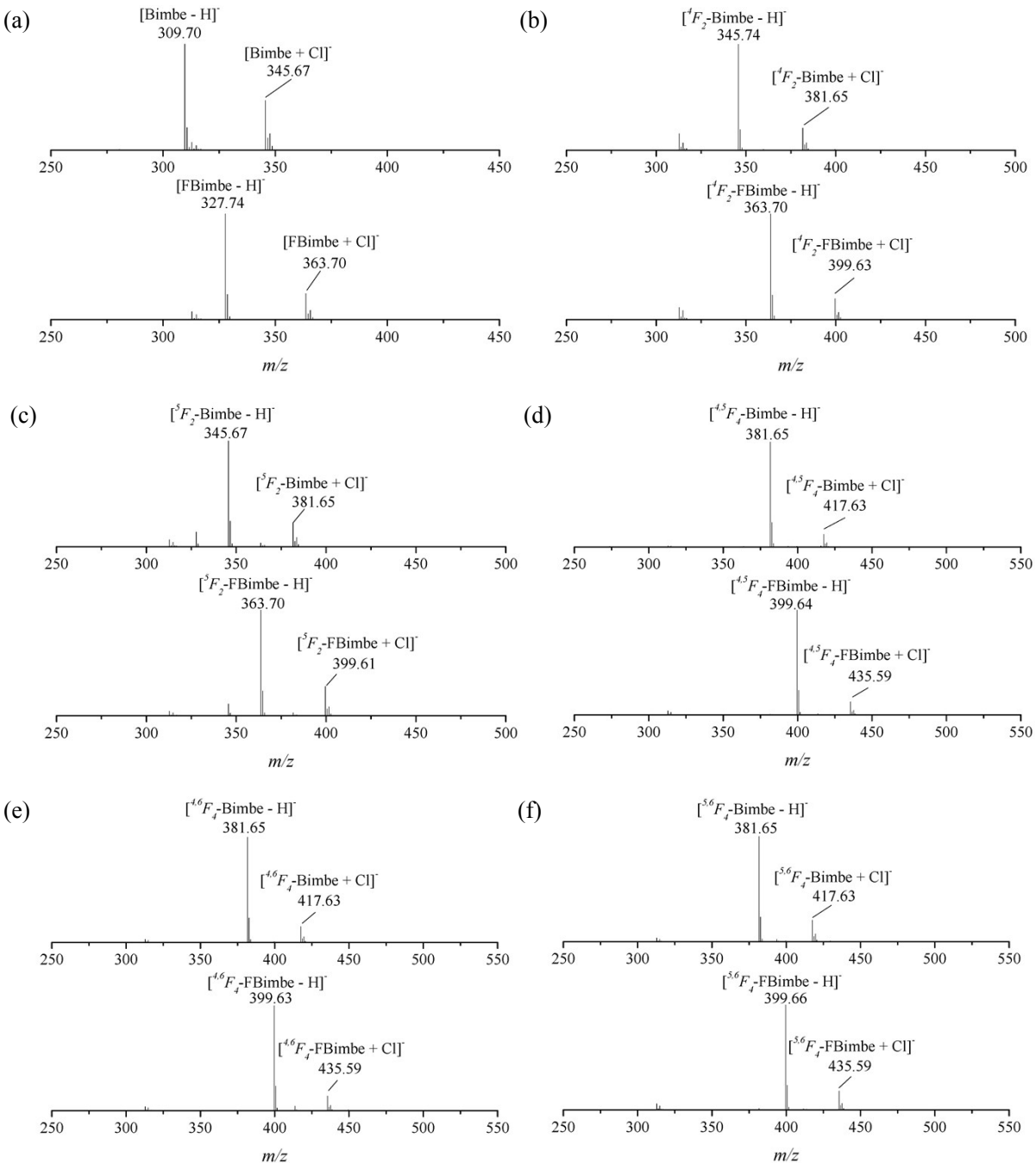

Fig S74. Negative ESI MS spectra of target compounds (1.0×10^{-3} M) mixed with TBACl (7.08×10^{-3} M) in CH_3CN.

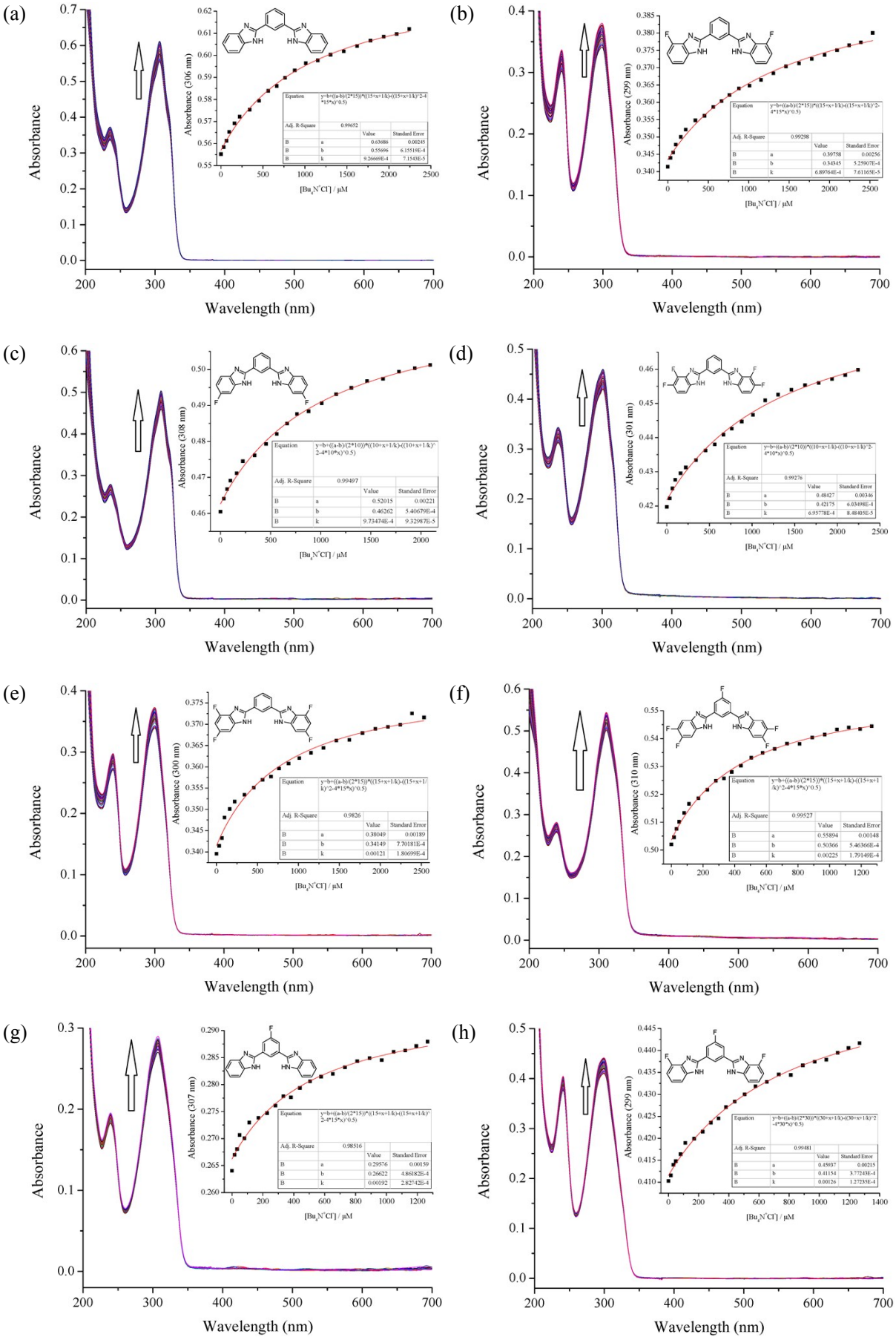
(a)
Absorbance
Wavelength (nm)
Absorbance (306 nm)
[Bu4N+Cl-] / μM
Equation
y=b+((a-b)/(2*15))*((15+x+1/k)-((15+x+1/k)^2-4*15*x)^0.5)
Adj. R-Square 0.99652
Value Standard Error
B a 0.63686 0.00245
B b 0.55696 6.15519E-4
B k 9.26669E-4 7.1543E-5
(b)
Absorbance
Wavelength (nm)
Absorbance (299 nm)
[Bu4N+Cl-] / μM
Equation
y=b+((a-b)/(2*15))*((15+x+1/k)-((15+x+1/k)^2-4*15*x)^0.5)
Adj. R-Square 0.99298
Value Standard Error
B a 0.39758 0.00256
B b 0.34345 5.25907E-4
B k 6.89764E-4 7.61165E-5
(c)
Absorbance
Wavelength (nm)
Absorbance (308 nm)
[Bu4N+Cl-] / μM
Equation
y=b+((a-b)/(2*10))*((10+x+1/k)-((10+x+1/k)^2-4*10*x)^0.5)
Adj. R-Square 0.99497
Value Standard Error
B a 0.52015 0.00221
B b 0.46262 5.40679E-4
B k 9.73474E-4 9.32987E-5
(d)
Absorbance
Wavelength (nm)
Absorbance (301 nm)
[Bu4N+Cl-] / μM
Equation
y=b+((a-b)/(2*10))*((10+x+1/k)-((10+x+1/k)^2-4*10*x)^0.5)
Adj. R-Square 0.99276
Value Standard Error
B a 0.48427 0.00346
B b 0.42175 6.03498E-4
B k 6.95778E-4 8.48405E-5
(e)
Absorbance
Wavelength (nm)
Absorbance (300 nm)
[Bu4N+Cl-] / μM
Equation
y=b+((a-b)/(2*15))*((15+x+1/k)-((15+x+1/k)^2-4*15*x)^0.5)
Adj. R-Square 0.9826
Value Standard Error
B a 0.38049 0.00189
B b 0.34149 7.70181E-4
B k 0.00121 1.80699E-4
(f)
Absorbance
Wavelength (nm)
Absorbance (310 nm)
[Bu4N+Cl-] / μM
Equation
y=b+((a-b)/(2*15))*((15+x+1/k)-((15+x+1/k)^2-4*15*x)^0.5)
Adj. R-Square 0.99527
Value Standard Error
B a 0.55894 0.00148
B b 0.50366 5.46366E-4
B k 0.00225 1.79149E-4
(g)
Absorbance
Wavelength (nm)
Absorbance (307 nm)
[Bu4N+Cl-] / μM
Equation
y=b+((a-b)/(2*15))*((15+x+1/k)-((15+x+1/k)^2-4*15*x)^0.5)
Adj. R-Square 0.98516
Value Standard Error
B a 0.29576 0.00159
B b 0.26622 4.86182E-4
B k 0.00192 2.82742E-4
(h)
Absorbance
Wavelength (nm)
Absorbance (299 nm)
[Bu4N+Cl-] / μM
Equation
y=b+((a-b)/(2*30))*((30+x+1/k)-((30+x+1/k)^2-4*30*x)^0.5)
Adj. R-Square 0.99481
Value Standard Error
B a 0.45937 0.00215
B b 0.41154 3.77243E-4
B k 0.00126 1.27235E-4

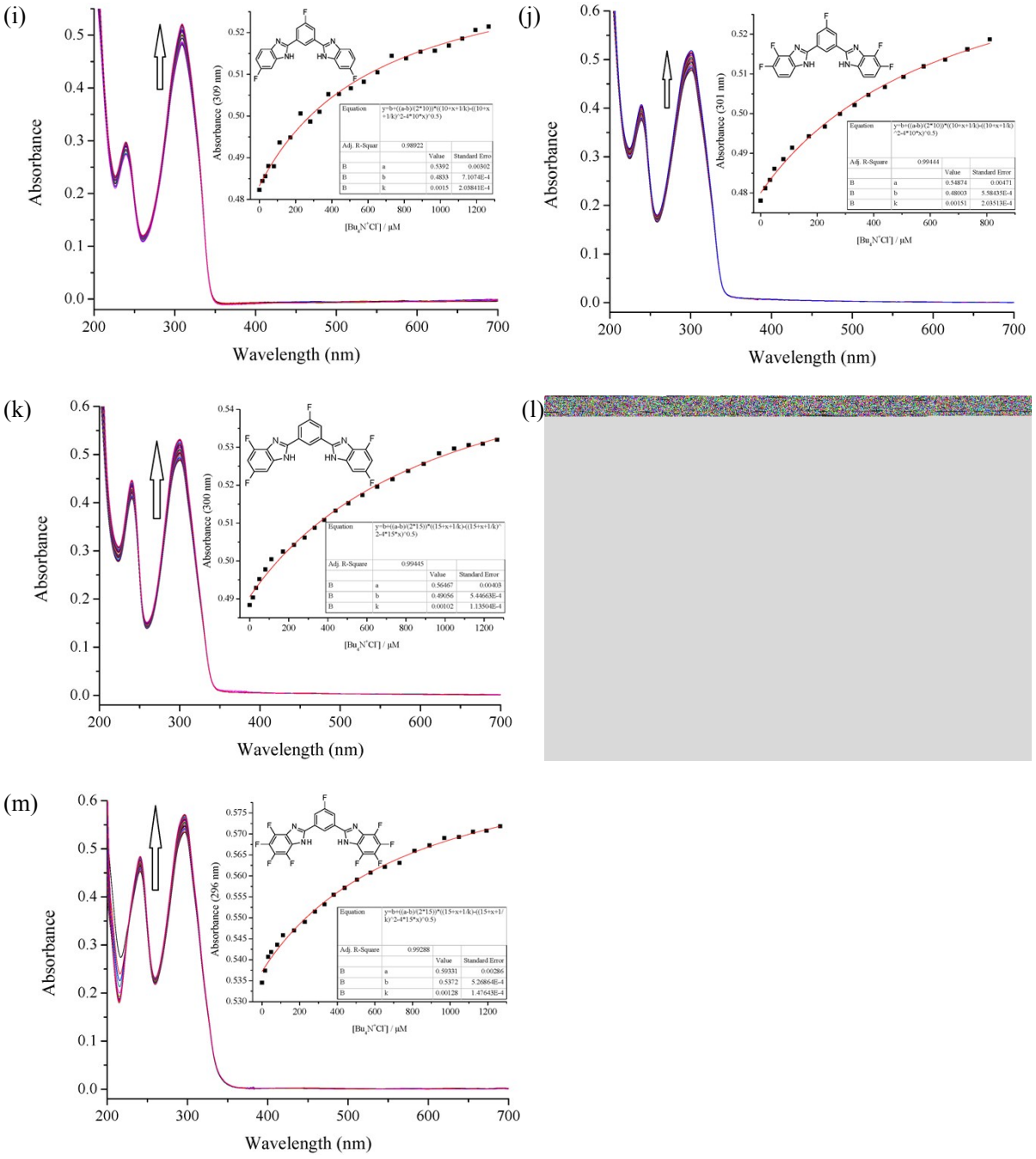

Fig. S75. Plot of the absorbance of (a) Bimbe **1**, (b) $^{4}F_{2}$-Bimbe **2**, (c) $^{5}F_{2}$-Bimbe **3**, (d) $^{4,5}F_{4}$-Bimbe **4**, (e) $^{4,6}F_{4}$-Bimbe **5**, (f) $^{5,6}F_{4}$-Bimbe **6**, (g) FBimbe **7**, (h) $^{4}F_{2}$-FBimbe **8**, (i) $^{5}F_{2}$-FBimbe **9**, (j) $^{4,5}F_{4}$-FBimbe **10**, (k) $^{4,6}F_{4}$-FBimbe **11**, (l) $^{5,6}F_{4}$-FBimbe **12** and (m) $^{4,5,6,7}F_{8}$-FBimbe **13** versus the concentrations of TBACl in a mixture of CH3CN and H2O (9/1, v/v). The solid line is the nonlinear least-squares fit of the experimental data according to a 1 : 1 binding model.

Table S1. Association constants (K_a's, M^{-1}) of compounds **1-13** with chloride anions [a]

Compound	Anion binding		Compound	Anion binding	
	K_a (M^{-1})	RA [b]		K_a (M^{-1}) [b]	RA [b]
Bimbe **1**	$(7.75\pm2.80)\times10^2$	1.0	FBimbe **7**	$(1.64\pm0.40)\times10^3$	2.1
$^{4}F_{2}$-Bimbe **2**	$(5.85\pm1.48)\times10^2$	0.8	$^{4}F_{2}$-FBimbe **8**	$(1.14\pm0.18)\times10^3$	1.5
$^{5}F_{2}$-Bimbe **3**	$(9.62\pm0.49)\times10^2$	1.2	$^{5}F_{2}$-FBimbe **9**	$(1.52\pm0.03)\times10^3$	2.0
$^{4,5}F_{4}$-Bimbe **4**	$(9.13\pm3.07)\times10^2$	1.2	$^{4,5}F_{4}$-FBimbe **10**	$(1.16\pm0.49)\times10^3$	1.5
$^{4,6}F_{4}$-Bimbe **5**	$(8.76\pm4.73)\times10^2$	1.1	$^{4,6}F_{4}$-FBimbe **11**	$(1.06\pm0.05)\times10^3$	1.4
$^{5,6}F_{4}$-Bimbe **6**	$(4.30\pm0.27)\times10^2$	0.6	$^{5,6}F_{4}$-FBimbe **12**	$(1.64\pm0.86)\times10^3$	2.1
			$^{4,5,6,7}F_{8}$-FBimbe **13**	$(9.12\pm5.20)\times10^2$	1.2

[a] Measured by means of spectrophotometric titrations in CH_3CN/H_2O (9/1).

[b] RA represents the relative binding affinity of each compound relative to Bimbe **1**.

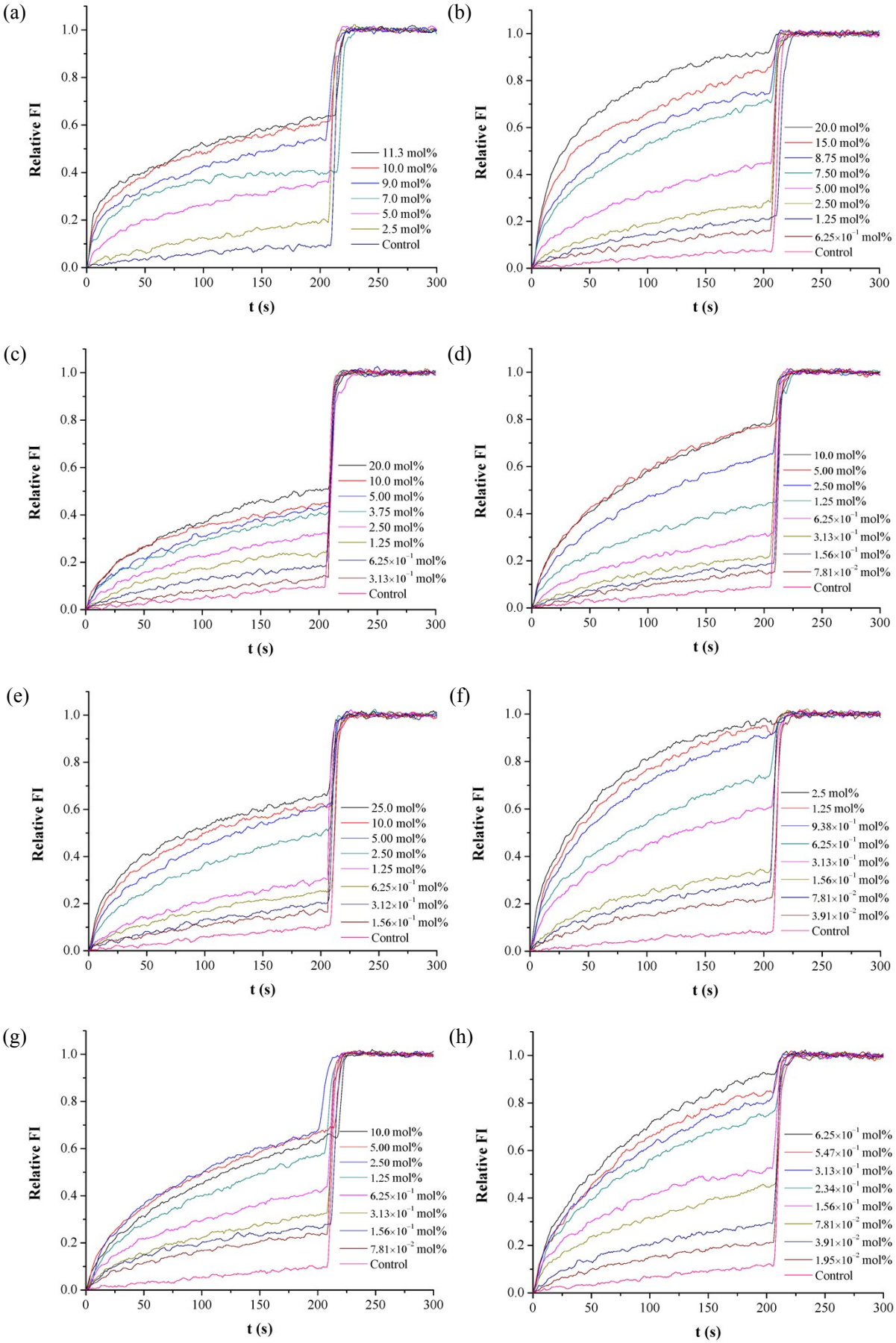
(a)
Relative FI
t (s)
11.3 mol%
10.0 mol%
9.0 mol%
7.0 mol%
5.0 mol%
2.5 mol%
Control
(b)
Relative FI
t (s)
20.0 mol%
15.0 mol%
8.75 mol%
7.50 mol%
5.00 mol%
2.50 mol%
1.25 mol%
6.25×10⁻¹ mol%
Control
(c)
Relative FI
t (s)
20.0 mol%
10.0 mol%
5.00 mol%
3.75 mol%
2.50 mol%
1.25 mol%
6.25×10⁻¹ mol%
3.13×10⁻¹ mol%
Control
(d)
Relative FI
t (s)
10.0 mol%
5.00 mol%
2.50 mol%
1.25 mol%
6.25×10⁻¹ mol%
3.13×10⁻¹ mol%
1.56×10⁻¹ mol%
7.81×10⁻² mol%
Control
(e)
Relative FI
t (s)
25.0 mol%
10.0 mol%
5.00 mol%
2.50 mol%
1.25 mol%
6.25×10⁻¹ mol%
3.12×10⁻¹ mol%
1.56×10⁻¹ mol%
Control
(f)
Relative FI
t (s)
2.5 mol%
1.25 mol%
9.38×10⁻¹ mol%
6.25×10⁻¹ mol%
3.13×10⁻¹ mol%
1.56×10⁻¹ mol%
7.81×10⁻² mol%
3.91×10⁻² mol%
Control
(g)
Relative FI
t (s)
10.0 mol%
5.00 mol%
2.50 mol%
1.25 mol%
6.25×10⁻¹ mol%
3.13×10⁻¹ mol%
1.56×10⁻¹ mol%
7.81×10⁻² mol%
Control
(h)
Relative FI
t (s)
6.25×10⁻¹ mol%
5.47×10⁻¹ mol%
3.13×10⁻¹ mol%
2.34×10⁻¹ mol%
1.56×10⁻¹ mol%
7.81×10⁻² mol%
3.91×10⁻² mol%
1.95×10⁻² mol%
Control

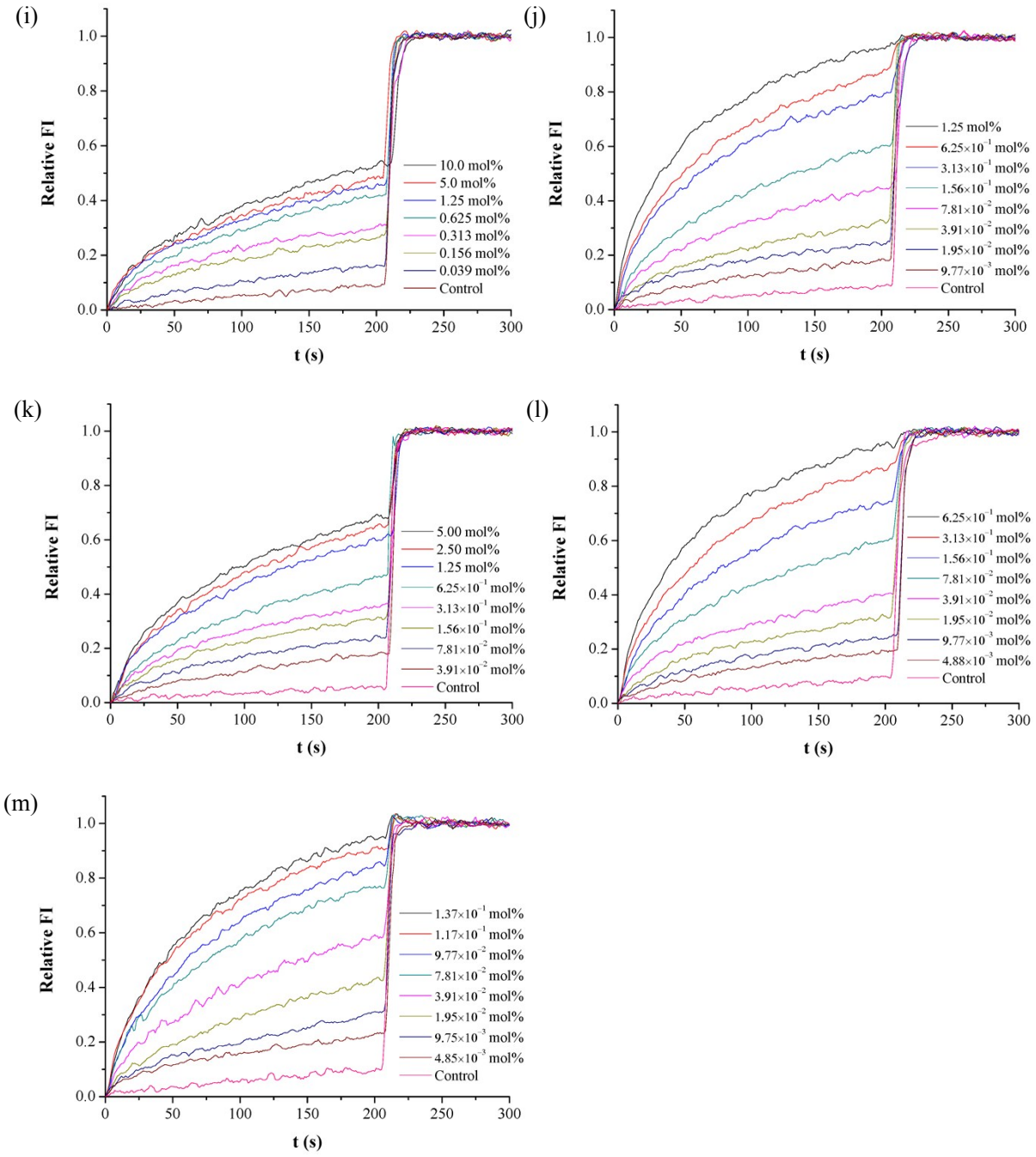

Fig. S76. Discharge of a pH gradient across EYPC-based liposomal membranes, mediated by (a) Bimbe **1**, (b) FBimbe **7**, (c) $^{4}F_{2}$-Bimbe **2**, (d) $^{4}F_{2}$-FBimbe **8**, (e) $^{5}F_{2}$-Bimbe **3**, (f) $^{5}F_{2}$-FBimbe **9**, (g) $^{4,5}F_{4}$-Bimbe **4**, (h) $^{4,5}F_{4}$-FBimbe **10**, (i) $^{4,6}F_{4}$-Bimbe **5**, (j) $^{4,6}F_{4}$-FBimbe **11**, (k) $^{5,6}F_{4}$-Bimbe **6**, (l) $^{5,6}F_{4}$-FBimbe **12** and (m) $^{4,5,6,7}F_{8}$-FBimbe **13** of varying concentrations. Intravesicular conditions: 0.1 mM pyranine in 25 mM HEPES (50 mM NaCl, pH 7.0); Extravesicular conditions: 25 mM HEPES (50 mM NaCl, pH 8.0). Ex 460 nm/Em 510 nm.

Table S2. Initial rate constants (k_{in}'s, s^{-1}) for pH discharge [a]

Compound	mol%	k_{in} (s^{-1})	Compound	mol%	k_{in} (s^{-1})
Bimbe **1**	11.25	$(1.46\pm0.16)\times10^{-2}$	FBimbe **7**	20.000	$(2.31\pm0.09)\times10^{-2}$
	10.00	$(1.32\pm0.11)\times10^{-2}$		15.000	$(2.07\pm0.09)\times10^{-2}$
	9.00	$(1.15\pm0.09)\times10^{-2}$		8.750	$(1.44\pm0.09)\times10^{-2}$
	7.00	$(0.92\pm0.06)\times10^{-2}$		7.500	$(1.22\pm0.06)\times10^{-2}$
	5.00	$(0.59\pm0.03)\times10^{-2}$		5.000	$(0.81\pm0.05)\times10^{-2}$
	2.50	$(0.22\pm0.02)\times10^{-2}$		2.500	$(0.31\pm0.02)\times10^{-2}$
	0	$(0.07\pm0.01)\times10^{-2}$		1.250	$(0.17\pm0.02)\times10^{-2}$
				0.625	$(0.14\pm0.01)\times10^{-2}$
				0	$(0.08\pm0.03)\times10^{-2}$
$^{4}F_{2}$-Bimbe **2**	20.000	$(0.82\pm0.03)\times10^{-2}$	$^{4}F_{2}$-FBimbe **8**	5.000	$(1.28\pm0.06)\times10^{-2}$
	10.000	$(0.73\pm0.04)\times10^{-2}$		2.500	$(0.97\pm0.05)\times10^{-2}$
	5.000	$(0.60\pm0.03)\times10^{-2}$		1.250	$(0.67\pm0.03)\times10^{-2}$
	3.750	$(0.56\pm0.03)\times10^{-2}$		0.625	$(0.47\pm0.01)\times10^{-2}$
	2.500	$(0.41\pm0.03)\times10^{-2}$		0.313	$(0.21\pm0.02)\times10^{-2}$
	1.250	$(0.26\pm0.01)\times10^{-2}$		0.156	$(0.18\pm0.01)\times10^{-2}$
	0.625	$(0.18\pm0.01)\times10^{-2}$		7.81×10^{-2}	$(0.10\pm0.01)\times10^{-2}$
	0.313	$(0.11\pm0.01)\times10^{-2}$		0	$(0.07\pm0.01)\times10^{-2}$
	0	$(0.04\pm0.01)\times10^{-2}$			
$^{5}F_{2}$-Bimbe **3**	25.000	$(1.33\pm0.09)\times10^{-2}$	$^{5}F_{2}$-FBimbe **9**	2.500	$(1.94\pm0.11)\times10^{-2}$
	10.000	$(1.25\pm0.06)\times10^{-2}$		1.250	$(1.85\pm0.06)\times10^{-2}$
	5.000	$(1.06\pm0.05)\times10^{-2}$		0.938	$(1.74\pm0.06)\times10^{-2}$
	2.500	$(0.81\pm0.04)\times10^{-2}$		0.625	$(1.54\pm0.09)\times10^{-2}$
	1.250	$(0.37\pm0.03)\times10^{-2}$		0.313	$(0.98\pm0.04)\times10^{-2}$
	0.625	$(0.33\pm0.02)\times10^{-2}$		0.156	$(0.50\pm0.03)\times10^{-2}$
	0.313	$(0.19\pm0.02)\times10^{-2}$		7.81×10^{-2}	$(0.35\pm0.01)\times10^{-2}$
	0.156	$(0.18\pm0.02)\times10^{-2}$		3.91×10^{-2}	$(0.24\pm0.01)\times10^{-2}$
	0	$(0.04\pm0.01)\times10^{-2}$		0	$(0.05\pm0.01)\times10^{-2}$
$^{4,5}F_{4}$-Bimbe **4**	10.000	$(1.22\pm0.07)\times10^{-2}$	$^{4,5}F_{4}$-FBimbe **10**	0.625	$(1.59\pm0.06)\times10^{-2}$
	5.000	$(1.22\pm0.07)\times10^{-2}$		0.547	$(1.49\pm0.09)\times10^{-2}$
	2.500	$(1.14\pm0.05)\times10^{-2}$		0.313	$(1.38\pm0.07)\times10^{-2}$
	1.250	$(0.97\pm0.03)\times10^{-2}$		0.234	$(1.23\pm0.06)\times10^{-2}$
	0.625	$(0.80\pm0.03)\times10^{-2}$		0.156	$(0.92\pm0.07)\times10^{-2}$
	0.313	$(0.48\pm0.02)\times10^{-2}$		7.81×10^{-2}	$(0.73\pm0.04)\times10^{-2}$
	0.156	$(0.36\pm0.01)\times10^{-2}$		3.91×10^{-2}	$(0.40\pm0.01)\times10^{-2}$
	7.81×10^{-2}	$(0.26\pm0.01)\times10^{-2}$		1.95×10^{-2}	$(0.27\pm0.01)\times10^{-2}$
	0	$(0.08\pm0.01)\times10^{-2}$		0	$(0.07\pm0.01)\times10^{-2}$

$^{4,6}F_4$-Bimbe **5**	10.000	(0.84±0.02)×10^{-2}	$^{4,6}F_4$-FBimbe **11**	1.250	(1.86±0.09)×10^{-2}
	5.000	(0.79±0.04)×10^{-2}		0.625	(1.63±0.08)×10^{-2}
	1.250	(0.73±0.04)×10^{-2}		0.313	(1.45±0.06)×10^{-2}
	0.625	(0.64±0.02)×10^{-2}		0.156	(1.00±0.04)×10^{-2}
	0.313	(0.44±0.03)×10^{-2}		7.81×10^{-2}	(0.76±0.02)×10^{-2}
	0.156	(0.37±0.01)×10^{-2}		3.91×10^{-2}	(0.47±0.01)×10^{-2}
	3.91×10^{-2}	(0.20±0.02)×10^{-2}		1.95×10^{-2}	(0.31±0.03)×10^{-2}
	0	(0.05±0.01)×10^{-2}		9.76×10^{-3}	(0.23±0.02)×10^{-2}
				0	(0.08±0.01)×10^{-2}
$^{5,6}F_4$-Bimbe **6**	5.000	(1.07±0.03)×10^{-2}	$^{5,6}F_4$-FBimbe **12**	0.625	(1.63±0.07)×10^{-2}
	2.500	(1.00±0.04)×10^{-2}		0.313	(1.48±0.07)×10^{-2}
	1.250	(0.95±0.04)×10^{-2}		0.156	(1.27±0.04)×10^{-2}
	0.625	(0.78±0.01)×10^{-2}		7.81×10^{-2}	(0.97±0.05)×10^{-2}
	0.313	(0.61±0.02)×10^{-2}		3.91×10^{-2}	(0.63±0.04)×10^{-2}
	0.156	(0.42±0.03)×10^{-2}		1.95×10^{-2}	(0.45±0.02)×10^{-2}
	7.81×10^{-2}	(0.33±0.01)×10^{-2}		9.76×10^{-3}	(0.26±0.01)×10^{-2}
	3.91×10^{-2}	(0.18±0.01)×10^{-2}		4.88×10^{-3}	(0.18±0.02)×10^{-2}
	0	(0.03±0.02)×10^{-2}		0	(0.08±0.02)×10^{-2}
$^{4,5,6,7}F_8$-FBimbe **13**	0.137	(1.48±0.05)×10^{-2}			
	0.117	(1.42±0.06)×10^{-2}			
	9.77×10^{-2}	(1.35±0.04)×10^{-2}			
	7.81×10^{-2}	(1.34±0.04)×10^{-2}			
	3.91×10^{-2}	(1.07±0.06)×10^{-2}			
	1.95×10^{-2}	(0.75±0.04)×10^{-2}			
	9.75×10^{-3}	(0.49±0.03)×10^{-2}			
	4.85×10^{-3}	(0.34±0.03)×10^{-2}			
	0	(0.08±0.02)×10^{-2}			

[a] See Fig. S76 for the measuring conditions.

(a)

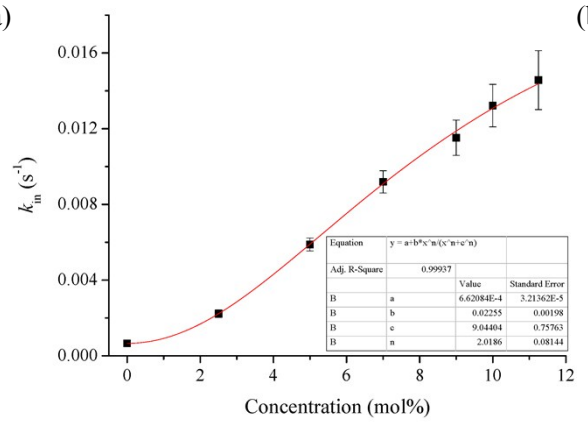

Equation	y = a+b*x^n/(x^n+c^n)		
Adj. R-Square	0.99937		
		Value	Standard Error
B	a	6.62084E-4	3.21362E-5
B	b	0.02255	0.00198
B	c	9.04404	0.75763
B	n	2.0186	0.08144

(b)

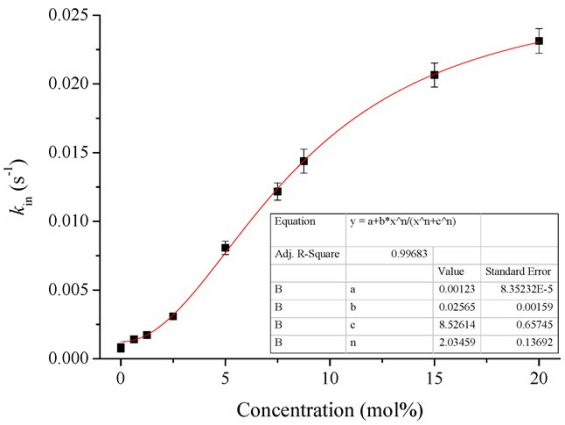

Equation	y = a+b*x^n/(x^n+c^n)		
Adj. R-Square	0.99683		
		Value	Standard Error
B	a	0.00123	8.35232E-5
B	b	0.02565	0.00159
B	c	8.52614	0.65745
B	n	2.03459	0.13692

(c)

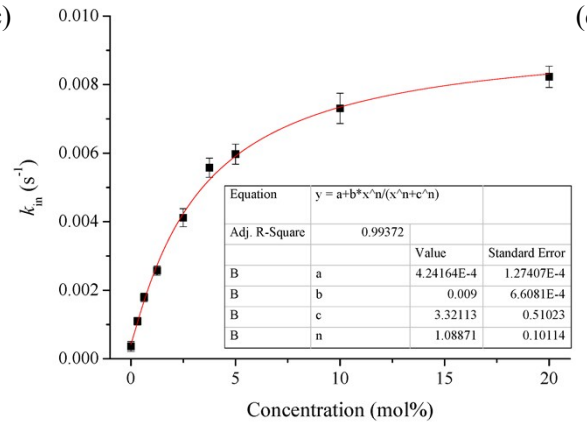

Equation	y = a+b*x^n/(x^n+c^n)		
Adj. R-Square	0.99372		
		Value	Standard Error
B	a	4.24164E-4	1.27407E-4
B	b	0.009	6.6081E-4
B	c	3.32113	0.51023
B	n	1.08871	0.10114

(d)

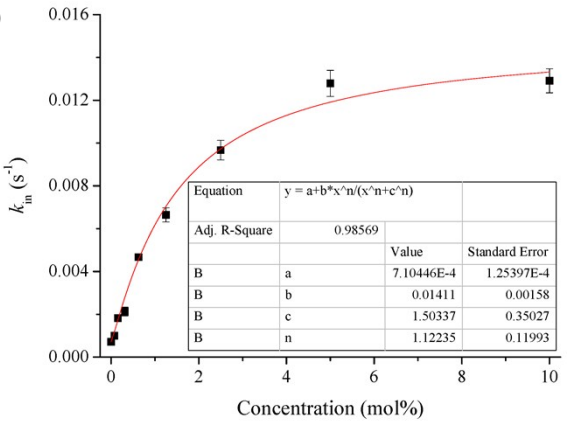

Equation	y = a+b*x^n/(x^n+c^n)		
Adj. R-Square	0.98569		
		Value	Standard Error
B	a	7.10446E-4	1.25397E-4
B	b	0.01411	0.00158
B	c	1.50337	0.35027
B	n	1.12235	0.11993

(e)

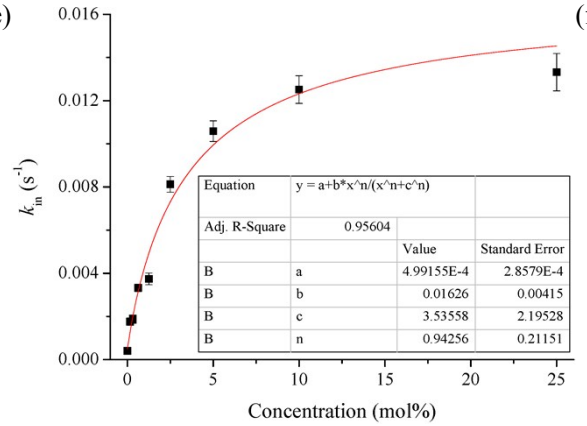

Equation	y = a+b*x^n/(x^n+c^n)		
Adj. R-Square	0.95604		
		Value	Standard Error
B	a	4.99155E-4	2.8579E-4
B	b	0.01626	0.00415
B	c	3.53558	2.19528
B	n	0.94256	0.21151

(f)

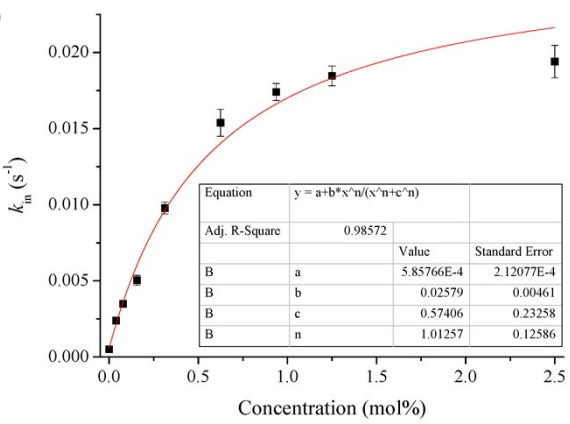

Equation	y = a+b*x^n/(x^n+c^n)		
Adj. R-Square	0.98572		
		Value	Standard Error
B	a	5.85766E-4	2.12077E-4
B	b	0.02579	0.00461
B	c	0.57406	0.23258
B	n	1.01257	0.12586

(g)

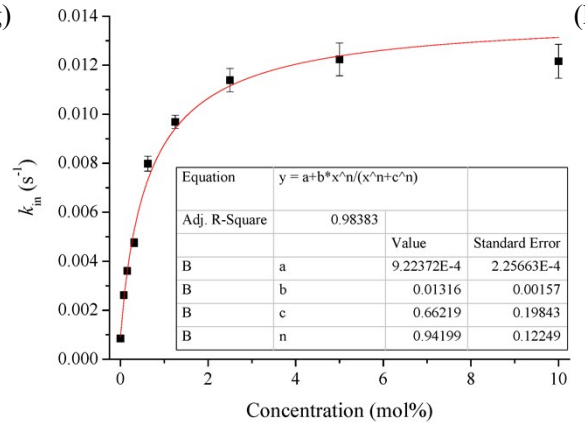

Equation	y = a+b*x^n/(x^n+c^n)		
Adj. R-Square	0.98383		
		Value	Standard Error
B	a	9.22372E-4	2.25663E-4
B	b	0.01316	0.00157
B	c	0.66219	0.19843
B	n	0.94199	0.12249

(h)

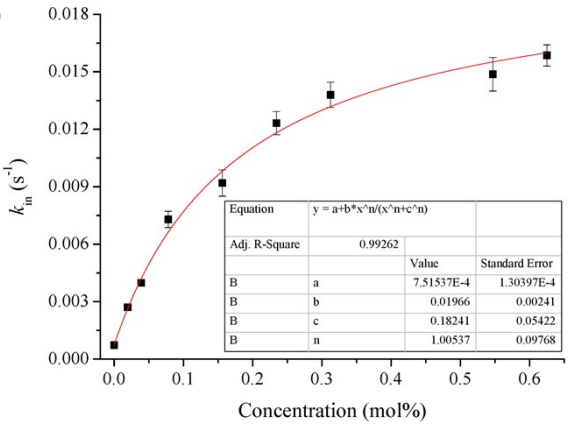

Equation	y = a+b*x^n/(x^n+c^n)		
Adj. R-Square	0.99262		
		Value	Standard Error
B	a	7.51537E-4	1.30397E-4
B	b	0.01966	0.00241
B	c	0.18241	0.05422
B	n	1.00537	0.09768

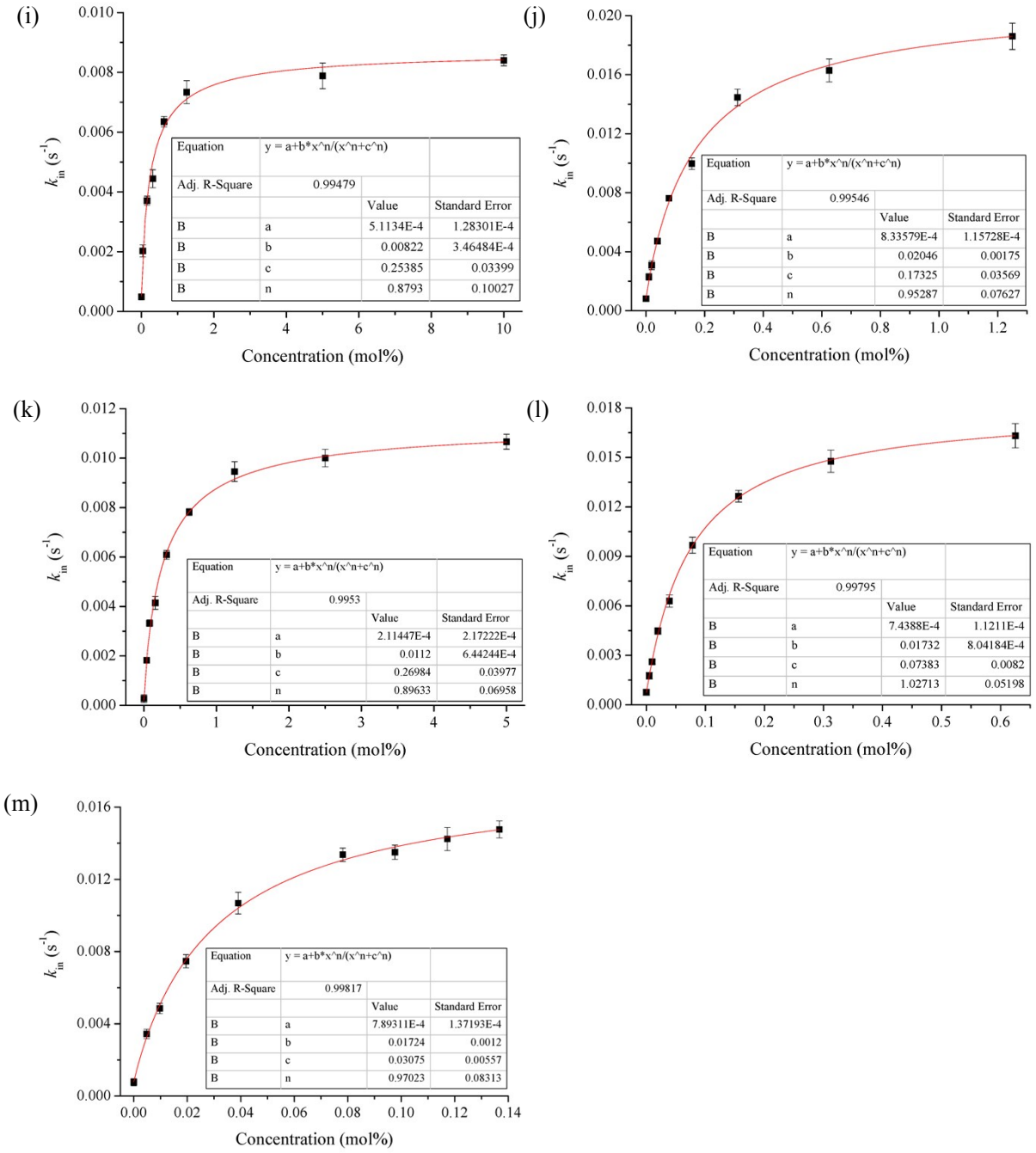

Fig. S77. Hill plots of the initial rate constants (k_{in}'s) *versus* the mol% concentrations for (a) Bimbe **1**, (b) FBimbe **7**, (c) $^{4}F_{2}$-Bimbe **2**, (d) $^{4}F_{2}$-FBimbe **8**, (e) $^{5}F_{2}$-Bimbe **3**, (f) $^{5}F_{2}$-FBimbe **9**, (g) $^{4,5}F_{4}$-Bimbe **4**, (h) $^{4,5}F_{4}$-FBimbe **10**, (i) $^{4,6}F_{4}$-Bimbe **5**, (j) $^{4,6}F_{4}$-FBimbe **11**, (k) $^{5,6}F_{4}$-Bimbe **6**, (l) $^{5,6}F_{4}$-FBimbe **12** and (m) $^{4,5,6,7}F_{8}$-FBimbe **13** in EYPC liposomes. The solid lines are nonlinear least-squares fit of the data according to the Hill Equation, $k_{in} = k_0+k_{max}\times[\text{compound}]^n/([\text{compound}]^n+[EC_{50}]^n)$.

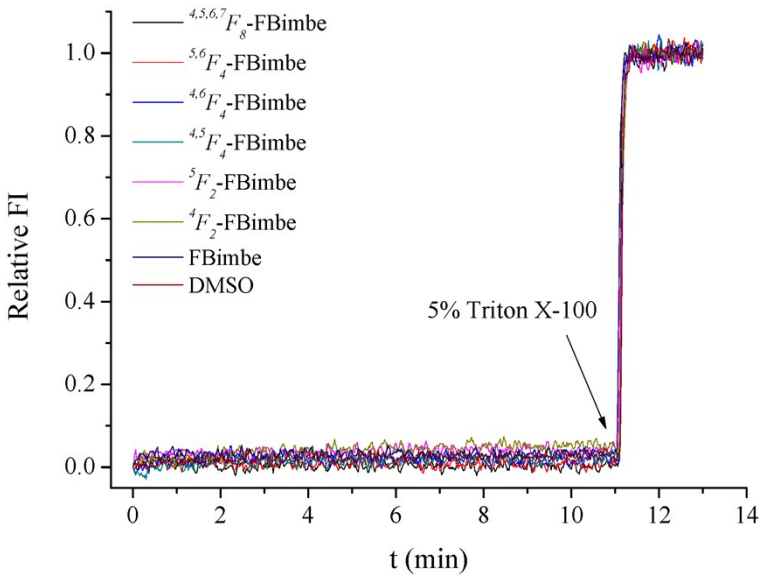

Fig. S78. Calcein leakage by FBimbe **7** (10 mol%), $^{4}F_2$-FBimbe **8** (10 mol%), $^{5}F_2$-FBimbe **9** (4 mol%), $^{4,5}F_4$-Bimbe **10** (2 mol%), $^{4,6}F_4$-FBimbe **11** (2 mol%), $^{5,6}F_4$-FBimbe **12** (1 mol%) and $^{4,5,6,7}F_8$-FBimbe **13** (1 mol%) from unilamellar EYPC vesicles loaded with 100 mM calcein buffered to pH 7.0 with 25 mM HEPES buffer and 500 mM NaCl. The vesicles were dispersed in 500 mM NaCl buffered to pH 7.0 with 25 mM HEPES buffer, followed by the addition of a DMSO solution of different compounds. At the end of the experiment (11 min), an aqueous solution of Triton X-100 (5 wt%) was added to lyse the vesicles. DMSO was used as a control. The results are shown as % calcein leaked from the vesicles.

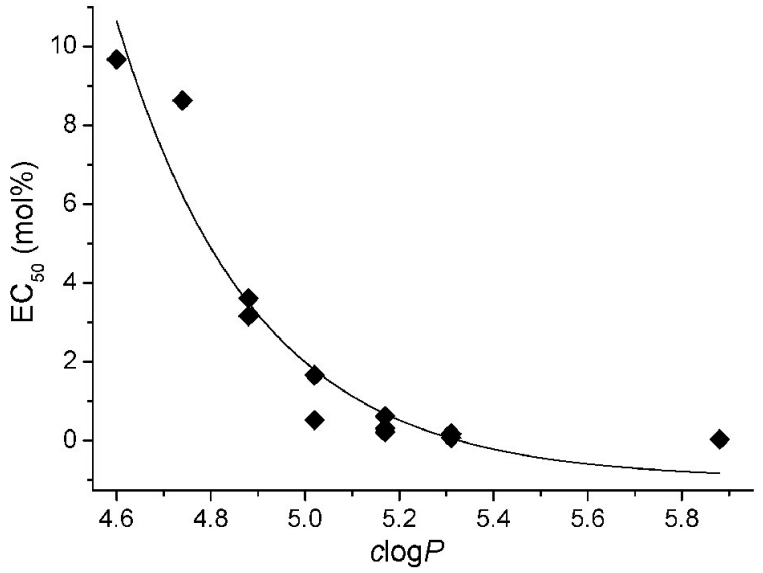

Fig. S79. Plot of the EC_{50} values of fluorinated Bimbe derivatives against their *c*log*P* values. The solid line was obtained by nonlinear least-square fitting according to the first-order exponential decay.

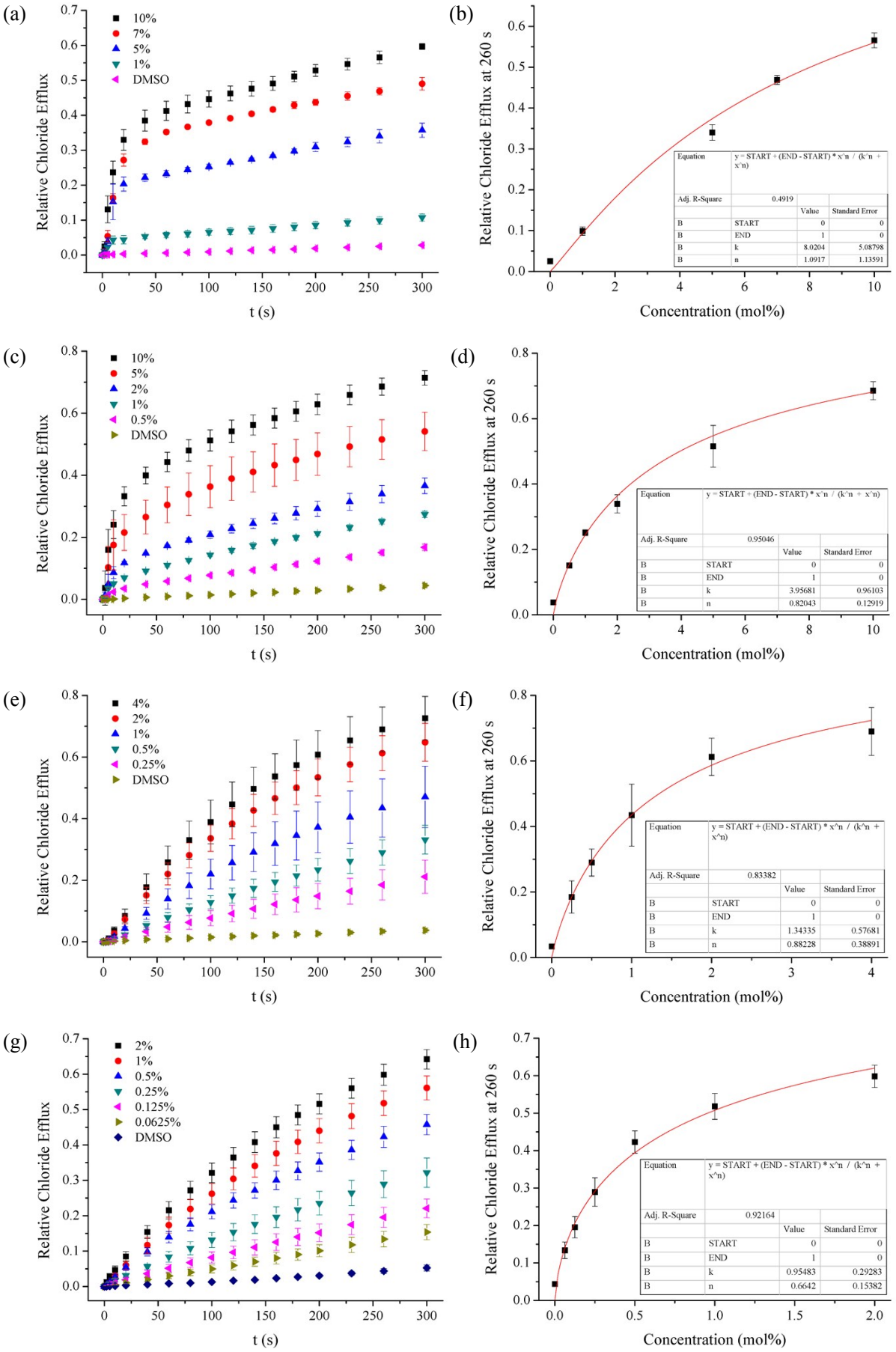
(a)
Relative Chloride Efflux
t (s)
10%
7%
5%
1%
DMSO
(b)
Relative Chloride Efflux at 260 s
Concentration (mol%)
Equation y = START + (END - START) * x^n / (k^n + x^n)
Adj. R-Square 0.4919
Value Standard Error
B START 0 0
B END 1 0
B k 8.0204 5.08798
B n 1.0917 1.13591
(c)
Relative Chloride Efflux
t (s)
10%
5%
2%
1%
0.5%
DMSO
(d)
Relative Chloride Efflux at 260 s
Concentration (mol%)
Equation y = START + (END - START) * x^n / (k^n + x^n)
Adj. R-Square 0.95046
Value Standard Error
B START 0 0
B END 1 0
B k 3.95681 0.96103
B n 0.82043 0.12919
(e)
Relative Chloride Efflux
t (s)
4%
2%
1%
0.5%
0.25%
DMSO
(f)
Relative Chloride Efflux at 260 s
Concentration (mol%)
Equation y = START + (END - START) * x^n / (k^n + x^n)
Adj. R-Square 0.83382
Value Standard Error
B START 0 0
B END 1 0
B k 1.34335 0.57681
B n 0.88228 0.38891
(g)
Relative Chloride Efflux
t (s)
2%
1%
0.5%
0.25%
0.125%
0.0625%
DMSO
(h)
Relative Chloride Efflux at 260 s
Concentration (mol%)
Equation y = START + (END - START) * x^n / (k^n + x^n)
Adj. R-Square 0.92164
Value Standard Error
B START 0 0
B END 1 0
B k 0.95483 0.29283
B n 0.6642 0.15382

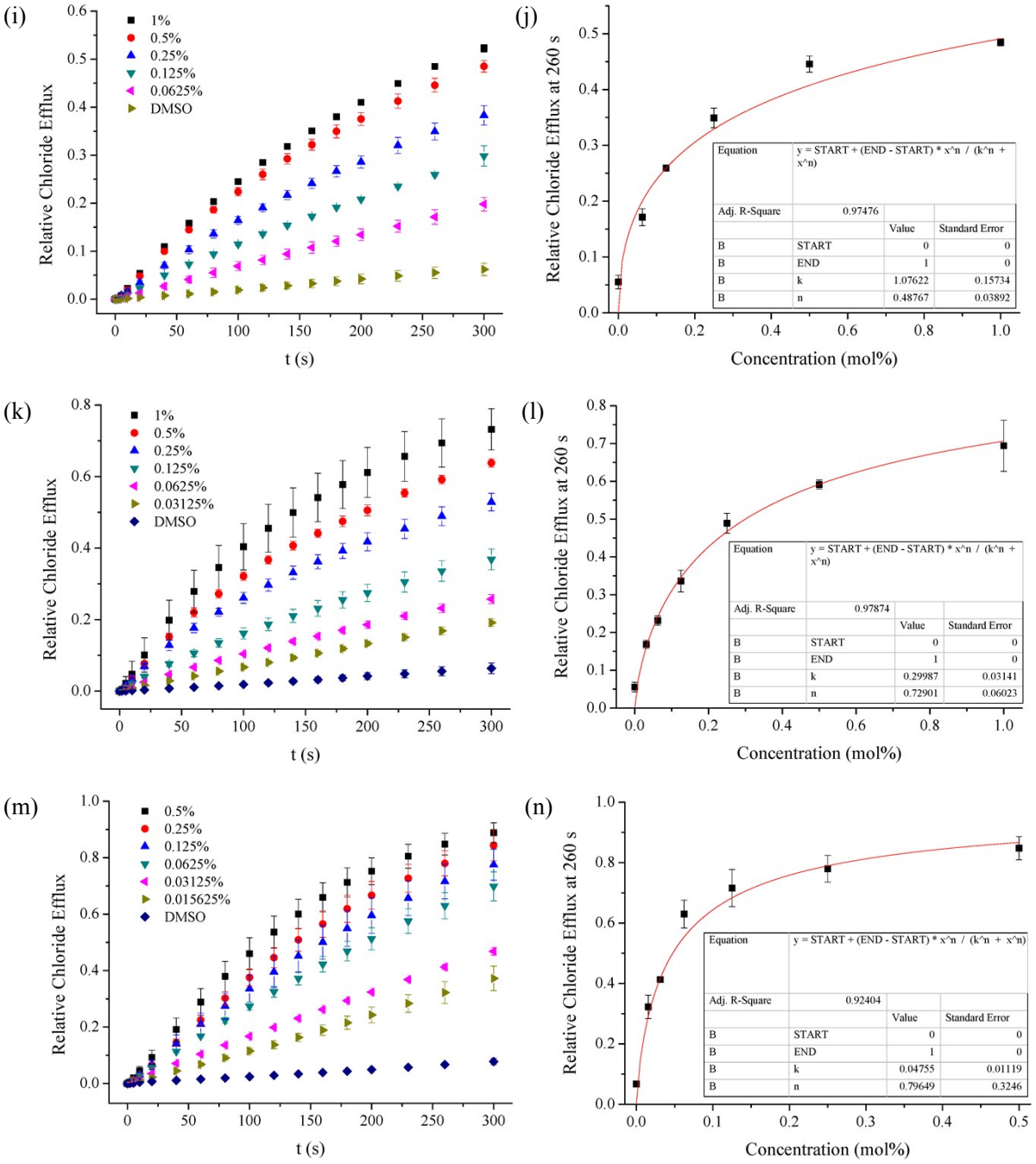

Fig. S80. Typical plots of the chloride efflux against time in the presence of (a) FBimbe **7**, (c) $^{4}F_{2}$-FBimbe **8**, (e) $^{5}F_{2}$-FBimbe **9**, (g) $^{4,5}F_{4}$-FBimbe **10**, (i) $^{4,6}F_{4}$-FBimbe **11**, (k) $^{5,6}F_{4}$-FBimbe **12** and (m) $^{4,5,6,7}F_{8}$-FBimbe **13** of varying concentrations in unilamellar EYPC vesicles loaded with 500 mM NaCl in 25 mM HEPES buffer (pH 7.0). The vesicles were dispersed in 500 mM $NaNO_3$ in 25 mM HEPES buffer (pH 7.0). Dose-response plots of the relative chloride efflux at 260 s *versus* the mol% concentrations of (b) FBimbe **7**, (d) $^{4}F_{2}$-FBimbe **8**, (f) $^{5}F_{2}$-FBimbe **9**, (h) $^{4,5}F_{4}$-FBimbe **10**, (j) $^{4,6}F_{4}$-FBimbe **11**, (l) $^{5,6}F_{4}$-FBimbe **12** and (n) $^{4,5,6,7}F_{8}$-FBimbe **13** in EYPC liposomes. EC_{50} and Hill coefficients (n value) were calculated by the Eq. $y = V_0 + (V_{max}–V_0)\times[compound]^n/([compound]^n + [EC_{50}]^n) = 100\%*[compound]^n/([compound]^n + [EC_{50}]^n)$, where y is the relative chloride efflux at 260 s at different concentration of compounds; V_{max} is the

maximum chloride efflux and is fixed at 1 as this is physically the possible maximum chloride efflux; V_0 is the relative chloride efflux at 260 s without the ionophore and is fixed at 0.

Table S3. Chloride efflux efficiency ($EC_{50,\ 260\ s}$) of each compound

Compound	Chloride efflux		Compound	Chloride efflux	
	$EC_{50,\ 260\ s}$ (mol%)	n		$EC_{50,\ 260\ s}$ (mol%)	n
Bimbe **1**	>10	/	FBimbe **7**	8.13±0.42	1.15±0.01
$^{4}F_2$-Bimbe **2**	>10	/	$^{4}F_2$-FBimbe **8**	4.31±0.66	0.82±0.07
$^{5}F_2$-Bimbe **3**	>10	/	$^{5}F_2$-FBimbe **9**	1.42±0.42	0.87±0.07
$^{4,5}F_4$-Bimbe **4**	>10	/	$^{4,5}F_4$-FBimbe **10**	0.96±0.17	0.66±0.04
$^{4,6}F_4$-Bimbe **5**	>10	/	$^{4,6}F_4$-FBimbe **11**	0.92±0.04	0.53±0.02
$^{5,6}F_4$-Bimbe **6**	>10	/	$^{5,6}F_4$-FBimbe **12**	0.31±0.05	0.73±0.06
			$^{4,5,6,7}F_8$-FBimbe **13**	0.04±0.01	0.77±0.07

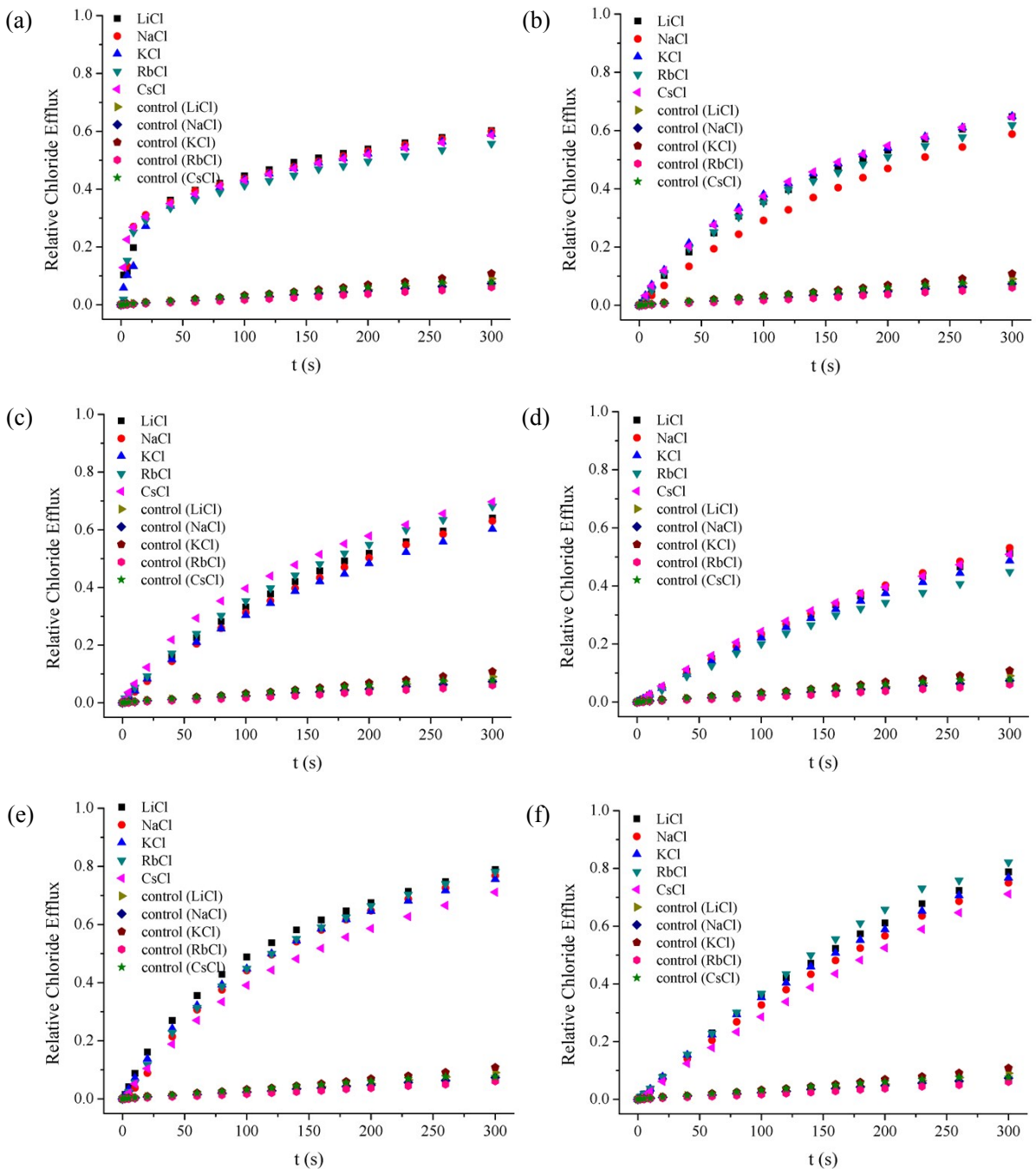

Fig. S81. Chloride efflux induced by (a) $^{4}F_{2}$-FBimbe **8** (5 mol%), (b) $^{5}F_{2}$-FBimbe **9** (2 mol%), (c) $^{4,5}F_{4}$-FBimbe **10** (2 mol%), (d) $^{4,6}F_{4}$-FBimbe **11** (1 mol%), (e) $^{5,6}F_{4}$-FBimbe **12** (1 mol%) and (f) $^{4,5,6,7}F_{8}$-FBimbe **13** (0.125 mol%) across EYPC-based liposomal membranes, under the measuring conditions of internal vesicles: 500 mM MCl, 25 mM HEPES, pH 7.0 (M = Li, Na, K, Rb and Cs) and external vesicles: 500 mM $NaNO_3$, 25 mM HEPES, pH 7.0.

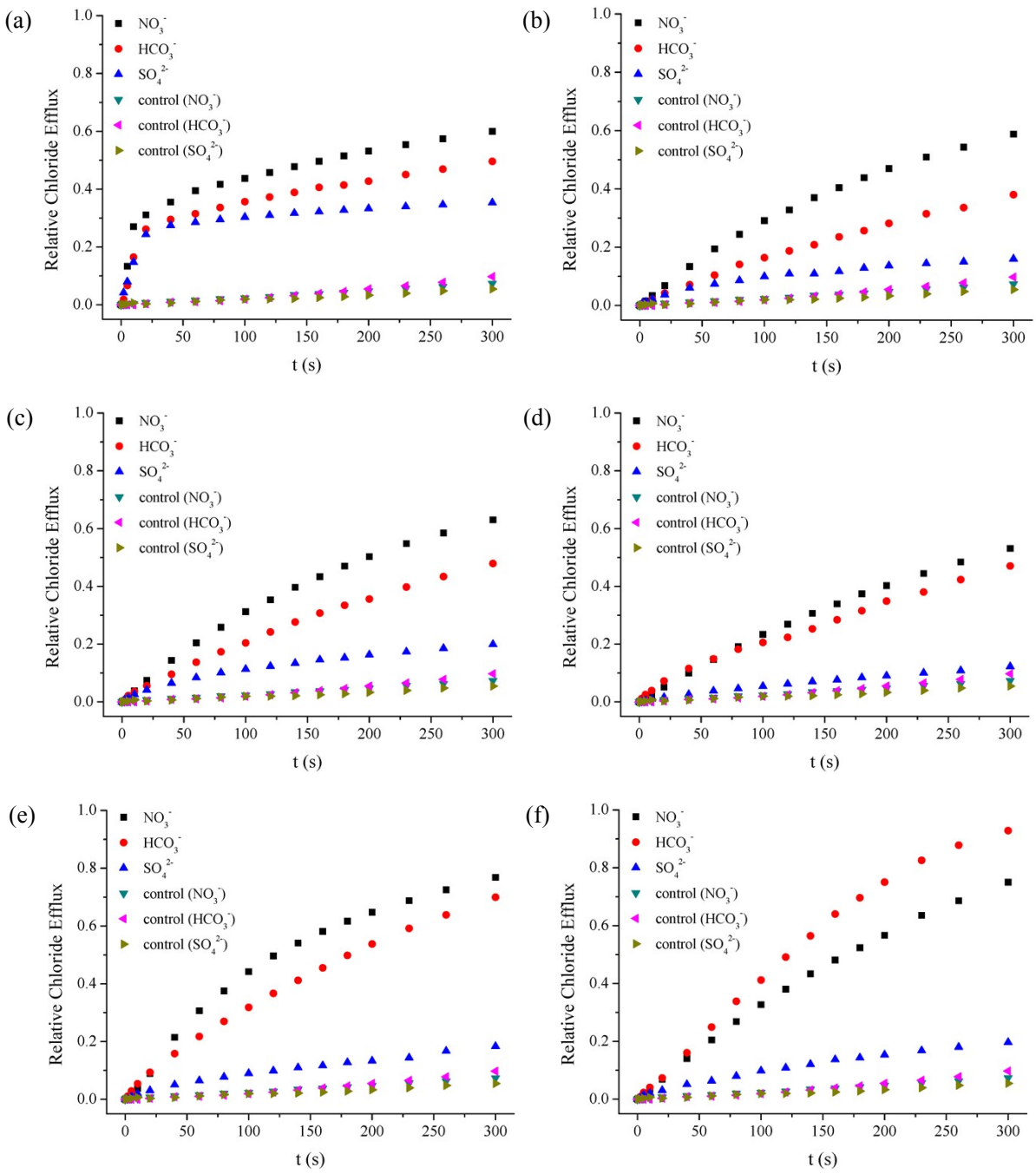

Fig. S82. Chloride efflux induced by (a) $^{4}F_{2}$-FBimbe **8** (5 mol%), (b) $^{5}F_{2}$-FBimbe **9** (2 mol%), (c) $^{4,5}F_{4}$-FBimbe **10** (2 mol%), (d) $^{4,6}F_{4}$-FBimbe **11** (1 mol%), (e) $^{5,6}F_{4}$-FBimbe **12** (1 mol%) and (f) $^{4,5,6,7}F_{8}$-FBimbe **13** (0.125 mol%) across EYPC-based liposomal membranes, under the measuring conditions of internal vesicles: 500 mM NaCl, 25 mM HEPES, pH 7.0 and external vesicles: 500 mM NaX, 25 mM HEPES, pH 7.0 (X = NO_3 or HCO_3) or 250 mM Na_2SO_4, 25 mM HEPES, pH 7.0.

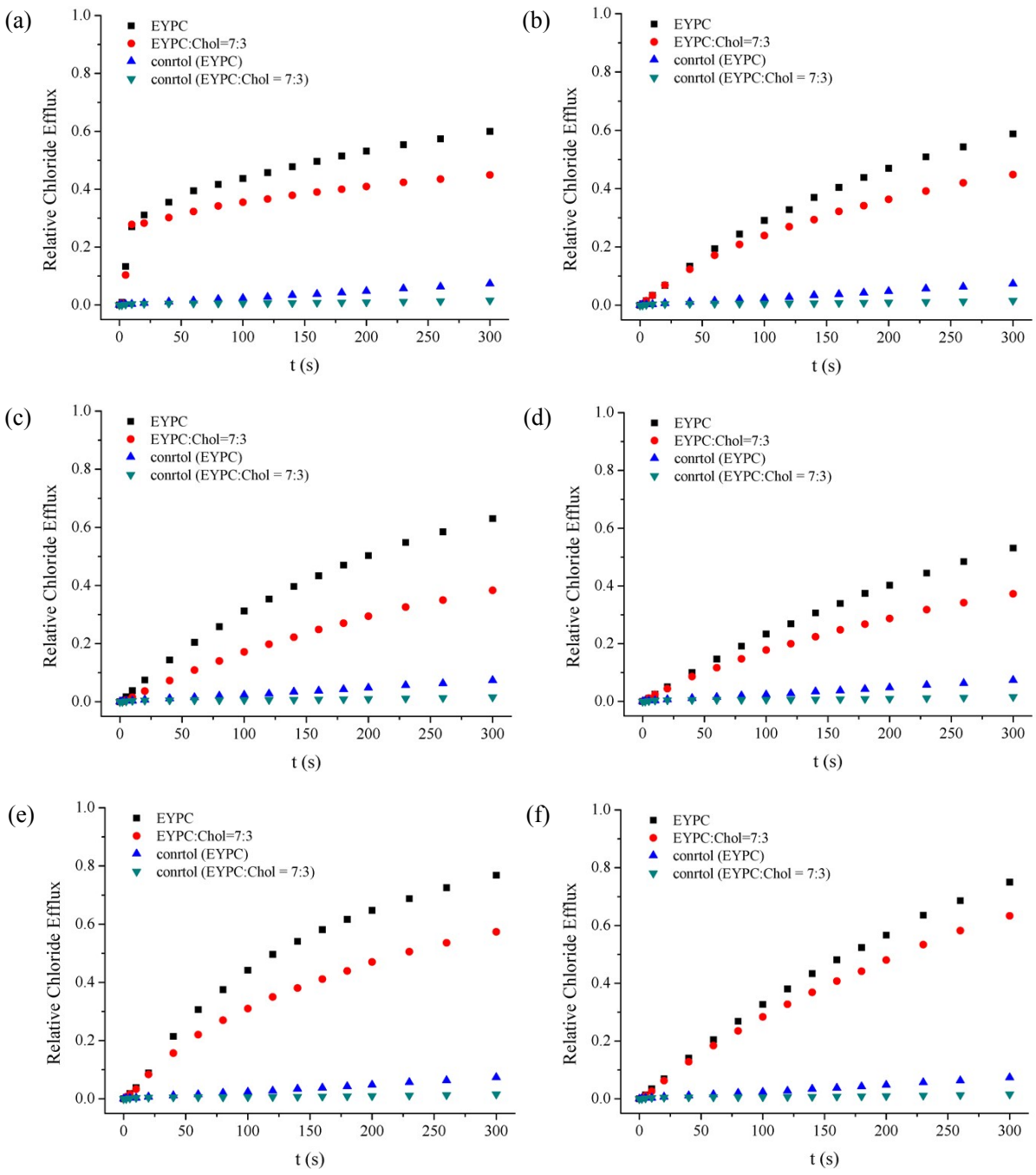

Fig. S83. Chloride efflux induced by (a) $^{4}F_{2}$-FBimbe **8** (5 mol%), (b) $^{5}F_{2}$-FBimbe **9** (2 mol%), (c) $^{4,5}F_{4}$-FBimbe **10** (2 mol%), (d) $^{4,6}F_{4}$-FBimbe **11** (1 mol%), (e) $^{5,6}F_{4}$-FBimbe **12** (1 mol%) and (f) $^{4,5,6,7}F_{8}$-FBimbe **13** (0.125 mol%) from EYPC vesicles or EYPC/cholesterol (7/3) vesicles, under the measuring conditions of internal vesicles: 500 mM NaCl, 25 mM HEPES, pH 7.0 and external vesicles: 500 mM $NaNO_3$, 25 mM HEPES, pH 7.0.

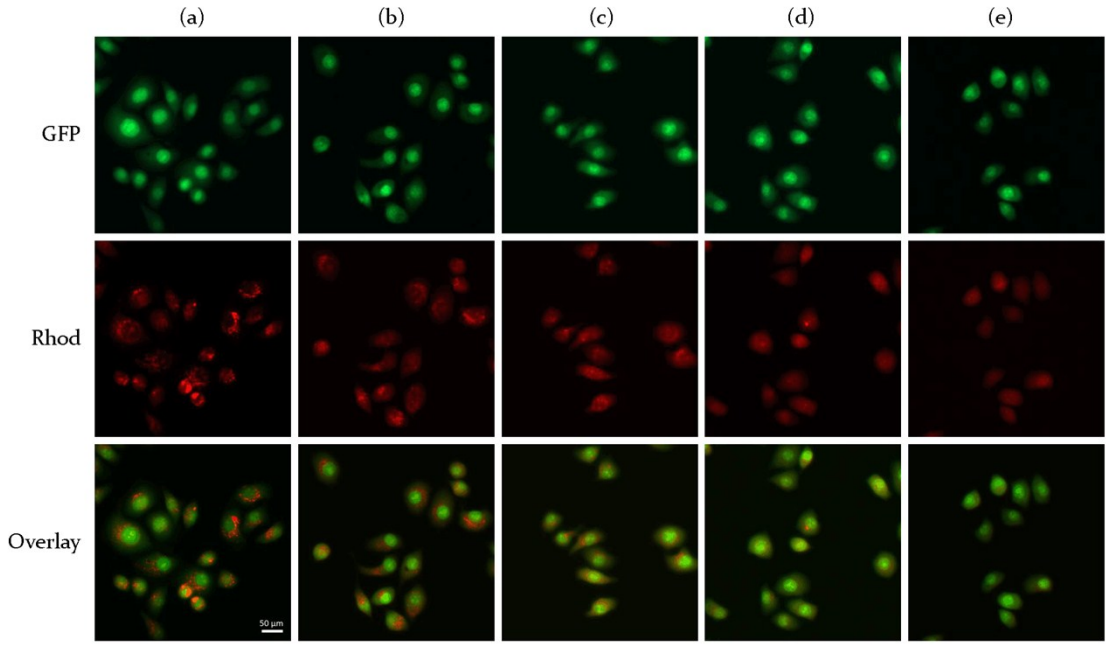

Fig. S84. Acridine orange staining of HeLa cells. (a) Untreated cells (control); (b)-(e) Cells treated with 10 μM of FBimbe **7**, $^{5}F_{2}$-FBimbe **9**, $^{5,6}F_{4}$-FBimbe **12** and $^{4,5,6,7}F_{8}$-FBimbe **13**, respectively, for 3 h.

Table S4. Cell viability (%) of Bimbe and its derivatives towards four solid tumor cells [a]

Compound	HeLa	A549	MCF-7	HepG2
Bimbe **1**	11.6±1.5	17.8±1.6	66.3±3.3	15.8±0.7
$^{4}F_{2}$-Bimbe **2**	54.1±0.2	84.4±4.7	94.0±3.7	66.7±5.6
$^{5}F_{2}$-Bimbe **3**	13.2±2.3	31.3±1.8	52.4±1.8	34.9±0.8
$^{4,5}F_{4}$-Bimbe **4**	73.3±2.4	66.3±2.8	96.6±3.1	77.0±4.6
$^{4,6}F_{4}$-Bimbe **5**	51.7±1.9	47.2±1.0	92.9±6.1	75.3±3.5
$^{5,6}F_{4}$-Bimbe **6**	54.1±1.3	9.7±1.8	56.8±4.7	23.1±2.4
FBimbe **7**	21.6±4.1	27.6±1.6	25.3±3.2	20.4±2.1
$^{4}F_{2}$-FBimbe **8**	52.3±1.0	72.7±2.8	70.6±1.2	68.6±2.9
$^{5}F_{2}$-FBimbe **9**	3.9±0.3	13.4±2.1	32.1±3.1	20.8±3.1
$^{4,5}F_{4}$-FBimbe **10**	21.9±1.8	23.5±2.7	29.1±1.7	49.5±3.4
$^{4,6}F_{4}$-FBimbe **11**	68.8±2.0	42.3±2.0	82.2±3.3	72.2±5.4
$^{5,6}F_{4}$-FBimbe **12**	15.8±1.5	4.2±3.0	3.2±0.2	5.4±2.2
$^{4,5,6,7}F_{8}$-FBimbe **13**	1.7±0.5	3.4±0.8	19.4±0.9	2.1±0.8

[a] The cell viability at 48 h was measured at the concentration of 50 μM.

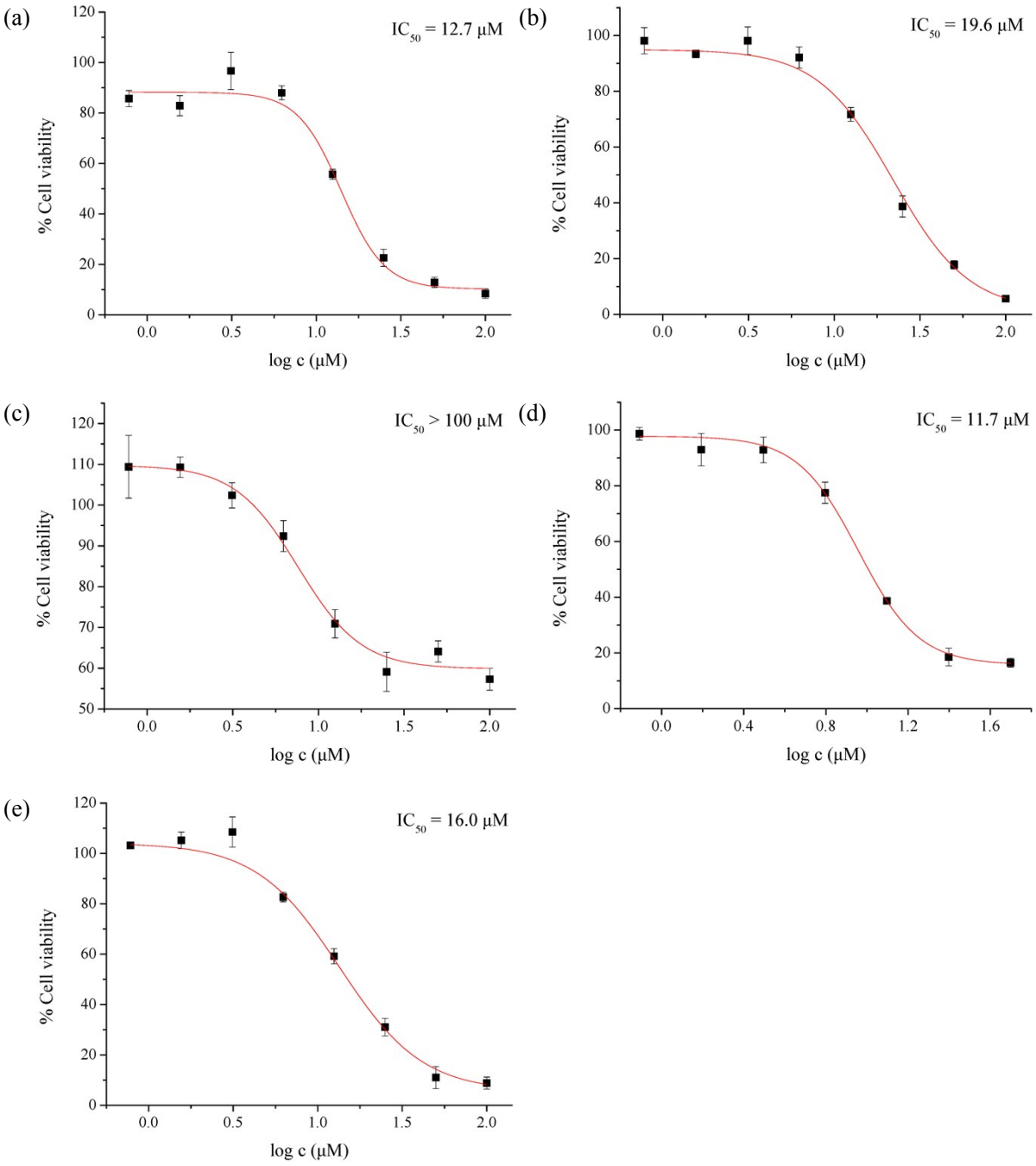

Fig. S85. Typical dose-response cell viability curves for HeLa (a), A549 (b), MCF-7 (c), HepG2 (d) and LO2 (e) cells treated with Bimbe **1** of varying doses.

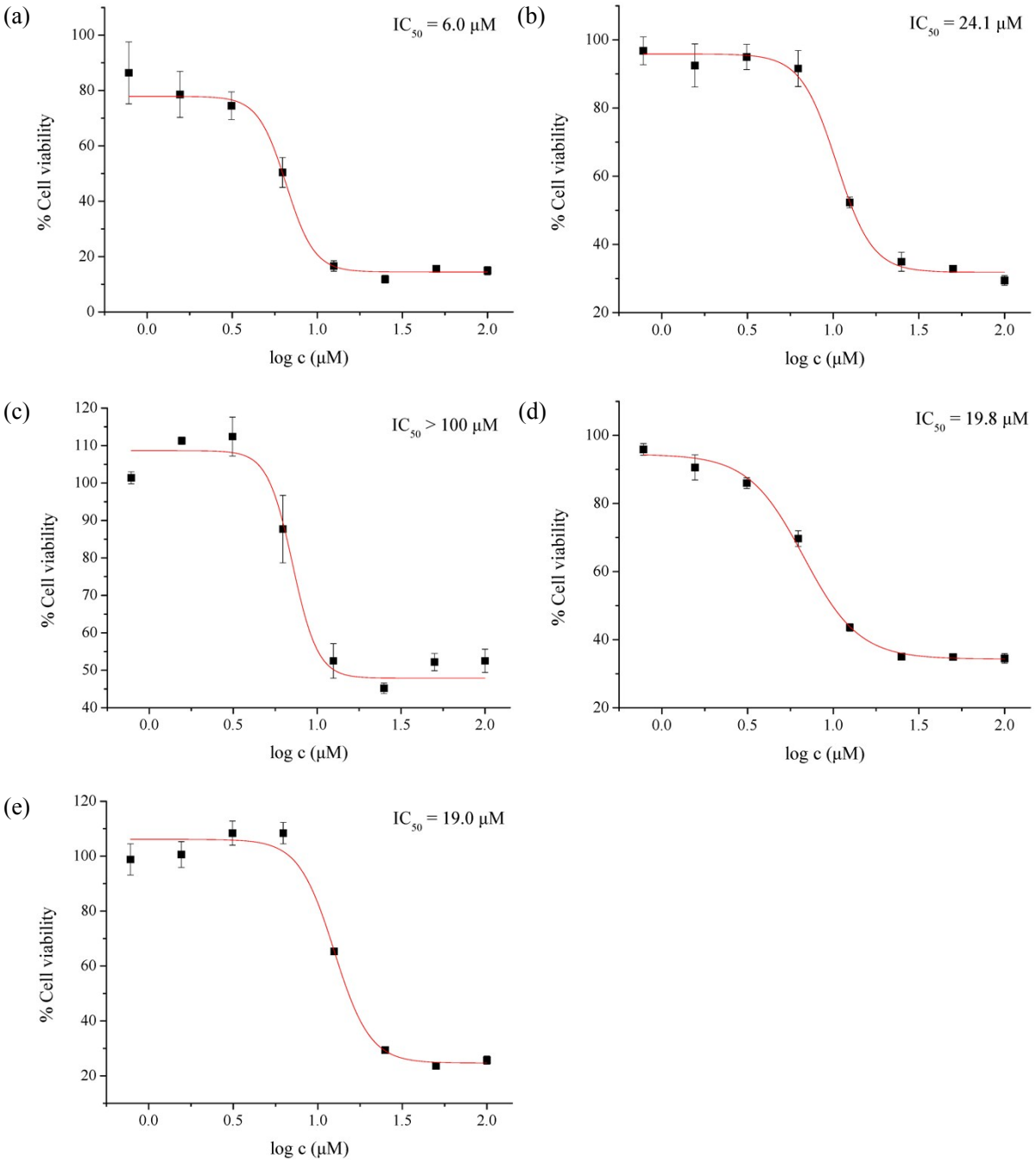

Fig. S86. Typical dose-response cell viability curves for HeLa (a), A549 (b), MCF-7 (c), HepG2 (d) and LO2 (e) cells treated with $^{5}F_{2}$-Bimbe **3** of varying doses.

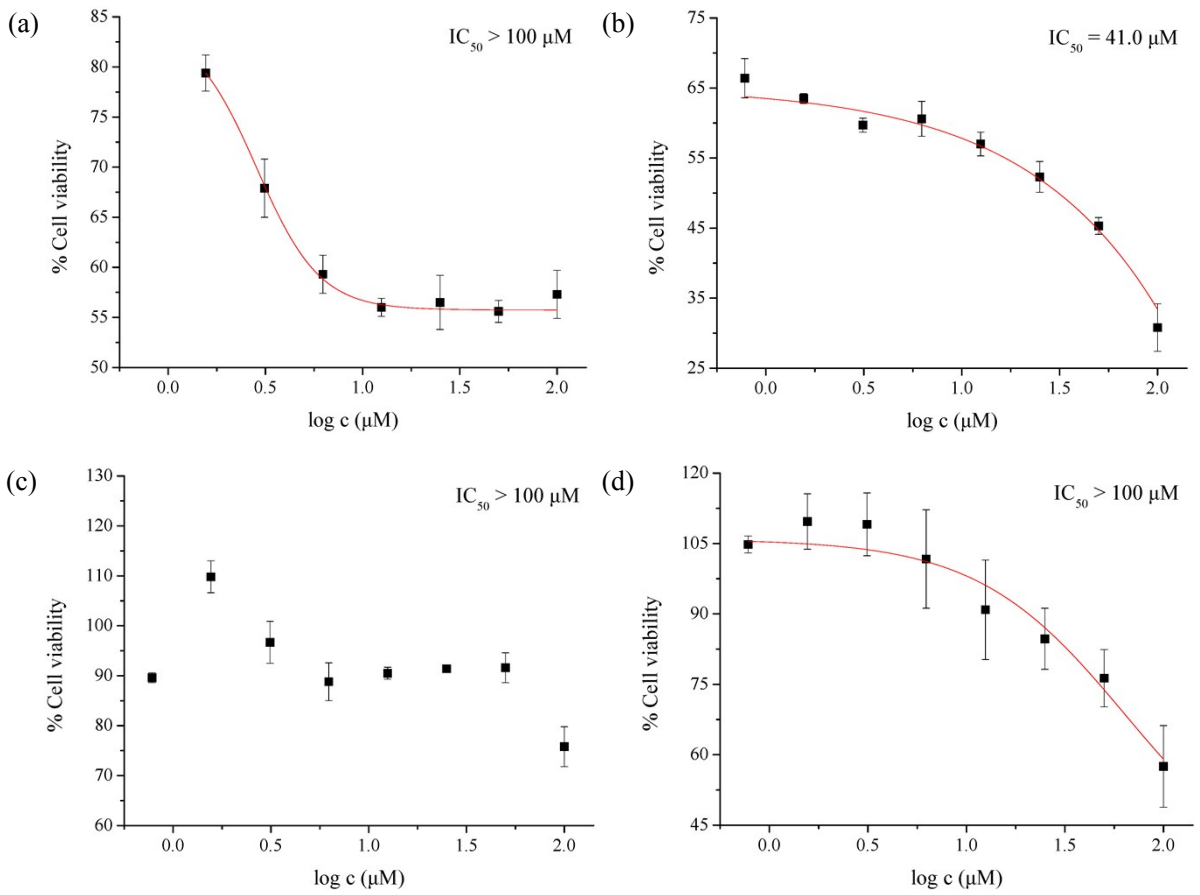

Fig. S87. Typical dose-response cell viability curves for HeLa (a), A549 (b), MCF-7 (c) and HepG2 (d) cells treated with $^{4,6}F_4$-Bimbe **5** of varying doses.

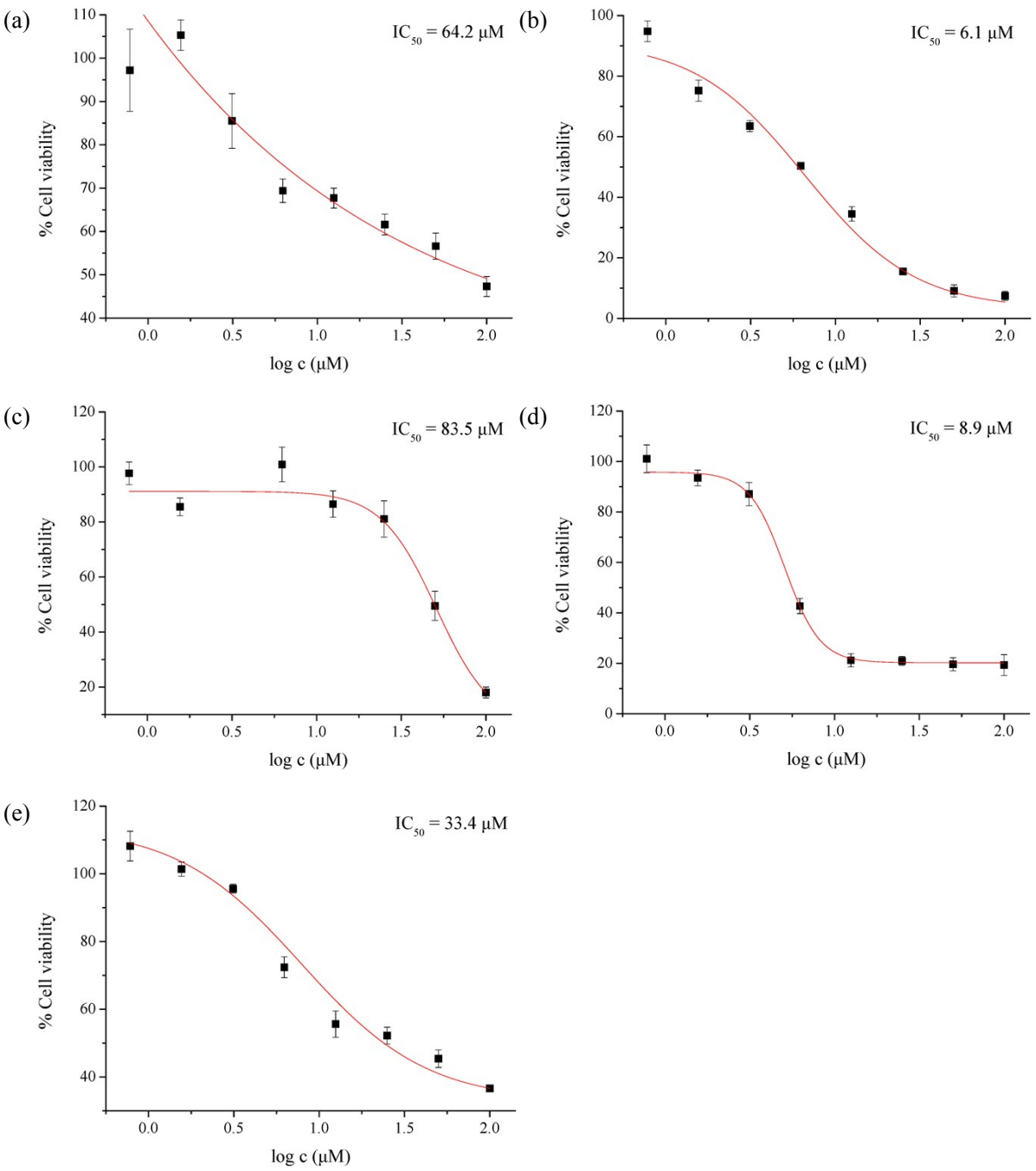

Fig. S88. Typical dose-response cell viability curves for HeLa (a), A549 (b), MCF-7 (c), HepG2 (d) and LO2 (e) cells treated with $^{5,6}F_4$-Bimbe **6** of varying doses.

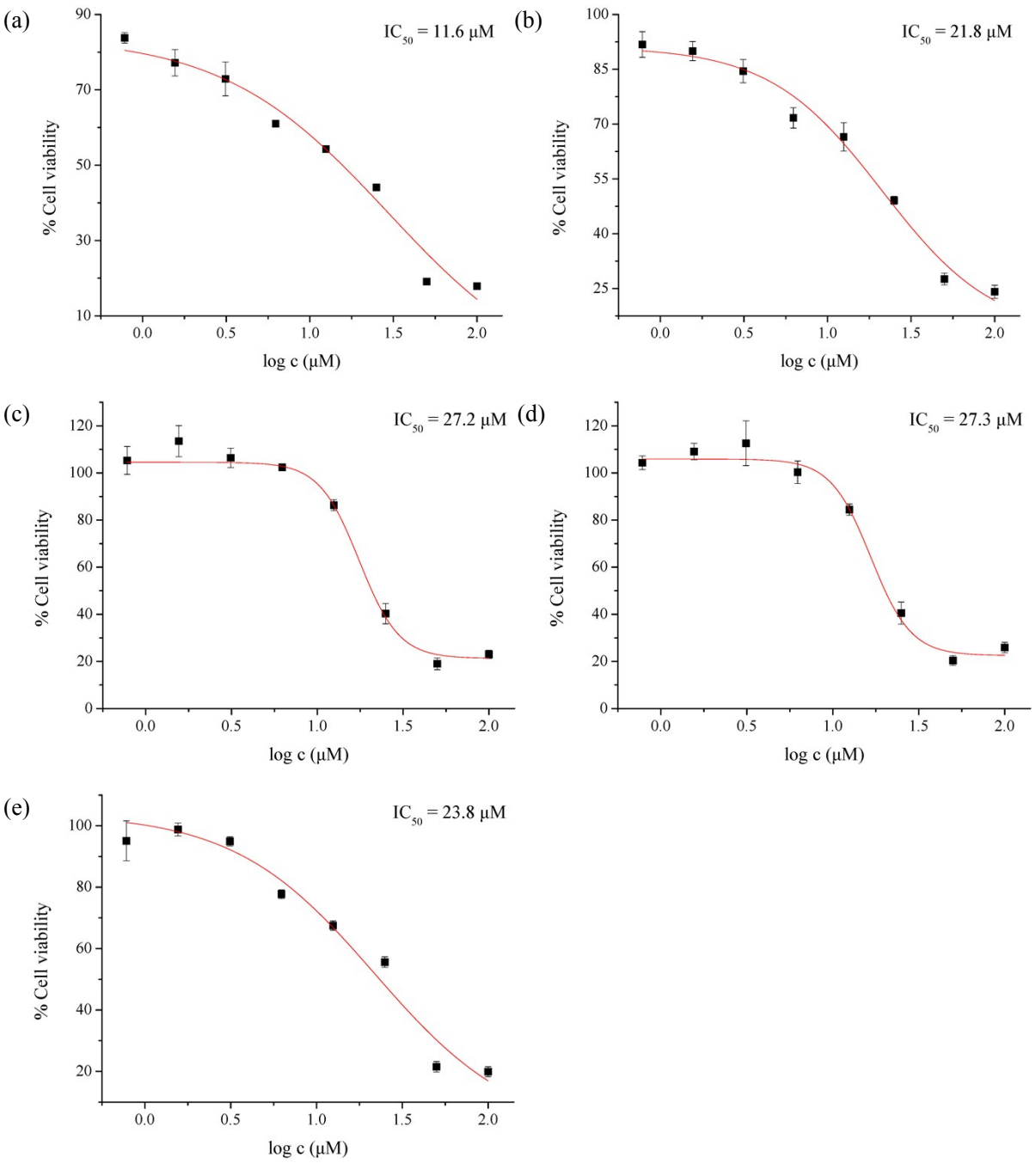

Fig. S89. Typical dose-response cell viability curves for HeLa (a), A549 (b), MCF-7 (c), HepG2 (d) and LO2 (e) cells treated with FBimbe **7** of varying doses.

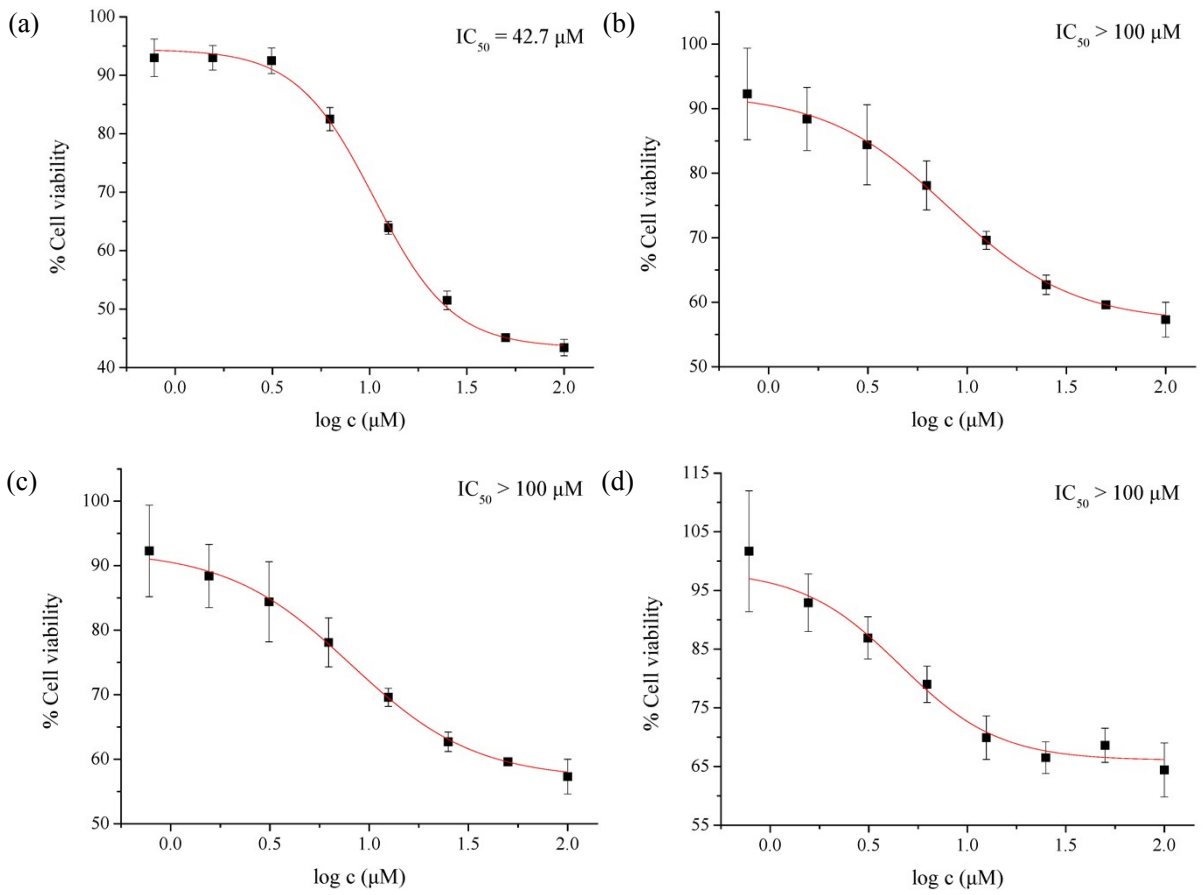

Fig. S90. Typical dose-response cell viability curves for HeLa (a), A549 (b), MCF-7 (c) and HepG2 (d) cells treated with $^4F_2$-FBimbe **8** of varying doses.

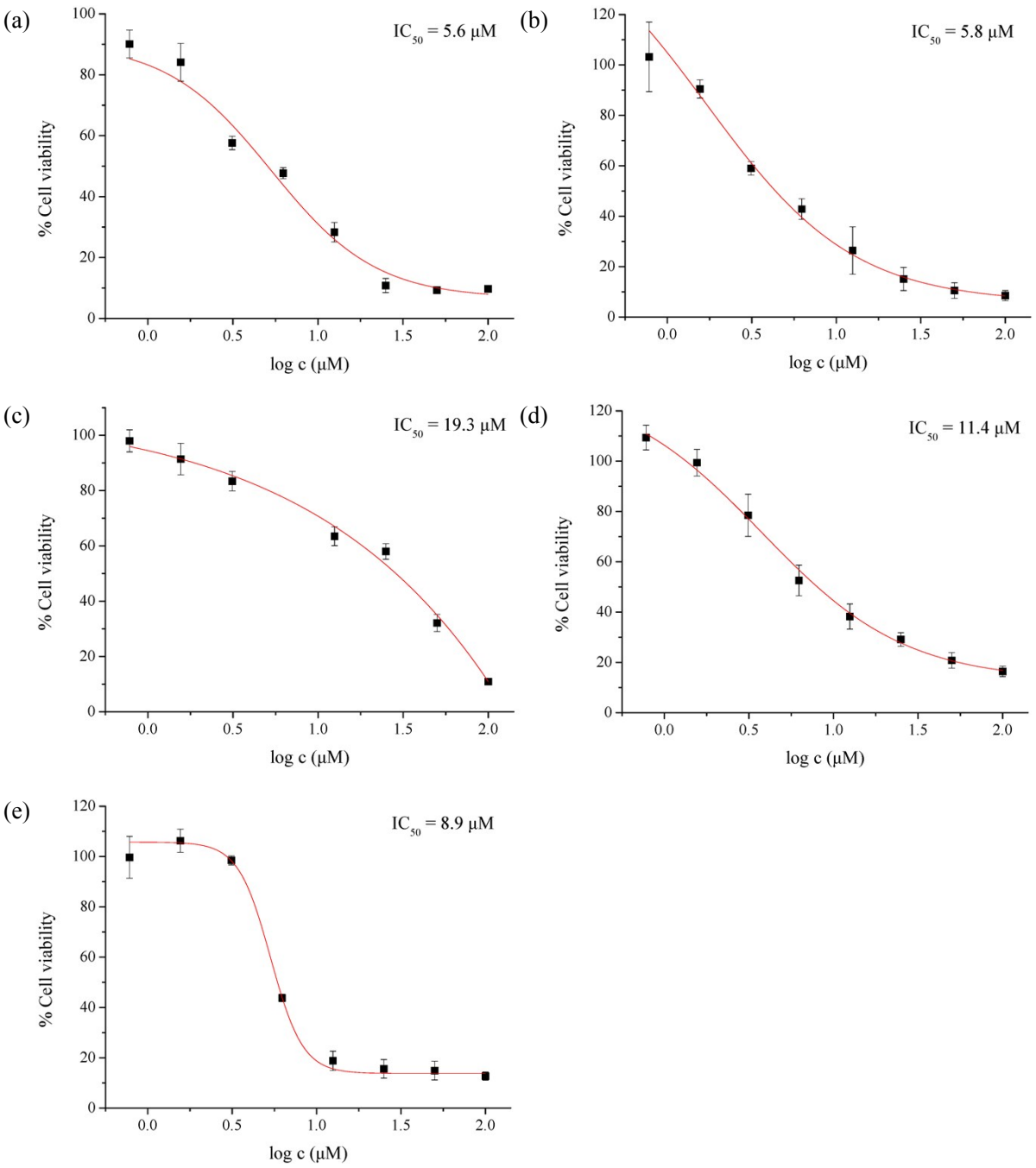

Fig. S91. Typical dose-response cell viability curves for HeLa (a), A549 (b), MCF-7 (c), HepG2 (d) and LO2 (e) cells treated with $^{5}F_{2}$-FBimbe **9** of varying doses.

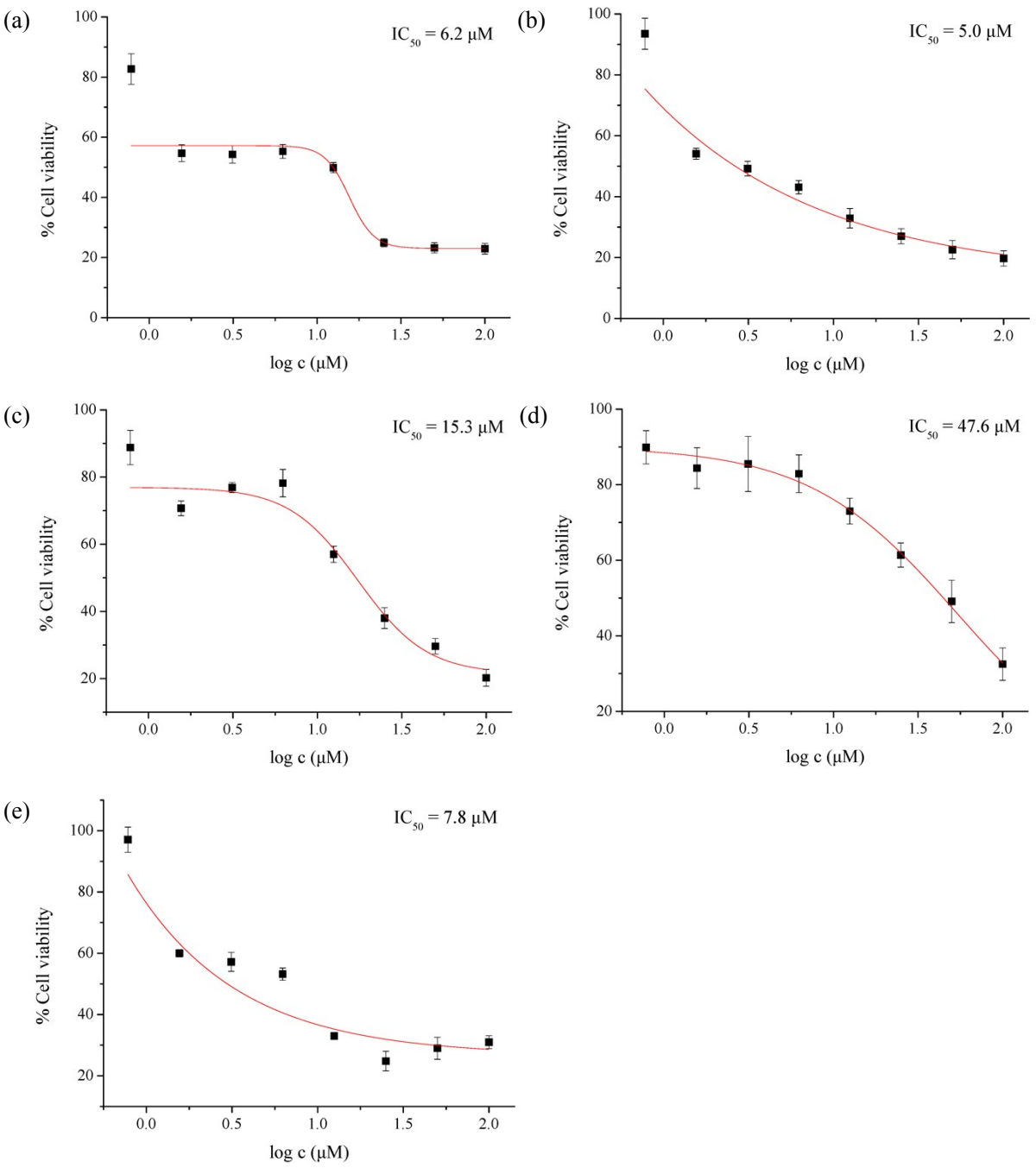

Fig. S92. Typical dose-response cell viability curves for HeLa (a), A549 (b), MCF-7 (c), HepG2 (d) and LO2 (e) cells treated with $^{4,5}F_4$-FBimbe **10** of varying doses.

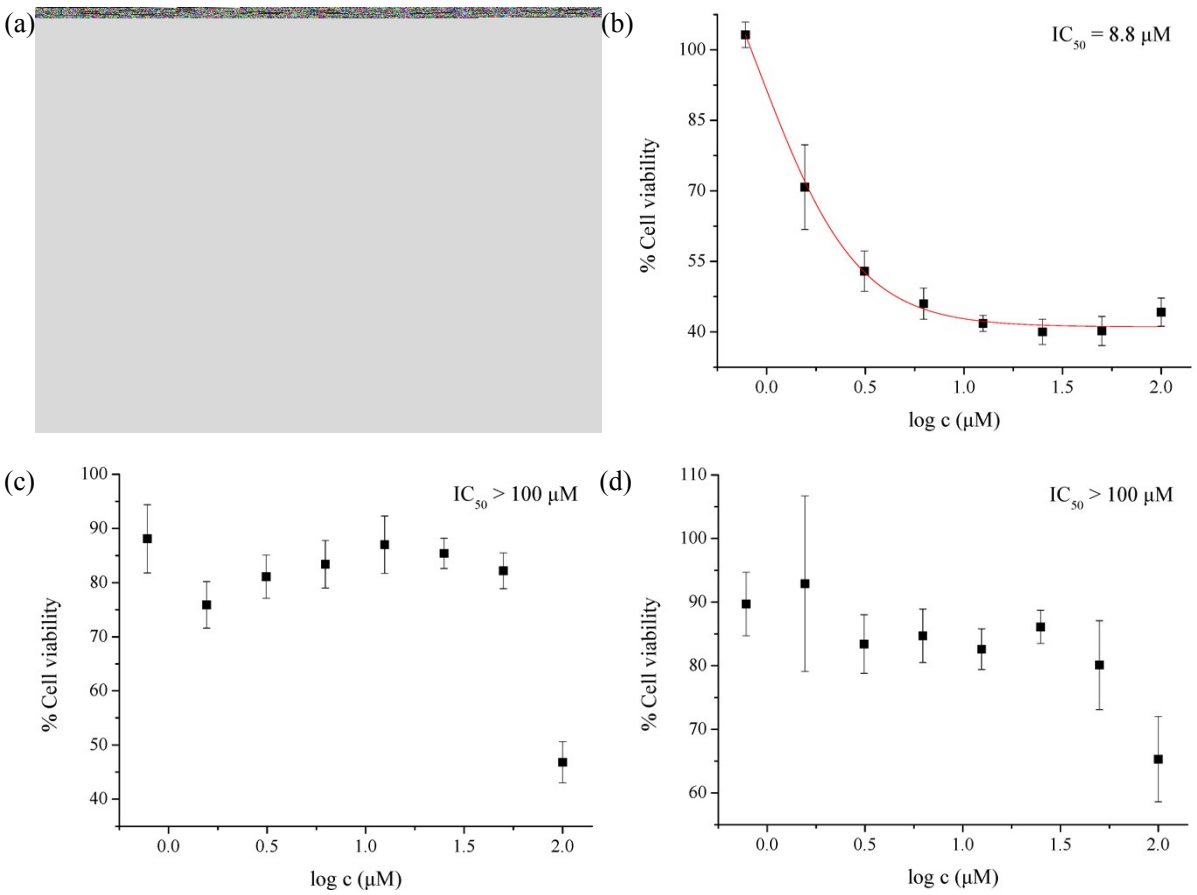

Fig. S93. Typical dose-response cell viability curves for HeLa (a), A549 (b), MCF-7 (c) and HepG2 (d) cells treated with $^{4,6}F_4$-FBimbe **11** of varying doses.

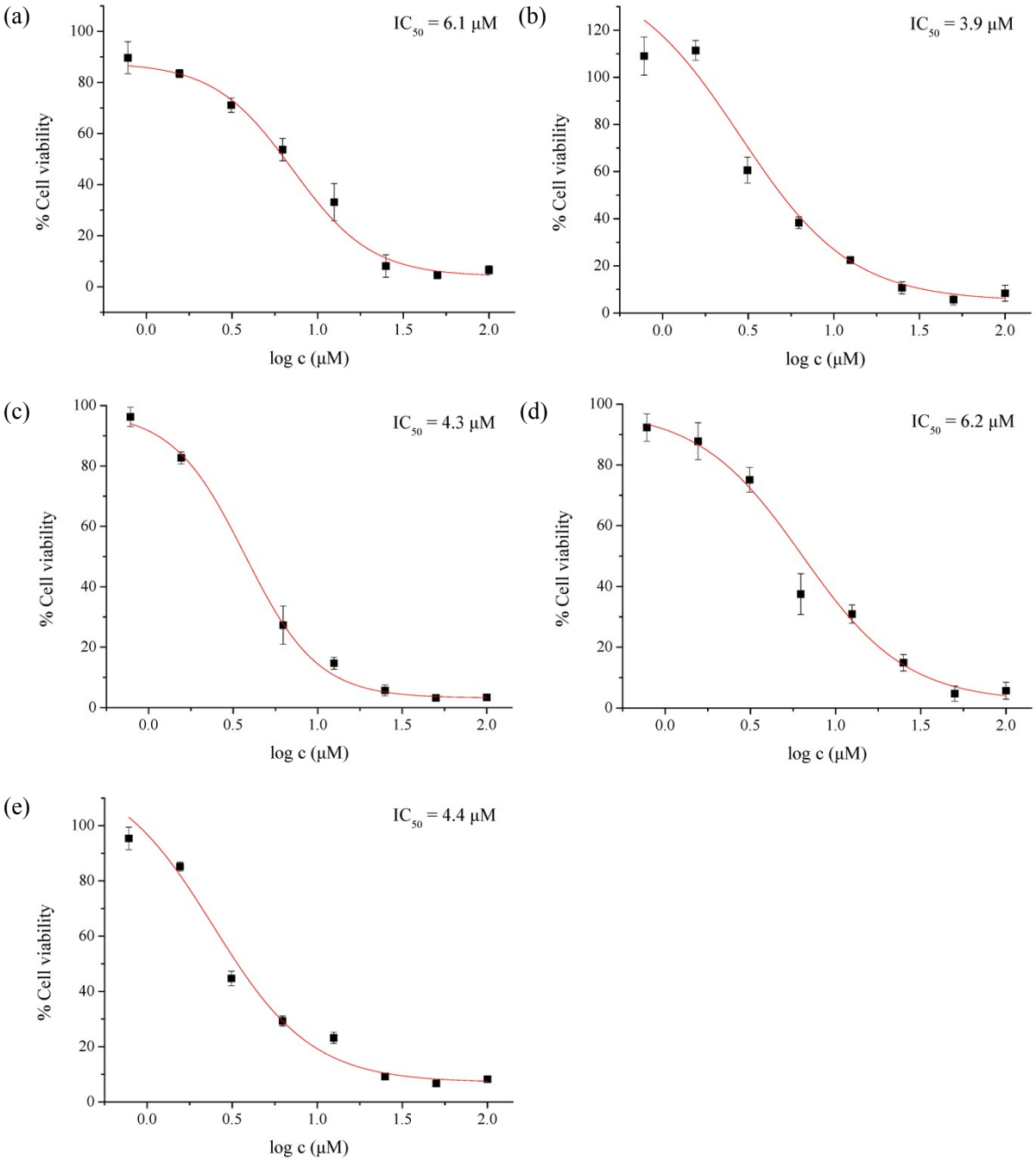

Fig. S94. Typical dose-response cell viability curves for HeLa (a), A549 (b), MCF-7 (c), HepG2 (d) and LO2 (e) cells treated with $^{5,6}F_4$-FBimbe **12** of varying doses.

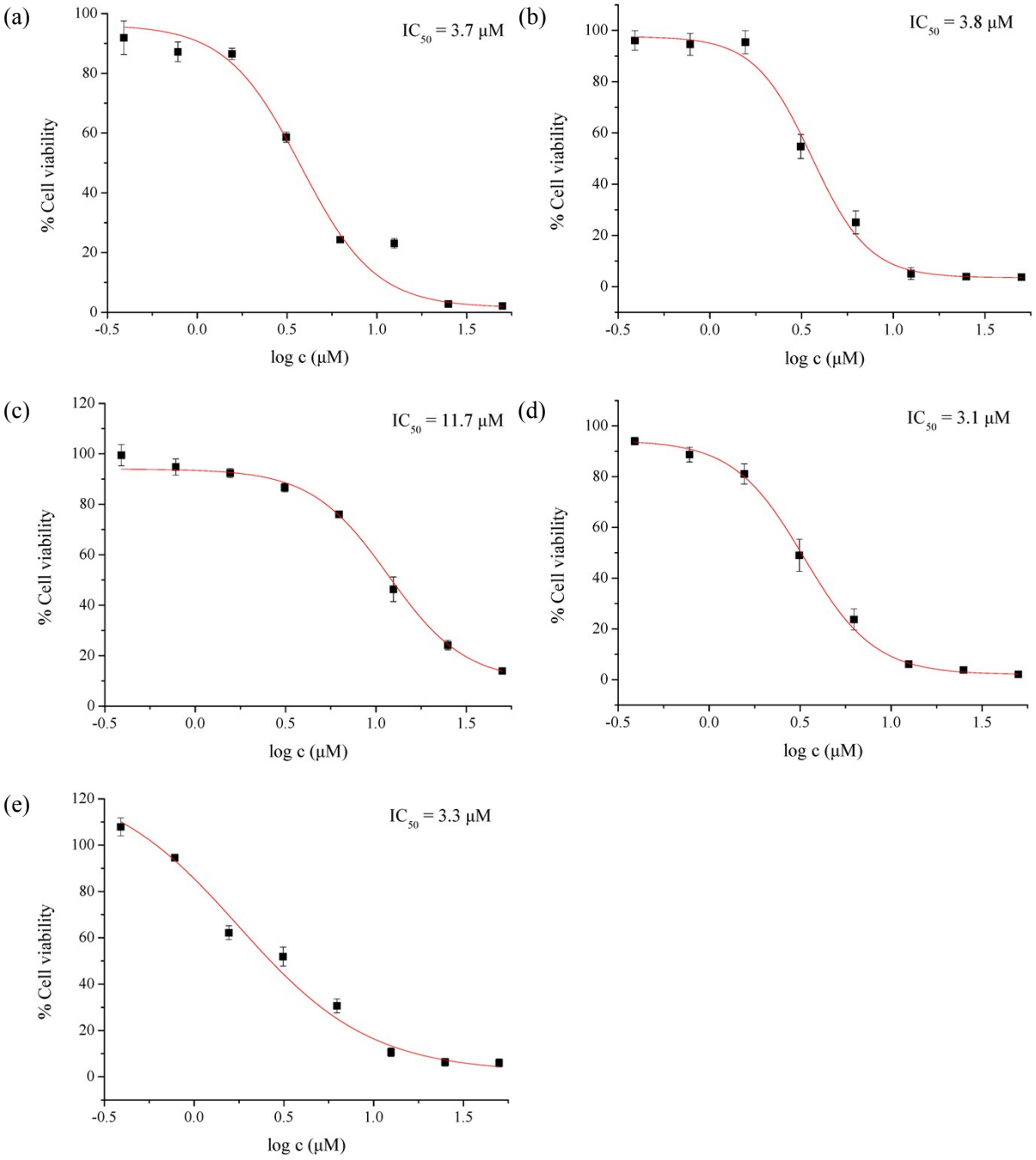

Fig. S95. Typical dose-response cell viability curves for HeLa (a), A549 (b), MCF-7 (c), HepG2 (d) and LO2 (e) cells treated with $^{4,5,6,7}F_8$-FBimbe **13** of varying doses.

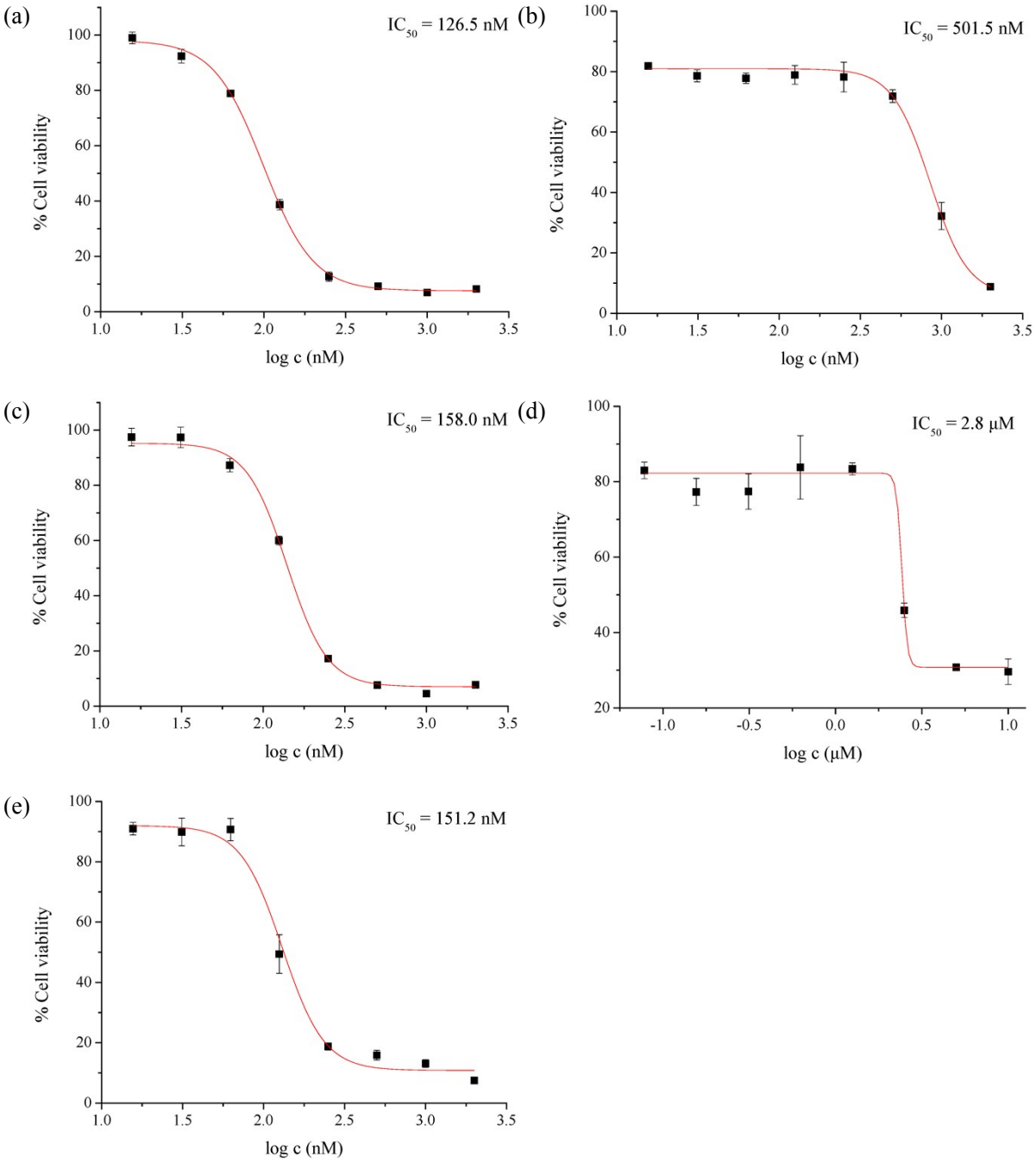

Fig. S96. Typical dose-response cell viability curves for HeLa (a), A549 (b), MCF-7 (c), HepG2 (d) and LO2 (e) cells treated with doxorubicin of varying doses.

Table S5. IC_{50} (μM) of Bimbe and its derivatives towards HeLa and A549 cells

Compound	HeLa				A549			
	1	2	3	Mean±SD	1	2	3	Mean±SD
Bimbe **1**	11.2	12.7	13.5	12.5±1.2	19.6	19.9	17.0	18.8±1.6
$^{4}F_{2}$-Bimbe **2**	>100	>100	>100	>100	>50	>50	>50	>50
$^{5}F_{2}$-Bimbe **3**	6.6	6.0	6.1	6.2±0.3	24.1	24.8	17.6	22.2±4.0
$^{4,5}F_{4}$-Bimbe **4**	>100	>100	>100	>100	>50	>50	>50	>50
$^{4,6}F_{4}$-Bimbe **5**	>100	>100	>100	>100	41.0	37.1	31.6	36.6±4.7
$^{5,6}F_{4}$-Bimbe **6**	64.2	61.3	50.0	58.5±7.5	6.2	6.1	6.4	6.2±0.2
FBimbe **7**	14.4	11.6	19.4	15.1±4.0	22.5	21.8	20.4	21.6±1.1
$^{4}F_{2}$-FBimbe **8**	47.9	51.4	42.7	47.3±4.4	>50	>50	>50	>50
$^{5}F_{2}$-FBimbe **9**	5.7	5.4	5.6	5.6±0.2	5.2	5.8	6.5	5.8±0.7
$^{4,5}F_{4}$-FBimbe **10**	6.2	7.9	5.3	6.5±1.3	5.0	4.9	3.6	4.5±0.8
$^{4,6}F_{4}$-FBimbe **11**	>100	>100	>100	>100	8.8	8.8	8.6	8.7±0.1
$^{5,6}F_{4}$-FBimbe **12**	6.5	10.1	6.1	7.6±2.2	2.8	3.9	2.8	3.2±0.6
$^{4,5,6,7}F_{8}$-FBimbe **13**	3.7	3.8	3.9	3.8±0.1	3.8	3.7	4.5	4.0±0.4
Doxorubicin	0.13	0.22	0.12	0.16±0.06	0.50	0.44	0.43	0.46±0.04

Table S6. IC_{50} (μM) of Bimbe and its derivatives towards MCF-7 and HepG2 cells

Compound	MCF-7				HepG2			
	1	2	3	Mean±SD	1	2	3	Mean±SD
Bimbe **1**	>100	>100	>100	>100	12.3	11.7	13.1	12.4±0.7
$^{4}F_{2}$-Bimbe **2**	>100	>100	>100	>100	>100	>100	>100	>100
$^{5}F_{2}$-Bimbe **3**	>100	>100	>100	>100	20.3	19.8	21.4	20.5±0.8
$^{4,5}F_{4}$-Bimbe **4**	>100	>100	>100	>100	>100	>100	>100	>100
$^{4,6}F_{4}$-Bimbe **5**	>100	>100	>100	>100	>100	>100	>100	>100
$^{5,6}F_{4}$-Bimbe **6**	64.1	83.5	75.6	74.4±9.8	10.1	8.9	10.3	9.8±0.8
FBimbe **7**	38.1	35.4	39.9	37.8±2.3	27.2	27.3	30.1	28.2±1.6
$^{4}F_{2}$-FBimbe **8**	>100	>100	>100	>100	>100	>100	>100	>100
$^{5}F_{2}$-FBimbe **9**	19.3	21.9	21.8	21.0±1.5	11.4	10.7	9.6	10.6±0.9
$^{4,5}F_{4}$-FBimbe **10**	15.2	16.6	15.3	15.7±0.8	45.1	47.6	39.3	44.0±4.3
$^{4,6}F_{4}$-FBimbe **11**	>100	>100	>100	>100	>100	>100	>100	>100
$^{5,6}F_{4}$-FBimbe **12**	5.5	4.3	4.0	4.6±0.8	6.3	6.3	6.2	6.3±0.1
$^{4,5,6,7}F_{8}$-FBimbe **13**	11.7	11.9	10.7	11.4±0.6	2.0	3.1	2.8	2.6±0.6
Doxorubicin	0.14	0.16	0.15	0.15±0.01	2.2	2.6	2.8	2.5±0.3

Table S7. IC_{50} (μM) of Bimbe and its derivatives towards LO2 cells

Compound	LO2			
	1	2	3	Mean±SD
Bimbe **1**	16.0	16.7	17.7	16.8±0.9
$^{4}F_{2}$-Bimbe **2**	> 50	> 50	> 50	> 50
$^{5}F_{2}$-Bimbe **3**	18.8	19.0	18.5	18.8±0.3
$^{4,5}F_{4}$-Bimbe **4**	> 50	> 50	> 50	> 50
$^{4,6}F_{4}$-Bimbe **5**	> 50	> 50	> 50	> 50
$^{5,6}F_{4}$-Bimbe **6**	33.4	30.1	27.2	30.2±3.1
FBimbe **7**	23.8	30.8	23.7	26.1±4.1
$^{4}F_{2}$-FBimbe **8**	> 50	> 50	> 50	> 50
$^{5}F_{2}$-FBimbe **9**	7.7	8.2	8.9	8.3±0.6
$^{4,5}F_{4}$-FBimbe **10**	5.2	7.8	6.0	6.3±1.3
$^{4,6}F_{4}$-FBimbe **11**	> 50	> 50	> 50	> 50
$^{5,6}F_{4}$-FBimbe **12**	4.1	3.9	4.4	4.1±0.3
$^{4,5,6,7}F_{8}$-FBimbe **13**	3.3	3.9	2.9	3.4±0.5
Doxorubicin	0.13	0.14	0.15	0.14±0.01

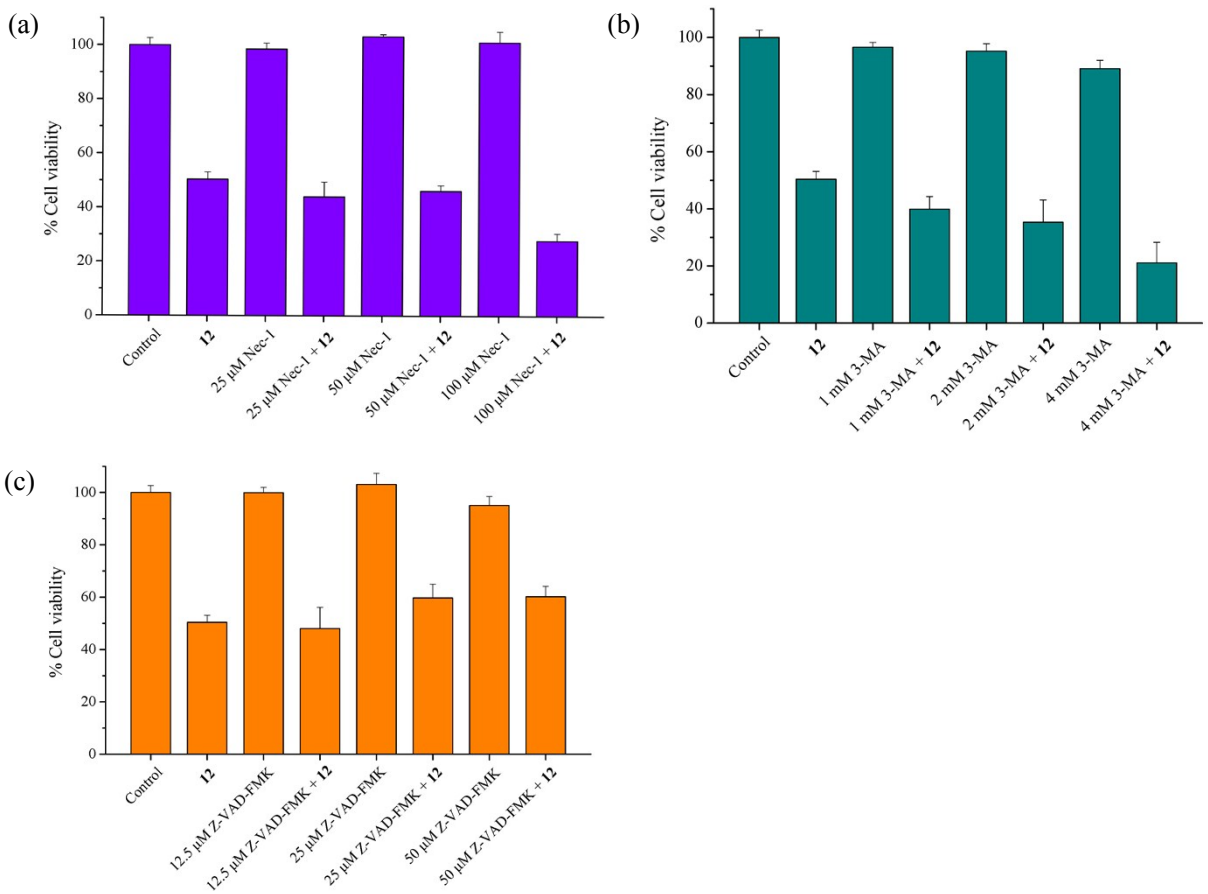

Fig. S97. Cell viability (%) of HeLa cells incubated with varying concentrations of Nec-1 (a), 3-MA (b) or Z-VAD-FMK (c) for 2 h, followed by the treatment with $^{5,6}F_4$-FBimbe **12** (10 μM) for 24 h.

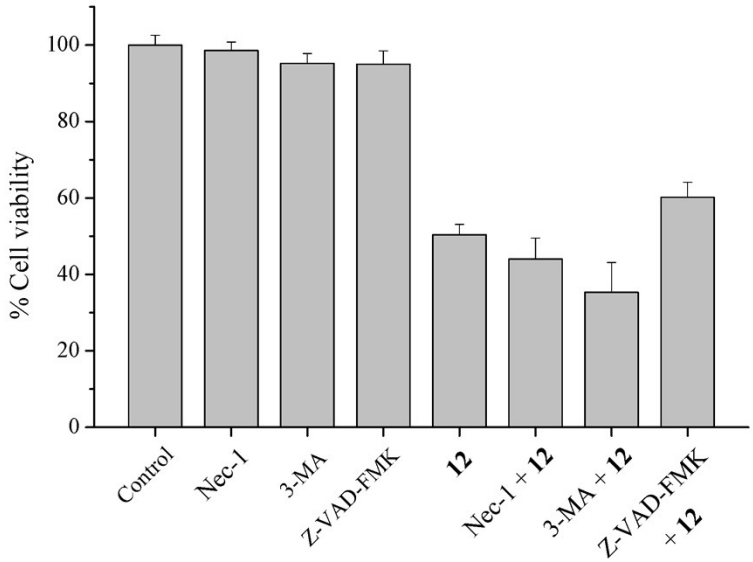

Fig. S98. Viability of HeLa cells incubated with Nec-1 (25 μM), 3-MA (2.0 mM) or Z-VAD-FMK (50 μM) for 2 h, followed by the treatment with $^{5,6}F_4$-FBimebe **12** of 10 μM for 24 h.

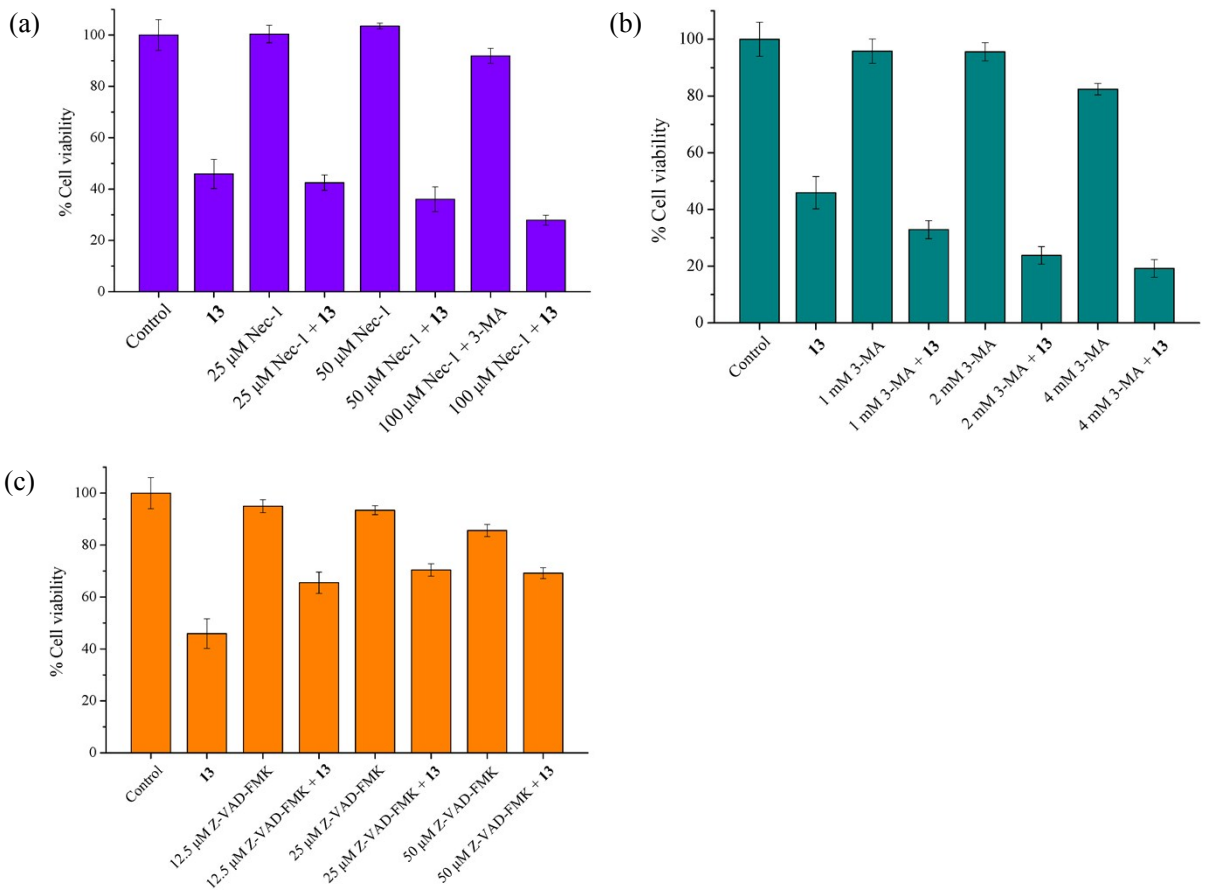

Fig. S99. Cell viability (%) of HeLa cells incubated with varying concentrations of Nec-1 (a), 3-MA (b) or Z-VAD-FMK (c) for 2 h, followed by the treatment with $^{4,5,6,7}F_8$-FBimbe **13** (10 μM) for 24 h.

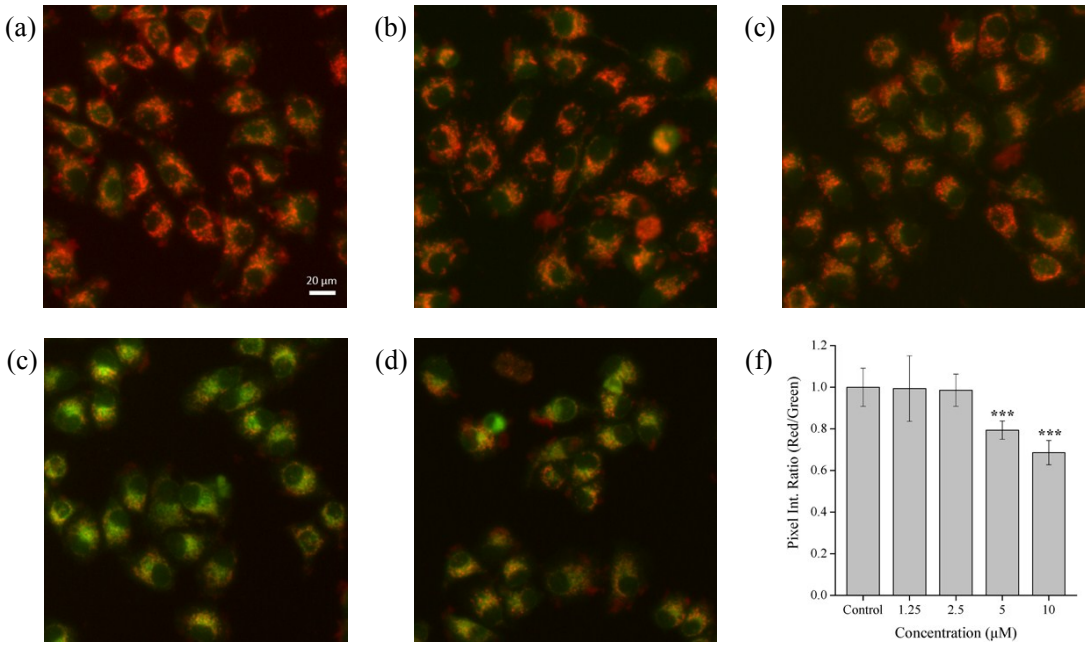

Fig. S100. JC-1 staining on HeLa cancer cells. (a) Untreated (control) cells; (b)-(e) cells treated with $^{5,6}F_4$-FBimbe at the concentrations of 1.25 μM, 2.5 μM, 5 μM and 10 μM, respectively; (d) The pixel ratio (red/green) for $^{5,6}F_4$-FBimbe **12** of varying concentrations, analyzed by ImageJ. (mean ± s.d., n = 9, ***P < 0.001, Independent-Sample T Test)